*- Supporting Information -*

# A Comprehensive Mechanistic Picture of the Isomerizing Alkoxycarbonylation of Plant Oils

Philipp Roesle,[a] Lucia Caporaso,[b,*] Manuel Schnitte,[a] Verena Goldbach,[a] Luigi Cavallo,[b,c] and Stefan Mecking[a,*]

a) Chair of Chemical Materials Science, Department of Chemistry, University of Konstanz, 78464 Konstanz, Germany.

b) Department of Chemistry, University of Salerno, Via Giovanni Paolo II, 84084-Fisciano (SA), Italy.

c) King Abdullah University of Science and Technology, Chemical and Life Sciences and Engineering, Kaust Catalysis Center, Thuwal 23955-6900, Saudi Arabia.

**Materials and general considerations**

Unless noted otherwise, all manipulations of phosphines or palladium complexes were carried out under an inert nitrogen or argon atmosphere using standard glovebox or Schlenk techniques. Pentane and methylene chloride were distilled from calcium hydride, THF and diethyl ether from blue sodium / benzophenone ketyl, methanol, ethanol, *n*-propanol and *iso*-propanol from activated (iodine) magnesium under argon prior to use. All other solvents were commercial grade. Trifluoromethanesulfonic acid, p-benzoquinone, *tert*-butyl chloride, 1,3-dichloropropane, magnesium chips, di-*iso*-propylphosphine, diethylphosphine, iodine, 3 Å molecular sieves, $^{13}CO$, trichlorophosphine (99 %), methyl oleate (99 %) and methyl linoleate (99 %) were purchased from Sigma-Aldrich, 1,2-bis((di-tert-butylphosphino)methyl)benzene (dtbpx) and silver triflate (99 %) from ABCR. *tert*-BuLi in hexanes, *n*-BuLi in hexanes and di-*tert*-butylmethylphosphine were obtained from Acros, palladium(II)-chloride from MCAT and CO 3.7 from AirLiquide. High oleic sunflower oil methyl ester 'Dakolub MB 9001' was donated by Dako AG. p-Benzoquinone was sublimed prior to use. Methyl oleate, methyl linoleate, high oleic sunflower oil methyl ester 'Dakolub MB 9001' and 1,3-dichloropropane were degassed by repetitive freeze/pump/thaw-cycles, stored over 3 Å molecular sieves and used without further purification. All other chemicals were used without further purification. [$Pd(dba)_2$],[1] dibenzylideneacetone (dba),[2] [$(COD)PdCl_2$],[3] [(COD)Pd(Me)Cl],[4] di-*tert*-butylphosphine,[5] di-*tert*-butylchlorophosphine,[6] 1,1-bis(di-*tert*-butylphosphino)methane (dtbpm),[6] 1,2-bis(di-*tert*-butylphosphino)ethane (dtbpe),[7] 1,3-bis(di-*tert*-butylphosphino)propane (dtbpp),[8] 1,4-bis(di-*tert*-butylphosphino)butane (dtbpb),[9] 1,3-bis(di-*iso*-propylphosphino)propane (dippp),[10] 1,3-bis(diethylphosphino)propane (depp),[11] [$(dtbpp)Pd(OTf)_2$],[17] [$(dtbpx)Pd(OTf)_2$][12] and [(dtbpx)Pd(Me)Cl][19] were synthesized according to literature procedures. [(dtbpx)Pd($^{13}$COMe)Cl] was generated in-situ according to a literature procedure.[19]

NMR spectra were recorded on a Varian Unity Inova 400 equipped with a 4NUC/switchable mode - 5 mm "direct detection" probe, a Bruker Avance III 400 equipped with a BBFO plus probe or a Bruker Avance III 600 equipped with a QXI-H/C/N/P quadruple resonance probe. $^1$H NMR spectra were referenced to residual protiated solvent signals. $^{13}$C NMR spectra were referenced to the solvent signals, $^{31}$P NMR spectra to external 85% $H_3PO_4$ and $^{19}$F NMR spectra to external $BF3{\cdot}OEt_2$. NMR spectra are reported as follows: chemical shift (δ ppm), multiplicity, coupling constant (Hz), and integration. Multiplicities are given as follows (or combinations thereof): s: singlet, d: doublet, t: triplet, q: quartet, quint: quintet, m: multiplet, v: virtual, br.: broad. The identity of metal complexes and detailed NMR assignments were

established by 2D NMR experiments ($^{1}$H,$^{1}$H-COSY, $^{1}$H,$^{13}$C-HSQC, $^{1}$H,$^{13}$C-HMBC and $^{1}$H,$^{31}$P-HMBC) in addition to 1D NMR experiments. Acquired data was processed and analyzed using MestReNova software.

Gas chromatography was carried out on a PerkinElmer (PE) Clarus 500 instrument with autosampler and FID detection on a PerkinElmer Elite-5 (5% Diphenyl- 95% Dimethylpolysiloxane) Series Capillary Columns (Length: 30 m, Inner Diameter: 0.25 mm, Film Thickness: 0.25 mm), using Helium as carrier gas at a flow rate of 1.5 mL min$^{-1}$. The injector temperature was 300 °C. When methyl oleate, methyl linoleate or 1-octadecen were used as substrates, the oven was kept isothermal at 90 °C for 1 min after injection, then heated with 30 K min$^{-1}$ to 280 °C, and kept isothermal at 280 °C for 8 min. When octenes were used as substrates, the oven was kept isothermal at 60 °C for 3 min after injection, then heated with 30 K min$^{-1}$ to 280 °C, and kept isothermal at 280 °C for 3 min. When ethylene was used as a substrate, the oven was kept isothermal at 40 °C for 7 min after injection, then heated with 40 K min$^{-1}$ to 280 °C, and kept isothermal at 280 °C for 3 min.

X-Ray diffraction analysis was performed at 100 K on a STOE IPDS-II diffractometer equipped with a graphite-monochromated radiation source ($\lambda$ = 0.71073 Å) and an image plate detection system. Crystals were mounted on a fine glass fiber with silicon grease. The selection, integration and averaging procedure of the measured reflex intensities, the determination of the unit cell dimensions and a least-squares fit of the $2\theta$ values as well as data reduction, LP-correction and space group determination were performed using the X-Area software package delivered with the diffractometer.[13] Unless noted otherwise, a semi empirical absorption correction was performed. The structures were solved by Patterson or Direct methods (SHELXS-97),[14] completed with difference Fourier syntheses, and refined with full-matrix least-square using SHELXL-97[15] minimizing w($F_0^2$-$F_c^2$)$^2$. Weighted $R$ factor ($wR_2$) and the goodness of fit GooF are based on $F^2$. All non-hydrogen atoms were refined with anisotropic displacement parameters. All hydrogen atoms were treated in a riding model. Graphical output (ORTEP plots) were created using ORTEP-3 V2.02 for Windows 7.[16]

**Carbonylation procedure I:**

Carbonylations were carried out in a 20 mL stainless steel pressure reactor equipped with heating jacket and a glass inlay. Mixing was provided by a magnetic stirring bar. Prior to a carbonylation experiment the reactor was purged several times with argon. The catalyst precursor was weighed into a Schlenk tube equipped with a magnetic stirring bar in a glovebox. The Schlenk tube was removed from the glovebox and all other reactants (olefinic substrate and

alcohol) were added using standard Schlenk techniques. Vigorous stirring afforded a homogenous reaction mixture, which was cannula-transferred into the reactor in an argon counter stream. The reactor was closed, pressurized with carbon monoxide and then heated to the desired reaction temperature. After the desired reaction time, the reactor was cooled to room temperature and vented. The reaction mixture was diluted with methylene chloride and filtered to remove Pd-black. Conversion and selectivity were determined by GC analysis.

**Carbonylation procedure II:**

Carbonylations in which the progress of the reaction was monitored over time were carried out in a 200 mL stainless steel mechanically stirred pressure reactor equipped with a heating/cooling jacket supplied by a thermostat controlled by a thermocouple dipping into the reaction mixture. Prior to a carbonylation experiment the reactor was purged several times with argon. The catalyst precursor was dissolved in 2 mL of the desired alcohol and transferred into a syringe. All other reagents (olefinic substrate and alcohol) were mixed in a Schlenk tube, stirred and cannula-transferred into the reactor in an argon counter stream. The reactor was closed and pressurized with 2 bar carbon monoxide. The catalyst solution was then injected into the reactor through a custom made rubber septa via a long needle attached to the syringe. The reactor was closed, pressurized with carbon monoxide and heated to the desired reaction temperature. To reach the desired reaction temperature as fast as possible (within 2 minutes) the thermostat was preheated to the desired reaction temperature + 4 °C and connected to the heating/cooling jacket of the reactor after pressurization. Samples for GC analysis were drawn via a bottom blow valve periodically. After the desired reaction time, the reactor was cooled to room temperature and vented. The reaction mixture was diluted with methylene chloride and filtered to remove Pd-black. Conversion and selectivity were determined by GC analysis.

**Carbonylation of ethylene:**

The reaction was carried out in a 200 mL stainless steel mechanically stirred pressure reactor equipped with a heating/cooling jacket supplied by a thermostat controlled by a thermocouple dipping into the reaction mixture. Prior to a methoxycarbonylation experiment the reactor was purged several times with argon. The catalyst precursor was weighed into a Schlenk tube equipped with a magnetic stirring bar in a glovebox. The Schlenk tube was removed from the glovebox and 180 mL methanol and methyl hexanoate (220 µL, 1.5 mmol) as internal standard were added. The catalyst / internal standard solution was cannula-transferred into the reactor in an argon counter stream. The reactor was closed, pressurized with 2-10 bar ethylene and

'saturated' for 5-10 minutes. The preheated thermostat (94 °C) was then connected and the reactor was pressurized with additional 20 bar CO after the reaction mixture reached 90 °C. Ethylene conversion was calculated from the total amount of methyl propionate formed after reaction times of ca. 15 minutes (note that already after 2-3 minutes the amount of methyl propionate did not change any more). The desired 29.5 mmol ethylene were obtained when an ethylene pressure of 5 bar was applied and the methanol solution was 'saturated' for 5 minutes.

**General synthesis of [(P^P)Pd(OTf)$_2$] - procedure I[17,18]**

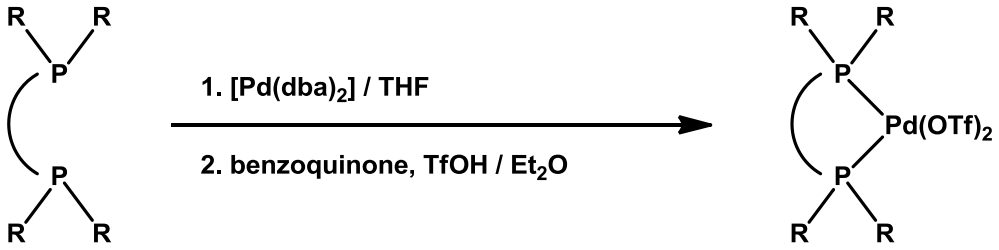


1 Equiv. diphosphine was dissolved in THF (c ~ 0.1 mol $L^{-1}$) and added to a deep red solution of 1 equiv. [Pd(dba)$_2$] in THF (c ~ 0.1 mol $L^{-1}$). The reaction mixture was stirred for two hours at room temperature. Insoluble parts (palladium black) were filtered off and the solvent was removed in vacuum. The yellow to red residue thus obtained was suspended in pentane and washed three more times with pentane to remove remaining diphosphine and dba. After drying in vacuum yellow to orange solids were obtained, which were used without further characterization. 1.1 Equiv. p-benzoquinone and $Et_2O$ (c ~ 0.05 mol $L^{-1}$) were then added resulting in a yellow to red suspension. After drop wise addition of 2.1 equiv. TfOH in $Et_2O$ (c ~ 0.5 mol $L^{-1}$) the suspension became clear and after 5-10 minutes the desired complexes precipitated as yellow to orange solids. After stirring overnight at room temperature, the solid was filtered off, washed with $Et_2O$ until the $Et_2O$ phase was colorless and the solids were dried in vacuum.

**General synthesis of [(P^P)Pd(OTf)$_2$] - procedure II[19]**

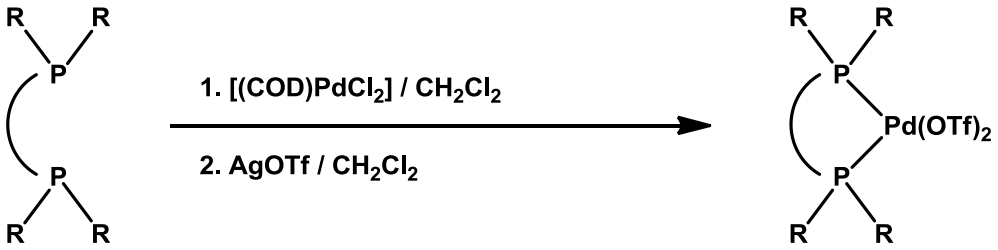


**a)** 1 Equiv. diphosphine, dissolved in $CH_2Cl_2$ (c ~ 0.1 mol $L^{-1}$) was added drop wise to a solution of 1 equiv. [(COD)$PdCl_2$] in $CH_2Cl_2$ (c ~ 0.1 mol $L^{-1}$) and stirred for 4 hours at room temperature. Insoluble parts were filtered off and the solvent was removed in vacuum. The residue was washed with $Et_2O$ and dried under reduced pressure. For further purification, the complex was dissolved in a minimum amount of methylene chloride, precipitated with pentane, filtered and washed with pentane yielding the desired [(P^P)$PdCl_2$] complex.
**b)** 1 Equiv. of the respective [(P^P)$PdCl_2$] complex was dissolved in $CH_2Cl_2$ (c ~ 0.1 mol $L^{-1}$) and 2 equiv. AgOTf were added as a solid and the reaction mixture was stirred for 20 minutes under the exclusion of light at room temperature. The white precipitate of AgCl was removed by filtration and the solvent was removed in vacuum. The crude product was washed with $Et_2O$ and dried in vacuum. For further purification, the complex was dissolved in a minimum amount of methylene chloride, precipitated with pentane, filtered and washed with pentane yielding the desired [(P^P)Pd(OTf)$_2$] complex.

**Synthesis of [(dtbpm)$PdCl_2$]**

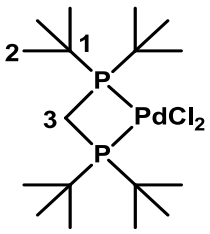


Following the general synthesis procedure II, [(dtbpm)$PdCl_2$] was obtained as a beige powder in 73 % yield. Crystals suitable for X-Ray diffraction were grown from a $CH_2Cl_2$ solution layered with $Et_2O$. **$^1$H NMR** (400 MHz, $CD_2Cl_2$, 298 K): δ 3.29 (t, $^2J_{PH}$ = 9.1, 2H, H-3), 1.58 (d, $^3J_{PH}$ = 15.9, 36H, H-2). **$^{31}$P{$^1$H} NMR** (162 MHz, $CD_2Cl_2$, 298 K): δ -15.9 (s). **$^{13}$C{$^1$H}**

**NMR** (100 MHz, $CD_2Cl_2$, 298 K): δ 38.9 (m, C-1), 31.2 (s, C-2), 27.8 (t, C-3). **Elemental analysis** (%) for $C_{17}H_{38}Cl_2P_2Pd$: calculated: C 42.38, H 7.95; found: C 42.26, H 7.99.

**Synthesis of [(dtbpm)Pd(OTf)$_2$]**

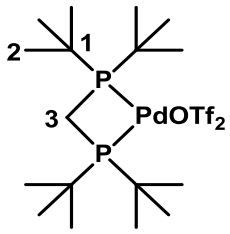


Following the general synthesis procedure I, [(dtbpm)Pd(OTf)$_2$] was obtained as a beige powder in 72 % yield. **$^1$H NMR** (400 MHz, $CD_2Cl_2$, 298 K): δ 3.96 (t, $^2J_{PH}$ = 10.2, 2H, H-3), 1.63 (d, $^3J_{PH}$ = 17.4, 36H, H-2). **$^{31}$P{$^1$H} NMR** (162 MHz, $CD_2Cl_2$, 298 K): δ -13.5 (s). **$^{13}$C{$^1$H} NMR** (100 MHz, $CD_2Cl_2$, 298 K): δ 121.5 (q, $^1J_{CF}$ = 321.1, *C*$F_3SO_3^-$), 41.0 (m, C-1), 31.4 (m, C-2), 27.3 (m, C-3). **$^{19}$F{$^1$H} NMR** (376 MHz, $CD_2Cl_2$, 298 K): δ -78.8 (s). **Elemental analysis** (%) for $C_{19}H_{38}F_6O_6P_2PdS_2$: calculated: C 32.19, H 5.40; found: C 32.59, H 5.78. **ESI-MS** (m/z) for $C_{19}H_{38}F_6O_6P_2PdS_2$: $[M - OTf]^+$ calculated: 559.1, found: 559.2; $[M + OTf]^-$ calculated: 857.0, found: 856.8.

**Synthesis of [(dtbpe)Pd(OTf)$_2$]**

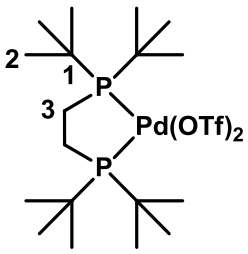


Following the general synthesis procedure II, [(dtbpe)Pd(OTf)$_2$] was obtained as an off-white powder in 70 % overall yield. Crystals suitable for X-Ray diffraction were grown from an acetone solution layered with $Et_2O$. **$^1$H NMR** (400 MHz, $CD_2Cl_2$, 298 K): δ 2.42 (m, 4H, H-3), 1.54 (d, $^3J_{PH}$ = 15.1, 36H, H-2). **$^{31}$P{$^1$H} NMR** (162 MHz, $CD_2Cl_2$, 298 K): δ 126.1 (s). **$^{13}$C{$^1$H} NMR** (100 MHz, $CD_2Cl_2$, 298 K): δ 121.5 (q, $^1J_{CF}$ = 320.9, *C*$F_3SO_3^-$), 41.3 (t, C-1), 30.7 (s, C-2), 25. 7 (m, C-3). **$^{19}$F{$^1$H} NMR** (376 MHz, $CD_2Cl_2$, 298 K): δ -78.7 (s). **ESI-MS** (m/z) for

$C_{20}H_{40}F_6O_6P_2PdS_2$: $[M - OTf]^+$ calculated: 573.1, found: 573.3; $[M + OTf]^-$ calculated: 871.0, found: 870.8.

**Synthesis of [(dtbpb)Pd(OTf)$_2$]**

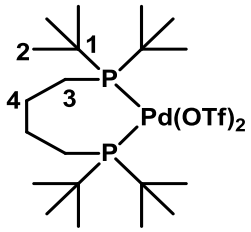


Following the general synthesis procedure I, [(dtbpb)Pd(OTf)$_2$] was obtained as an orange powder in 81 % yield. Crystals suitable for X-Ray diffraction were grown from a $CH_2Cl_2$ solution layered with $Et_2O$. **$^1$H NMR** (400 MHz, $CD_2Cl_2$, 298 K): δ 2.41 (m, 4H, H-3), 2.10 (m, 4H, H-4), 1.57 (d, $^3J_{PH}$ = 15.4, 36H, H-2). **$^{31}$P{$^1$H} NMR** (162 MHz, $CD_2Cl_2$, 298 K): δ 94.8 (s). **$^{13}$C{$^1$H} NMR** (100 MHz, $CD_2Cl_2$, 298 K): δ 120.6 (q, $^1J_{CF}$ = 319.6, *C*$F_3SO_3^-$), 42.6 (m, C-1), 31.3 (s, C-2), 20.8 (s, C-4), 18.2 (m, C-3). **$^{19}$F{$^1$H} NMR** (376 MHz, $CD_2Cl_2$, 298 K): δ -77.5 (s). **ESI-MS** (m/z) for $C_{22}H_{44}F_6O_6P_2PdS_2$: $[M - OTf]^+$ calculated: 601.2, found: 601.3; $[M + OTf]^-$ calculated: 899.1, found: 898.9.

**Synthesis of [(dippp)Pd(OTf)$_2$]**

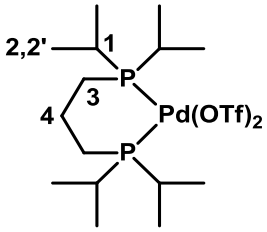


Following the general synthesis procedure I, [(dippp)Pd(OTf)$_2$] was obtained as an orange powder in 70 % yield. Crystals suitable for X-Ray diffraction were grown from a $CH_2Cl_2$ solution layered with $Et_2O$. **$^1$H NMR** (400 MHz, $CD_2Cl_2$, 298 K): δ 2.79 (m br., 4H, H-1), 2.13 (m br., 2H, H-4), 1.68 (m br., 4H, H-3), 1.50 (dd, $^3J_{PH}$ = 19.1, $^3J_{HH}$ = 7.2, 12H, H-2), 1.33 (dd, $^3J_{PH}$ = 16.3, $^3J_{HH}$ = 7.0, 12H, H-2'). **$^{31}$P{$^1$H} NMR** (162 MHz, $CD_2Cl_2$, 298 K): δ 55.1 (s). **$^{13}$C{$^1$H} NMR** (100 MHz, $CD_2Cl_2$, 298 K): δ 120.2 (q, $^1J_{CF}$ = 319.3, *C*$F_3SO_3^-$), 28.4 (d, $^2J_{CP}$ =

28.6, C-1), 21.7 (s br., C-4), 21.3 (s, C-2), 19.0 (d, $^2J_{CP}$ = 3.6, C-2'), 14.6 (dd, $J_{CP}$ = 30.6, 7.2, C-3). **$^{19}$F{$^1$H} NMR** (376 MHz, $CD_2Cl_2$, 298 K): δ -77.5 (s). **Elemental Analysis** (%) for $C_{17}H_{34}F_6O_6P_2S_2Pd \cdot C_4H_{10}O$: calculated: C 33.40, H 5.87; found: C 33.48, H 5.65.

**Synthesis of [(depp)Pd(OTf)$_2$]**

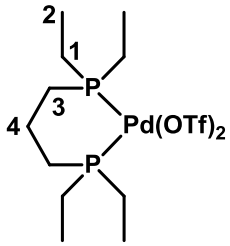


Following the general synthesis procedure I, crude [(depp)Pd(OTf)$_2$] was obtained, which was purified by dissolving in $CH_2Cl_2$ and precipitation by addition of $Et_2O$ yielding the desired product as a yellowish powder in 60 % yield. Crystals suitable for X-Ray diffraction were grown from a $CH_2Cl_2$ solution layered with $Et_2O$. **$^1$H NMR** (400 MHz, $CD_2Cl_2$, 298 K): δ 2.36 (m br., 4H, H-1), 2.10 (m br., 6H, H-4 and H-1), 1.78 (m br., 4H, H-3), 1.34 (dt, $^3J_{PH}$ = 19.6, $^3J_{HH}$ = 7.6, 12H, H-2). **$^{31}$P{$^1$H} NMR** (162 MHz, $CD_2Cl_2$, 298 K): δ 35.2 (s). **$^{13}$C{$^1$H} NMR** (100 MHz, $CD_2Cl_2$, 298 K): δ 120.4 (q, $^1J_{CF}$ = 318.9, *C*$F_3SO_3^-$), 19.6 - 18.6 (m, C-3, C-4 and C-1), 9.0 (s br., C-2). **$^{19}$F{$^1$H} NMR** (376 MHz, $CD_2Cl_2$, 298 K): δ -77.4 (s). **Elemental Analysis** (%) for $C_{13}H_{26}F_6O_6P_2S_2Pd$: calculated: C 24.99, H 4.19; found: C 24.13, H 4.47.

**General synthesis of [(P^P)Pd(Me)Cl][19]**

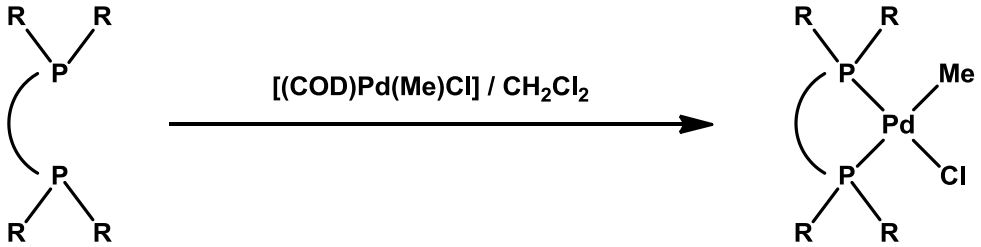


1 Equiv. diphosphine, dissolved in $CH_2Cl_2$ (c ~ 0.2 mol $L^{-1}$) was added drop wise to a solution of [(COD)Pd(Me)Cl] in $CH_2Cl_2$ (c ~ 0.2 mol $L^{-1}$) and stirred for 30 minutes at room temperature. The solvent was removed, and the resulting solid was washed with $Et_2O$ and pentane. For further purification, the complex was dissolved in a minimum amount of

methylene chloride, precipitated with pentane, filtered and washed with pentane yielding the desired [(P^P)Pd(Me)Cl] complex.

**Synthesis of [(dtbpm)Pd(Me)Cl]**

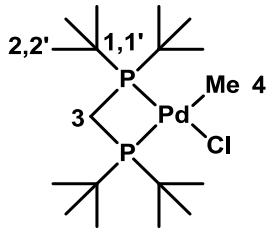


Following the general procedure, [(dtbpm)Pd(Me)Cl] was obtained as a white solid in 92 % yield. **$^{1}$H NMR** (400 MHz, $CD_2Cl_2$, 298 K): δ 3.03 (dd, $^{2}J_{PH}$ = 9.0, 5.3, 2H, H-3), 1.45 (vt, $^{3}J_{PH}$ = 13.6, 36H, H-2, H-2'), 0.54 (dd, $^{3}J_{PH}$ = 8.8, 1.4, 3H, H-4). **$^{31}$P{$^{1}$H} NMR** (162 MHz, $CD_2Cl_2$, 298 K): δ 24.5 (d, $^{2}J_{PP}$ = 29.5), -3.3 (d, $^{2}J_{PP}$ = 29.5). **$^{13}$C{$^{1}$H} NMR** (100 MHz, $CD_2Cl_2$, 298 K): δ 37.7 (dd, $J_{PC}$ = 11.4, 3.5, C-1), 35.8 (dd, $J_{PC}$ = 5.8, 3.0, C-1'), 31.4 (d, $J_{PC}$ = 4.4, C-2), 31.2 (d, $J_{PC}$ = 6.4 , C-2'), 27.9 (dd, $J_{PC}$ = 15.3, 4.4, C-3), -0.6 (dd, $^{2}J_{PC\,trans}$ = 115.2, $^{2}J_{PC\,cis}$ = 4.6, C-4). **Elemental Analysis** (%) for $C_{18}H_{41}ClP_2Pd$: calculated: C 46.86, H 8.96; found: C 46.49, H 9.30.

**Synthesis of [(dtbpe)Pd(Me)Cl]**

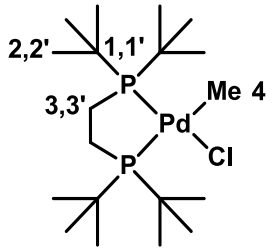


Following the general procedure, [(dtbpe)Pd(Me)Cl] was obtained as a beige solid in 86 % yield. **$^{1}$H NMR** (400 MHz, $CD_2Cl_2$, 298 K): δ 2.03 (m, 2H, H-3), 1.67 (m, 2H, H-3'), 1.37(d, $^{3}J_{PH}$ = 12.3, 18H, H-2'), 1.35 (d, $^{3}J_{PH}$ = 13.4, 18H, H-2'), 0.78 (dd, $^{3}J_{PH}$ = 7.6, 2.0, 3H, H-4). **$^{31}$P{$^{1}$H} NMR** (162 MHz, $CD_2Cl_2$, 298 K): δ 87.8 (d, $^{2}J_{PP}$ = 14.9), 75.2 (d, $^{2}J_{PP}$ = 14.9). **$^{13}$C{$^{1}$H} NMR** (100 MHz, $CD_2Cl_2$, 298 K): δ 38.1 (d, $J_{PC}$ = 19.1 , C-1), 36.0 (d, $J_{PC}$ = 6.5, C-1'), 30.8

(d, $^2J_{PC}$ = 3.8, C-2), 30.6 (d, $^2J_{PC}$ = 5.0, C-2'), 27.6 (dd, $J_{PC}$ = 23.3, 20.8, C-3), 20.5 (dd, $J_{PC}$ = 13.2, 8.6, C-3'), 3.2 (dd, $^2J_{PC\,trans}$ = 103.7, $^2J_{PC\,cis}$ = 3.4, C-4).

**Synthesis of [(dtbpp)Pd(Me)Cl]**

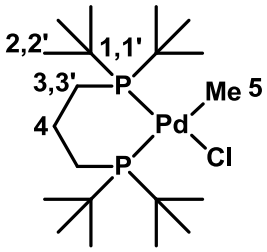


Following the general procedure, [(dtbpp)Pd(Me)Cl] was obtained as a white solid in 82 % yield. **$^1$H NMR** (400 MHz, $CD_2Cl_2$, 298 K): δ 1.95 (m br., 2H, H-4), 1.83 (m br., 2H, H-3), 1.65 (m br., 2H, H-3'), 1.38 (d, $^3J_{PH}$ = 12.4, 18H, H-2), 1.37 (d, $^3J_{PH}$ = 13.2, 18H, H-2'), 0.92 (dd, $^3J_{PH}$ = 7.0, 2.2, 3H, H-5). **$^{31}$P{$^1$H} NMR** (162 MHz, $CD_2Cl_2$, 298 K): δ 48.8 (d, $^2J_{PP}$ = 33.3), 19.5 (d, $^2J_{PP}$ = 33.3). **$^{13}$C{$^1$H} NMR** (100 MHz, $CD_2Cl_2$, 298 K): δ 38.4 (d, $J_{PC}$ = 19.1 , C-1), 36.2 (d, $J_{PC}$ = 7.1, C-1'), 31.8 (d, $J_{PC}$ = 3.6, C-2), 30.8 (d, $J_{PC}$ = 5.3, C-2'), 23.0 (dd, $J_{PC}$ = 8.0, 1.8) and 22.8 (dd, $J_{PC}$ = 18.3, 10.9, C-3 and C-4), 22.0 (dd, $J_{PC}$ = 8.2, 1.2, C-3'), 5.3 (dd, $^2J_{PC\,trans}$ = 93.9, $^2J_{PC\,cis}$ = 3.6, C-5). **Elemental Analysis** (%) for $C_{20}H_{45}ClP_2Pd$: calculated: C 49.08, H 9.27; found: C 48.99, H 9.58.

**Synthesis of [(dtbpx)Pd(η$^3$-C$_4$H$_7$)]$^+$(OTf)$^-$[20]**

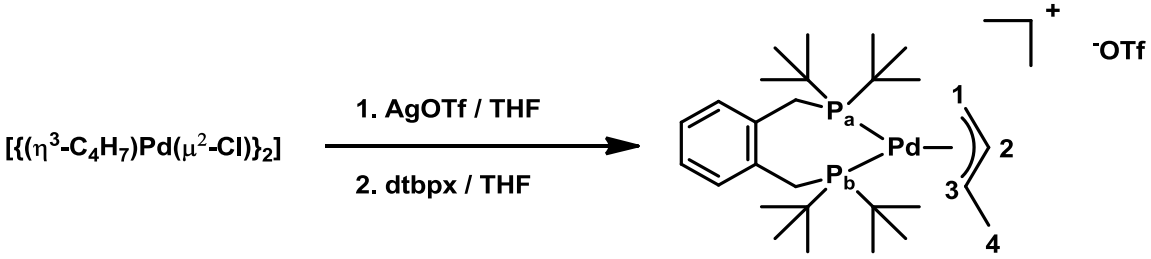


According to ref. 20, 100 mg [{(η$^3$-C$_4$H$_7$)Pd(μ$^2$-Cl)}$_2$] (0.26 mmol, 0.5 equiv.) were dissolved in 2 mL THF. 130 mg AgOTf (0.52 mmol, 1.0 equiv.) dissolved in 3 mL THF were added drop wise. A white precipitate forms immediately. The reaction mixture was stirred at room temperature under exclusion of light for 30 minutes and then filtered. 200 mg dtbpx (0.52 mmol,

1.0 equiv.) dissolved in 3 mL THF were added drop wise and the reaction mixture was stirred for 2 hours. After removing the solvent in vacuum, the crude product was washed with pentane (3 x 3 mL) to give 297 mg of the pure product (94 %, 0.49 mmol). **$^{1}$H NMR** (400 MHz, $CD_2Cl_2$, 298 K): δ 7.44 (m, 2H, aromatic CH), 7.25 (m, 2H, aromatic CH), 6.52 (m, 1H, H-3), 5.15 (ddd, *J* = 13.2, 7.5, 6.6, 1H, H-2), 4.59 (vt, *J* = 7.5, 1H, H-1), 3.84 - 3.54 (m, 4H, benzylic $CH_2$), 3.34 (dd, *J* = 13.2, 9.7, 1H, H-1), 1.69 - 1.02 (m, 39H, $^{t}$Bu-H and H-4). **$^{31}$P{$^{1}$H} NMR** (162 MHz, $CD_2Cl_2$, 298 K): δ 50.3 (d, $^{2}J_{PP}$ = 39.9, $P_a$), 44.4 - 41.8 (s br., $P_b$). **$^{13}$C{$^{1}$H} NMR** (100 MHz, $CD_2Cl_2$, 298 K): *δ* 135.4 (s, aromatic C), 133.9 (s, aromatic CH), 128.2 (s, aromatic CH), 112.1 (s br., C-2), 94.5 (d, $J_{CP}$ = 23.8, C-3), 59.0 (d, $J_{CP}$ = 32.4, C-1), 39.6 - 38.1 (m, $^{t}$Bu-*C*$(CH_3)_3$), 31.5 - 30.2 (m, $^{t}$Bu-C(*C*$H_3)_3$), 29.6 - 28.5 (m, benzylic $CH_2$), 16.9 (d, $J_{CP}$ = 4.6, C-4), note that *C*$F_3SO_3^-$ was not detected. **$^{1}$H NMR** (400 MHz, MeOD, 298 K): δ 7.53 (m, 2H, aromatic CH), 7.23 (m, 2H, aromatic CH), 6.62 (m, 1H, H-3), 5.29 (m, 1H, H-2), 4.64 (vt, *J* = 7.3, 1H, H-1), 3.97 - 3.69 (m, 4H, benzylic $CH_2$), 3.45 (dd, $J_{PH}$ = 13.2, 10.4, 1H, H-1), 1.64 - 1.12 (m, 39H, $^{t}$Bu-H and H-4). **Elemental Analysis** (%) for $C_{19}H_{51}F_3O_3P_2PdS$: calculated: C 49.40, H 7.29; found: C 49.68, H 7.34.

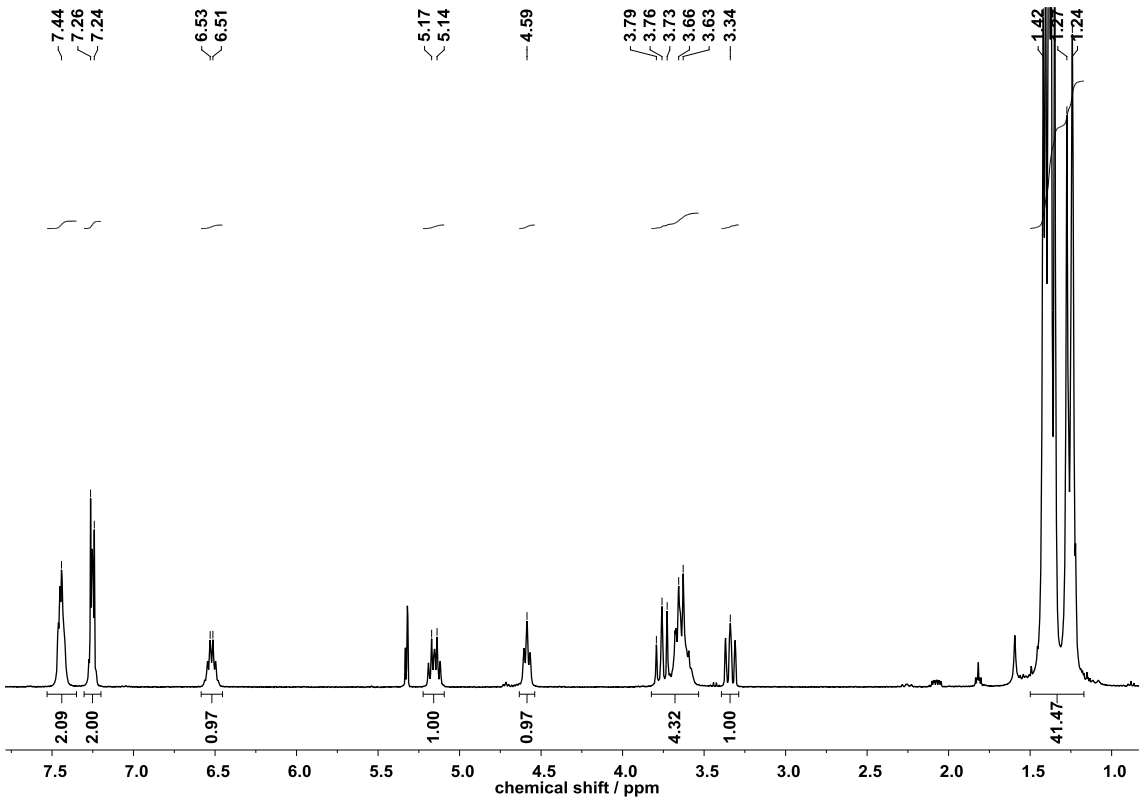


Figure S1: $^{1}$H NMR spectrum of $[(dtbpx)Pd(\eta^3\text{-}C_4H_7)]^+(OTf)^-$ in $CD_2Cl_2$ at 25 °C.

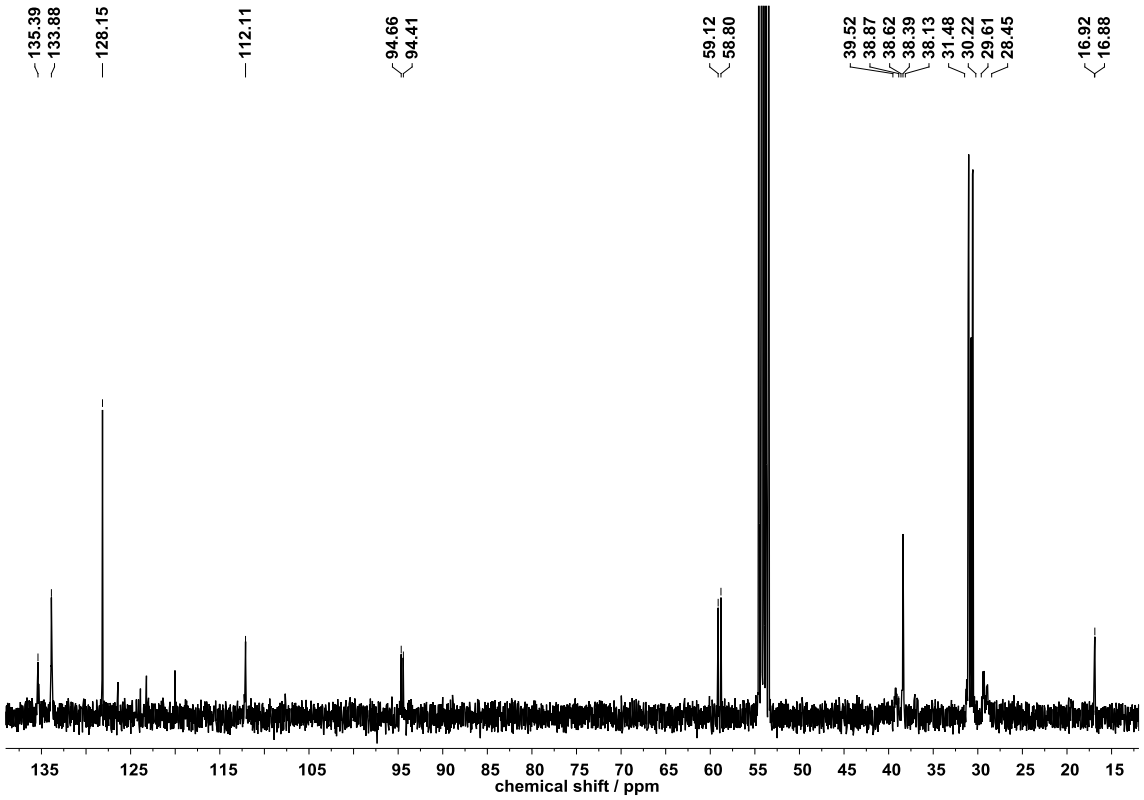


Figure S2: $^{13}C\{^{1}H\}$ NMR spectrum of $[(dtbpx)Pd(\eta^3\text{-}C_4H_7)]^+(OTf)^-$ in $CD_2Cl_2$ at 25 °C.

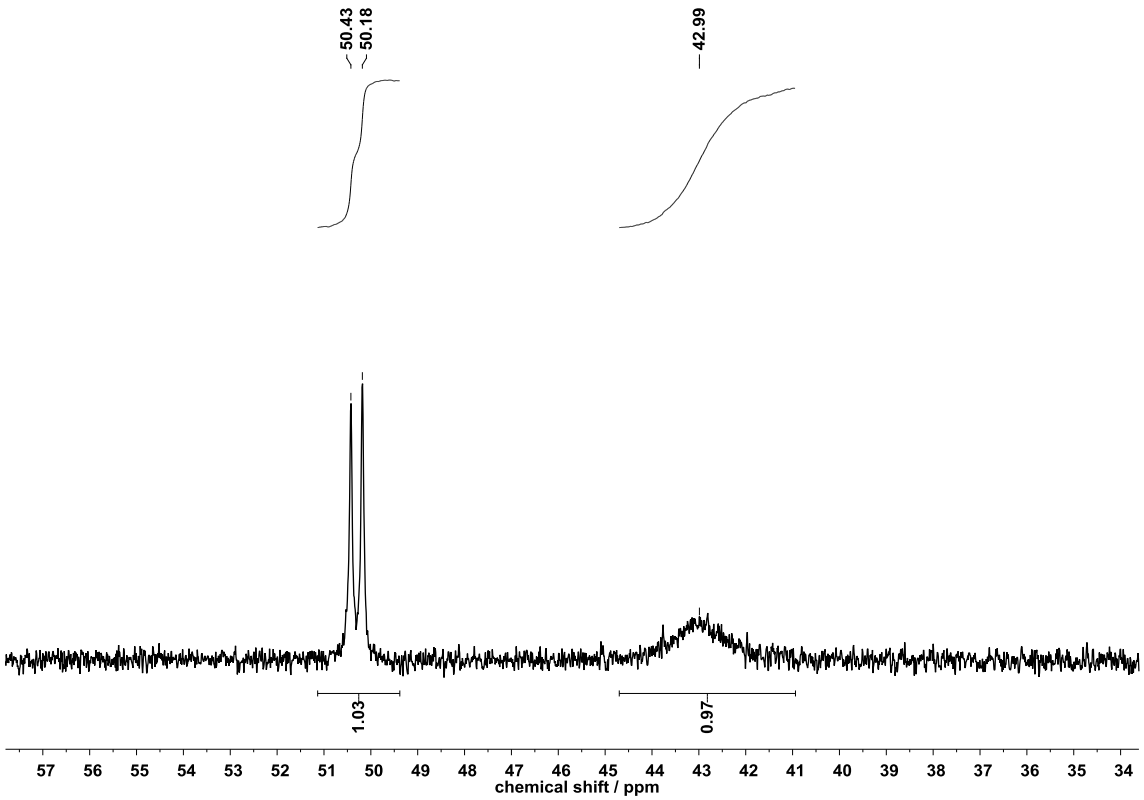


Figure S3: $^{31}P\{^{1}H\}$ NMR spectrum of $[(dtbpx)Pd(\eta^3\text{-}C_4H_7)]^+(OTf)^-$ in $CD_2Cl_2$ at 25 °C.

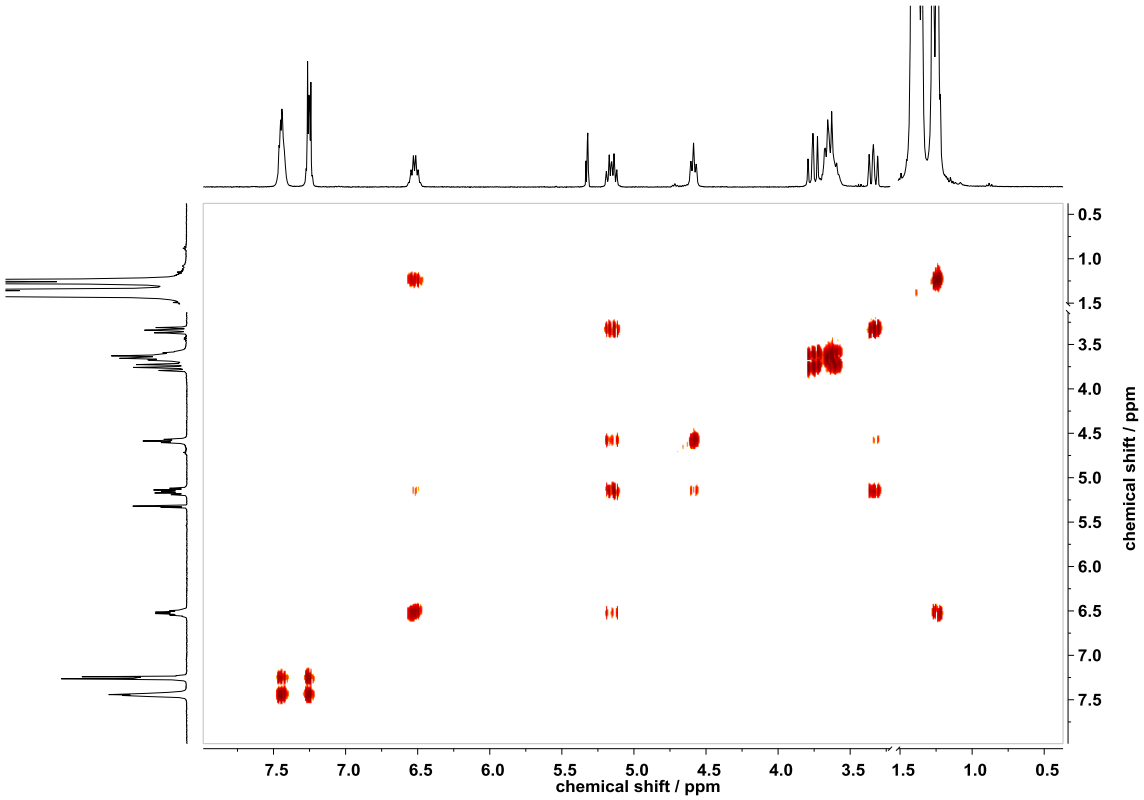


Figure S4: $^{1}H,^{1}H$-COSY NMR spectrum of $[(dtbpx)Pd(\eta^{3}\text{-}C_4H_7)]^{+}(OTf)^{-}$ in $CD_2Cl_2$ at 25 °C.

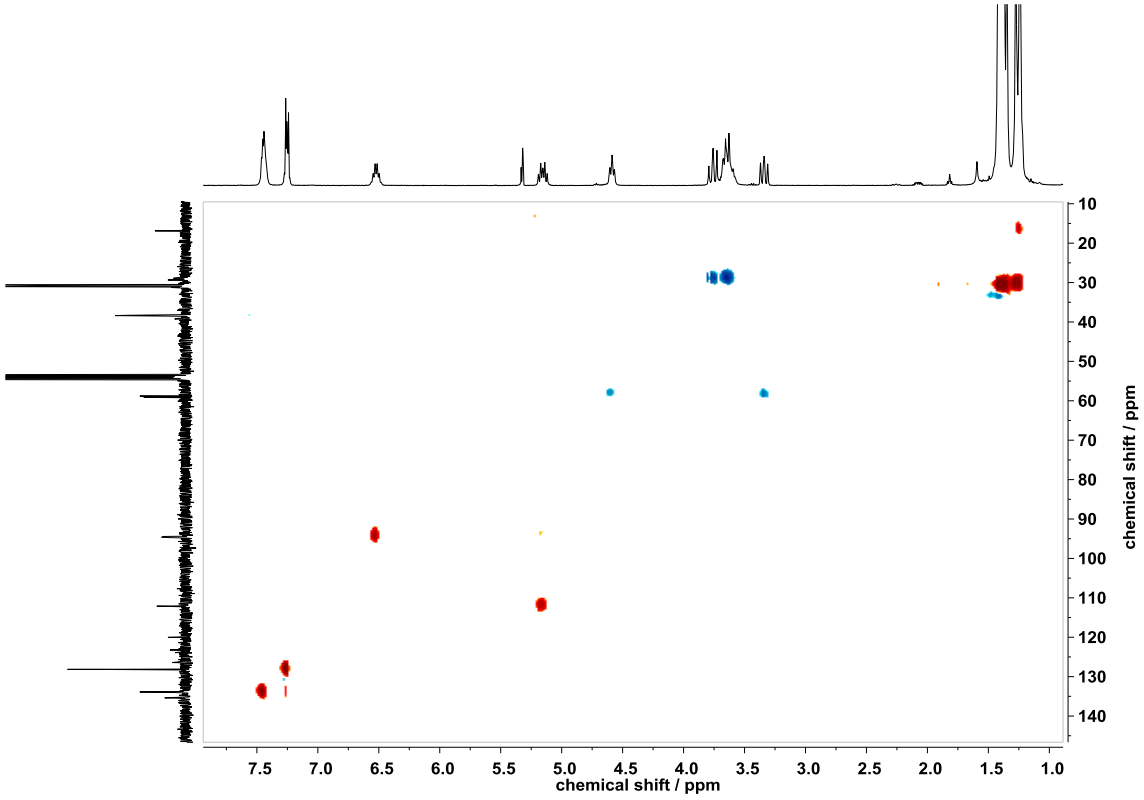


Figure S5: $^{1}H,^{13}C$-HSQC NMR spectrum of $[(dtbpx)Pd(\eta^{3}\text{-}C_4H_7)]^{+}(OTf)^{-}$ in $CD_2Cl_2$ at 25 °C.

**General procedure for NMR tube experiments:**

NMR tubes were charged with solid reagents and the appropriate solvent or solvent mixture in a glove box. All tubes were sealed with rubber septa. Liquid reactants were added with µL Hamilton syringes and tubes were thoroughly shaken after each addition. Carbon monoxide was added at low temperatures, since solubility of carbon monoxide is increased at lower temperatures. Using a three-way stopcock, a compressed gas cylinder equipped with a pressure relief valve was connected to a vacuum line and a small Schlenk flask sealed with a rubber septum. The system was evacuated, and back filled with 1 atmosphere (ambient pressure) of $^{13/12}$CO. Gas was transferred into the NMR tubes with 1 mL syringes and tubes were briefly shaken after addition. For calculating the appropriate volume, ideal gas conditions were assumed. For NMR experiments in which pressures of up to 6 bar CO were applied, a 5 mm Medium Wall Precision Pressure/Vacuum Valve NMR Sample Tube from Wilmad-LabGlass was used. By a custom made three-way pipeline system the tube was connected to the vacuum line and to the compressed gas cylinder equipped with a pressure relief valve. The NMR tube was evacuated at low temperature (-78 °C) prior to pressurization with CO.

**In-situ generation of [(dtbpe)Pd(*µ*-H/D)(*µ*-$^{(13/12)}$CO)Pd(dtbpe)]$^+$(OTf)$^-$**

10 mg [(dtbpe)Pd(OTf)$_2$] were dissolved in a mixture of 0.5 mL MeOH and 0.1 mL $C_6D_6$ or in 0.6 mL methanol-*d*$_4$ in a NMR tube. Ca. 6 equiv. $^{13}$CO were added. After heating to 90 °C for 3 h formation of [(dtbpe)Pd(*µ*-H)(*µ*-$^{13}$CO)Pd(dtbpe)]$^+$OTf$^-$ or [(dtbpe)Pd(*µ*-D)(*µ*-$^{13}$CO)Pd(dtbpe)]$^+$OTf$^-$ was observed. Using $^{12}$CO instead of $^{13}$CO under otherwise identical conditions results in formation of [(dtbpe)Pd(*µ*-H)(*µ*-CO)Pd(dtbpe)]$^+$OTf$^-$ and [(dtbpe)Pd(*µ*-D)(*µ*-CO)Pd(dtbpe)]$^+$OTf$^-$ respectively. $^1$H NMR resonances are identical to the respective $^{13}$CO labeled species, in $^{31}$P NMR spectroscopy no $J_{PC}$ couplings are observed.

[(dtbpe)Pd(*µ*-H)(*µ*-$^{13}$CO)Pd(dtbpe)]$^+$(OTf)$^-$: **$^1$H NMR** (400 MHz, $CH_3OH$ / $C_6D_6$ (0.5 mL / 0.1 mL)), referenced to residual $C_6D_5H$, 298 K): δ 1.84 (dd, $J_{PH}$ = 6.3, 1.9 Hz, 8H, C*H*$_2$), 1.10 (m br., 72H, $^t$Bu-H), - 5.70 (quint., $^2J_{PH}$ = 43.1 Hz, 1H, *µ*-H). **$^{31}$P{$^1$H} NMR** (162 MHz, $CH_3OH$ / $C_6D_6$ (0.5 mL / 0.1 mL), 298 K): δ 75.77 (d, $^2J_{PC}$ = 32.5 Hz). **$^{13}$C{$^1$H} NMR** (100 MHz, $CH_3OH$ / $C_6D_6$ (0.5 mL / 0.1 mL), referenced to $C_6D_6$, 298 K): δ 247.64 (quint, $^2J_{PC}$ = 32.5 Hz, *µ*-$^{13}$CO), 184.64 (s br., non-coordinated $^{13}$CO), 35.56 (s br., $^t$Bu-*C*(CH$_3$)$_3$), 30.19 (s br., $^t$Bu-C(*C*H$_3$)$_3$), 23.49 (s br., *C*H$_2$).

[(dtbpe)Pd(*µ*-D)(*µ*-$^{13}$CO)Pd(dtbpe)]$^+$(OTf)$^-$: **$^1$H NMR** (400 MHz, $CD_3OD$, 298 K) δ 2.18 (dd, $J_{PH}$ = 6.4, 2.0 Hz, 8H, C*H*$_2$), 1.34 (m br., 72H, $^t$Bu-H). **$^{31}$P{$^1$H} NMR** (162 MHz, $CD_3OD$, 298 K): δ 75.08 (dt, $^2J_{PC}$ = 32.7 Hz, $^2J_{PD}$ = 6.5 Hz). **$^{13}$C{$^1$H} NMR** (100 MHz, $CD_3OD$, 298 K): δ

248.33 (quint., $^{2}J_{PC}$ = 32.7 Hz, $\mu$-$^{13}$CO), 185.43 (s br., non coordinated $^{13}$CO), 36.44 (s br., $^{t}$Bu-*C*(CH$_3$)$_3$), 30.93 (s br., $^{t}$Bu-C(*C*H$_3$)$_3$), 24.35 (s br., *C*H$_2$).

[(dtbpe)Pd($\mu$-H)($\mu$-CO)Pd(dtbpe)]$^{+}$(OTf)$^{-}$: **$^{1}$H NMR** (400 MHz, CH$_3$OH / C$_6$D$_6$ (0.5 mL / 0.1 mL)), referenced to residual C$_6$D$_5$H, 298 K): δ 1.84 (dd, $J_{PH}$ = 6.3, 1.9 Hz, 8H, C*H*$_2$), 1.10 (m br., 72H, $^{t}$Bu-H), - 5.70 (quint., $^{2}J_{PH}$ = 43.1 Hz, 1H, $\mu$-H). **$^{31}$P{$^{1}$H} NMR** (162 MHz, CH$_3$OH / C$_6$D$_6$ (0.5 mL / 0.1 mL), 298 K): δ 75.77 (s).

[(dtbpe)Pd($\mu$-D)($\mu$-CO)Pd(dtbpe)]$^{+}$(OTf)$^{-}$: **$^{1}$H NMR** (400 MHz, CD$_3$OD, 298 K) δ 2.18 (dd, $J_{PH}$ = 6.4, 2.0 Hz, 8H, C*H*$_2$), 1.34 (m br., 72H, $^{t}$Bu-H). **$^{31}$P{$^{1}$H} NMR** (162 MHz, CD$_3$OD, 298 K): δ 75.08 (t, $^{2}J_{PD}$ = 6.5 Hz).

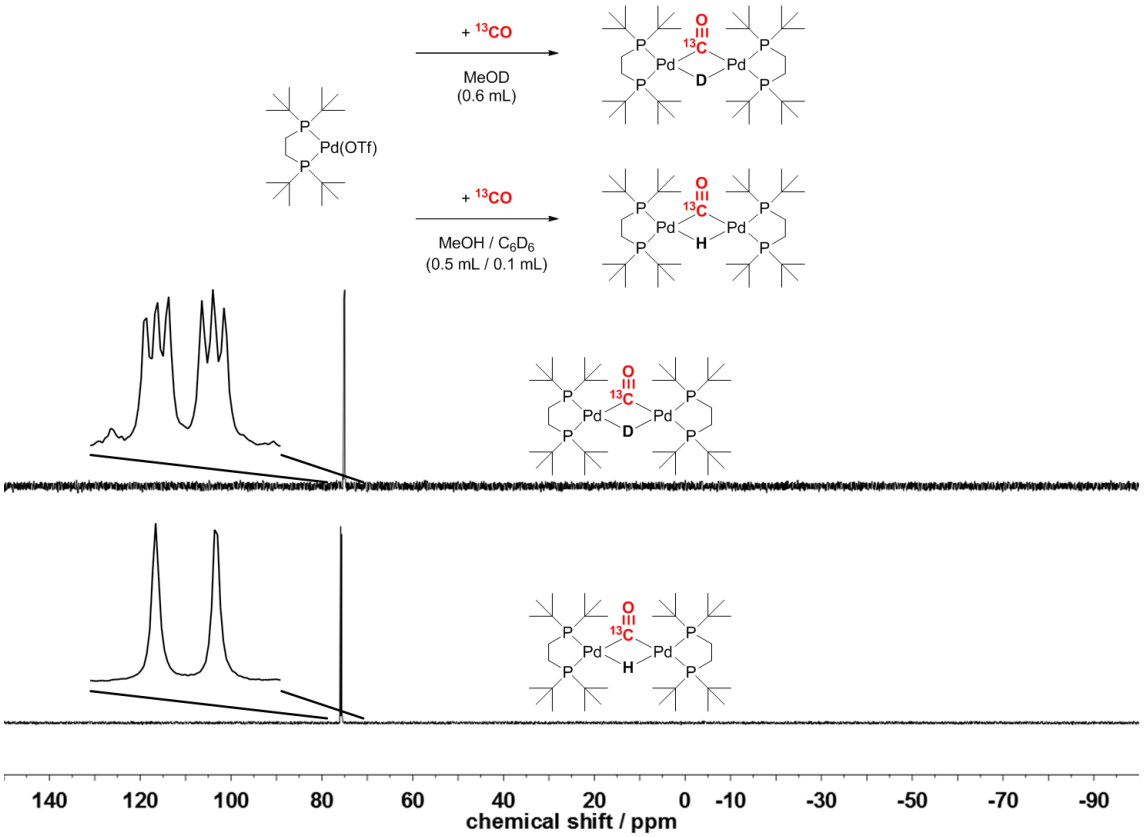


Figure S6: $^{31}$P{$^{1}$H} NMR spectra of [(dtbpe)Pd($\mu$-D)($\mu$-$^{13}$CO)Pd(dtbpe)]$^{+}$(OTf)$^{-}$ in methanol-*d*$_4$ (top) and [(dtbpe)Pd($\mu$-H)($\mu$-$^{13}$CO)Pd(dtbpe)]$^{+}$(OTf)$^{-}$ in MeOH / C$_6$D$_6$ (bottom) at 25 °C.

**General method for in-situ generation of [(P^P)Pd(COMe)Cl]**

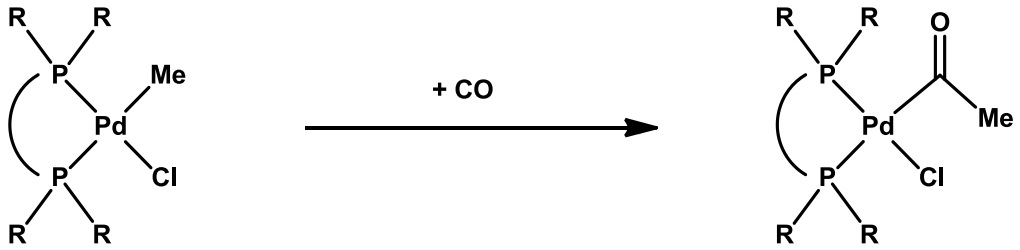


10 - 15 mg [(P^P)Pd(Me)Cl] were dissolved in 0.6 mL of the desired solvent in an NMR tube. 1 - 3 Equiv. $^{13}$CO were then added via syringe (the appropriate amount of CO was calculated assuming ideal gas conditions) and the NMR tube was thoroughly shaken. Formation of the desired [(P^P)Pd(COMe)Cl] species was proved by NMR spectroscopy. Note that formation of the cationic Pd(II) species $[(P\text{^}P)Pd(COMe)CO]^{+}(Cl)^{-}$ was not observed, even in when CO was used in excess (> 1 equiv.), and free CO was detected via $^{13}$C NMR spectroscopy.

**In-situ generation of [(dtbpm)Pd(COMe)Cl]**

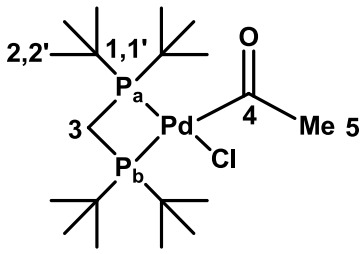


Following the general procedure, [(dtbpm)Pd(COMe)Cl] was generated in methylene chloride within 5 minutes. **$^{1}$H NMR** (400 MHz, $CD_2Cl_2$, 298 K): δ 2.81 (m br., 2H, H-3), 2.47 (d, $^{2}J_{CH}$ = 4.6, 3H, H-5), 1.46 and 1.43 (s br. each, 36H, H-2 and H-2'). **$^{31}$P{$^{1}$H} NMR** (162 MHz, $CD_2Cl_2$, 298 K): δ 30.0 (dd, $^{2}J_{PP}$ = 27.5, $^{2}J_{PC\textit{cis}}$ = 22.8, $P_a$), 7.4 (dd, $^{2}J_{PC\textit{trans}}$ = 131.4, $^{2}J_{PP}$ = 27.5, $P_b$). **$^{13}$C{$^{1}$H} NMR** (100 MHz, $CD_2Cl_2$, 298 K): δ 236.7 (dd, $^{2}J_{PC\textit{trans}}$ = 131.4, $^{2}J_{PC\textit{cis}}$ = 22.8, C-4), 40.4 (detected by HSQC, C-5), 37.1 and 35.6 (m each, C-1 and C-1'), 31.3 (d, $J_{PC}$ = 7.0, C-2), 31.0 (d, $J_{PC}$ = 4.6 Hz, C-2'), 25.3 (d, $J_{PC}$ = 15.4 Hz, C-3). When $^{13}$CO was used in excess, non-coordinated $^{13}$CO was observed at δ 185.4 (s).

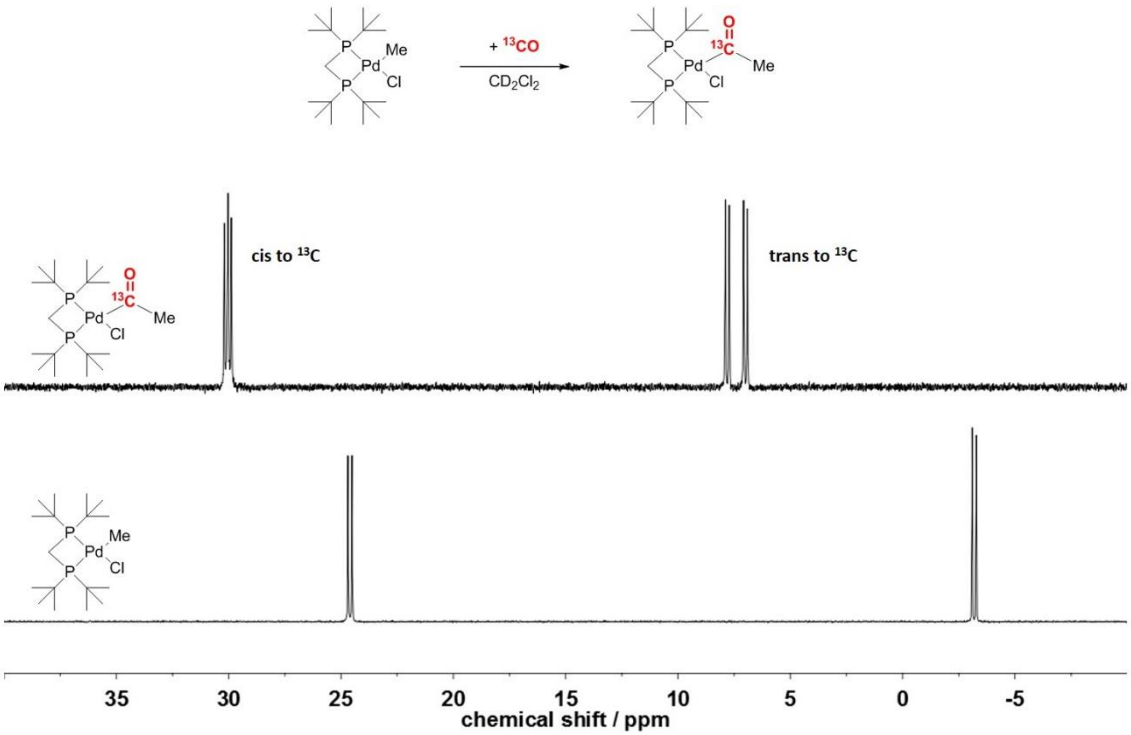


Figure S7: $^{31}P\{^{1}H\}$ NMR spectra of [(dtbpm)Pd($^{13}$COMe)Cl] (top) and [(dtbpm)Pd(Me)Cl] (bottom) in $CD_2Cl_2$ at 25 °C.

**In-situ generation of [(dtbpe)Pd(COMe)Cl]**

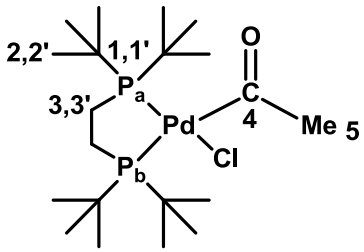


Following the general procedure, [(dtbpe)Pd(COMe)Cl] was generated in methylene chloride within 5 minutes. **$^{1}$H NMR** (400 MHz, $CD_2Cl_2$, 298 K): δ 2.56 (d, $^{2}J_{CH}$ = 5.3, 3H, H-5), 1.99 (m, 2H, H-3), 1.64 (m, 2H, H-3'), 1.38 (d, $^{3}J_{PH}$ = 12.4, 18H, H-2), 1.33 (d, $^{3}J_{PH}$ = 13.7, 18H, H-2'). **$^{31}$P{$^{1}$H} NMR** (162 MHz, $CD_2Cl_2$, 298 K): δ 74.4 (dd, $^{2}J_{PP}$ = 32.8, $^{2}J_{PC\,cis}$ = 12.1, $P_a$), 66.3 (dd, $^{2}J_{PC\,trans}$ = 125.6, $^{2}J_{PP}$ = 32.8, $P_b$). **$^{13}$C{$^{1}$H} NMR** (100 MHz, $CD_2Cl_2$, 298 K): δ 243.3 (dd, $^{2}J_{PC\,trans}$ = 125.6, $^{2}J_{PC\,cis}$ = 12.1, C-4), 40.8 (ddd, $J$ = 37.9, 21.3, 16.1, C-5), 37.0 (d, $J_{PC}$ = 16.4, C-1), 35.5 (dd, $J_{PC}$ = 4.0, 1.3, C-1'), 30.5 (2 x d, C-2, C-2'), 26.6 (vt, $J_{PC}$ = 22.7, C-3), 19.76 (dd, $J_{PC}$ = 11.6, 7.8, C-3'). When $^{13}$CO was used in excess, non-coordinated $^{13}$CO was observed at δ 184.8 (s).

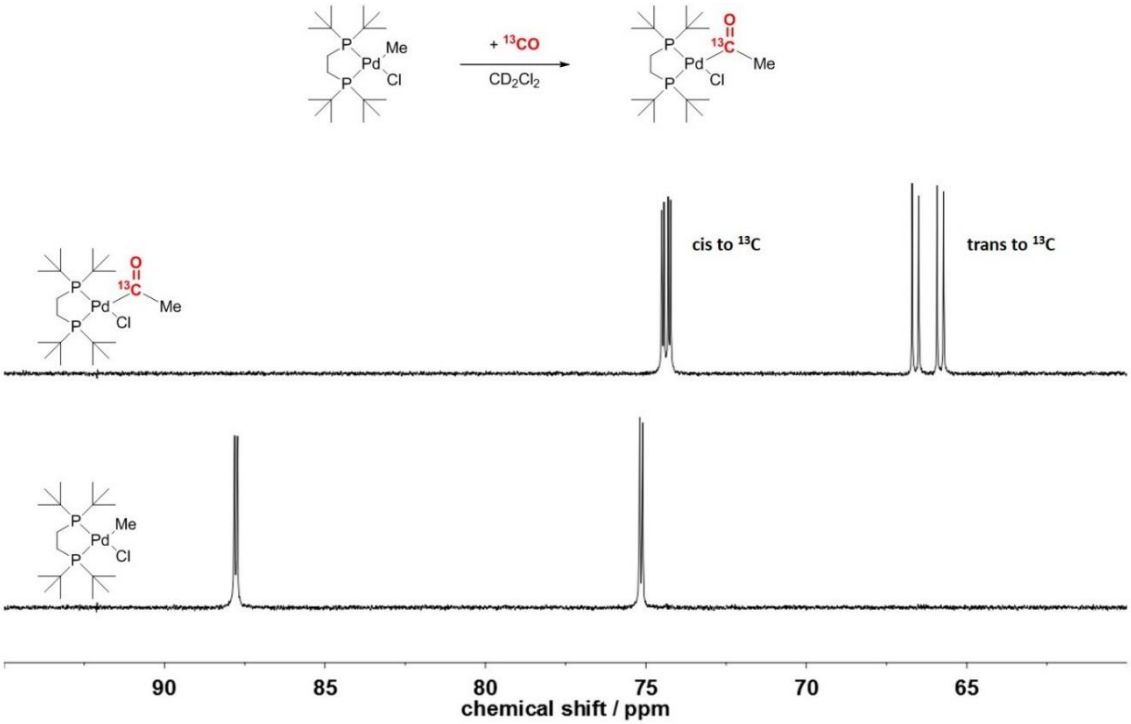


Figure S8: $^{31}P\{^{1}H\}$ NMR spectra of [(dtbpe)Pd($^{13}$COMe)Cl] (top) and [(dtbpe)Pd(Me)Cl] (bottom) in $CD_2Cl_2$ at 25 °C.

**In-situ generation of [(dtbpp)Pd(COMe)Cl]**

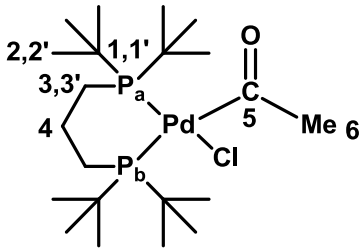


Following the general procedure, [(dtbpp)Pd(COMe)Cl] was generated in methylene chloride within 5 minutes. **$^{1}$H NMR** (400 MHz, $CD_2Cl_2$, 298 K): δ 2.66 (d, $^{2}J_{CH}$ = 5.4, 3H, H-6), 1.95 (m br., 2H, H-4), 1.76 (m br., 2H, H-3), 1.61 (m br., 2H, H-3'), 1.40 (d, $^{3}J_{PH}$ = 12.2, 18H, H-2), 1.35 (d, $^{3}J_{PH}$ = 13.4, 18H, H-2'). **$^{31}P\{^{1}H\}$ NMR** (162 MHz, $CD_2Cl_2$, 298 K): δ 39.6 (dd, $^{2}J_{PP}$ = 54.1, $^{2}J_{PCcis}$ = 13.8, $P_a$), 16.7 (dd, $^{2}J_{PCtrans}$ = 111.2, $^{2}J_{PP}$ = 54.1, $P_b$). **$^{13}C\{^{1}H\}$ NMR** (100 MHz, $CD_2Cl_2$, 298 K): δ 235.3 (dd, $^{2}J_{PCtrans}$ = 111.2, $^{2}J_{PCcis}$ = 13.8, C-5), 40.0 (detected by HSQC, C-6), 36.91 and 35.72 (m each, C-1 and C-1'), 30.9 and 30.7 (m each, C-2 and C-2'), 22.86 (m, C-4), 22.62 and 21.71 (m each, C-3 and C-3'). When $^{13}$CO was used in excess, non-coordinated $^{13}$CO was observed at δ 185.10 (s).

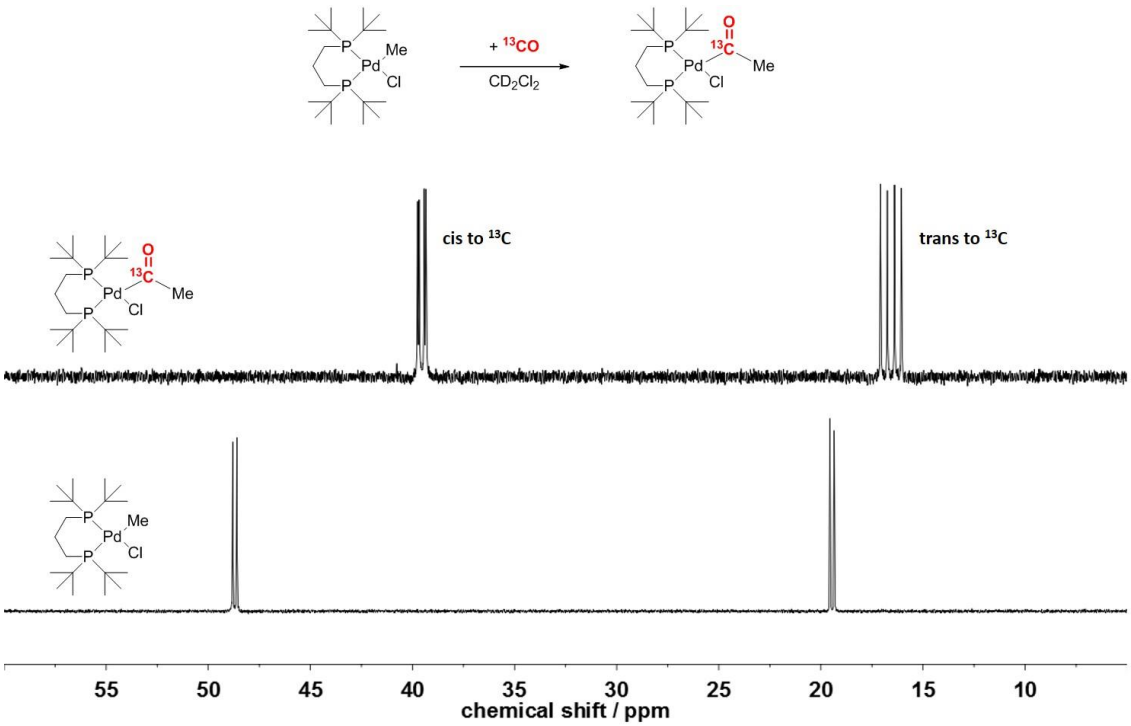


Figure S9: $^{31}P\{^{1}H\}$ NMR spectra of [(dtbpp)Pd($^{13}$COMe)Cl] (top) and [(dtbpp)Pd(Me)Cl] (bottom) in $CD_2Cl_2$ at 25 °C.

**Methanolysis of [(P^P)Pd(COMe)Cl]**

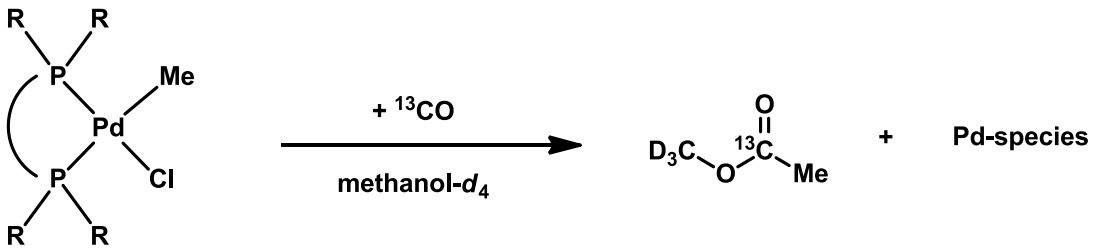


The desired acyl complexes [(P^P)Pd(COMe)Cl] were generated in-situ in methanol-$d_4$ as described above using 2 equiv. of $^{13}$CO. The NMR tube was shaken thoroughly and introduced into the NMR spectrometer. The methanolysis reaction was then followed by $^{1}$H NMR spectroscopy. Note that in case of [(dtbpp)Pd(COMe)Cl] the methanolysis reaction was already finished before recording the NMR spectrum.

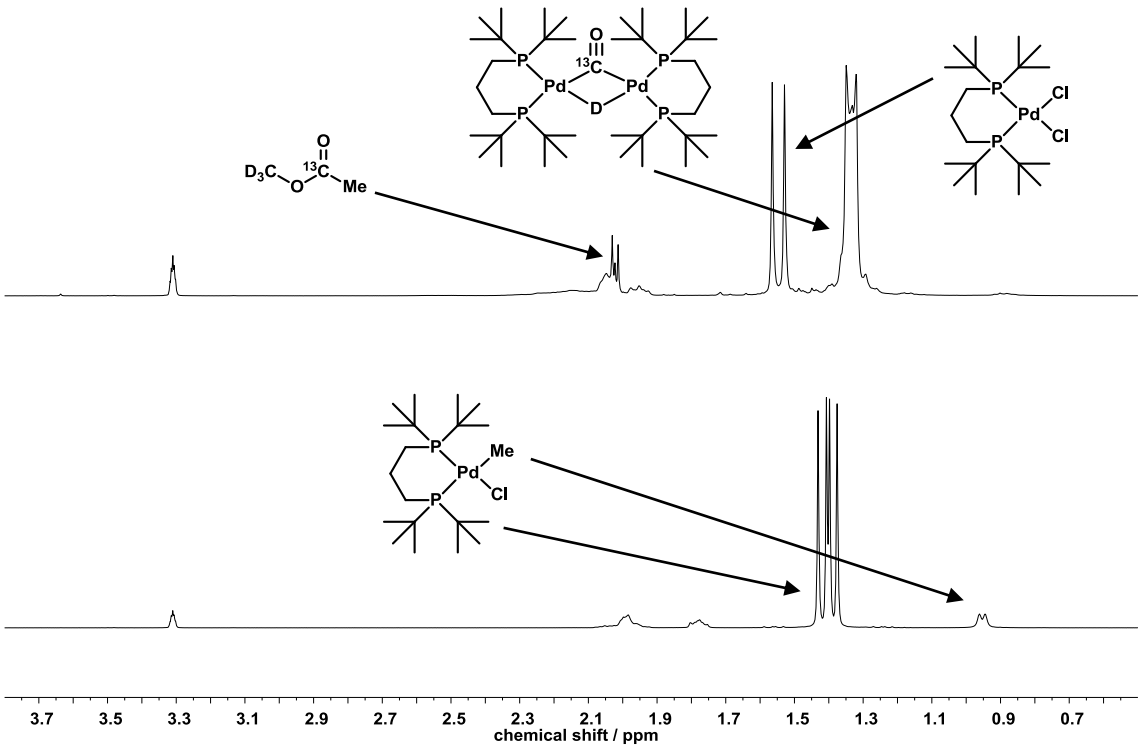


Figure S10: $^{1}$H NMR spectra of [(dtbpp)Pd(Me)Cl] in methanol-$d_4$ at 25 °C before (bottom) and directly after (top) addition of 2 equiv. $^{13}$CO (Me-groups are assigned).

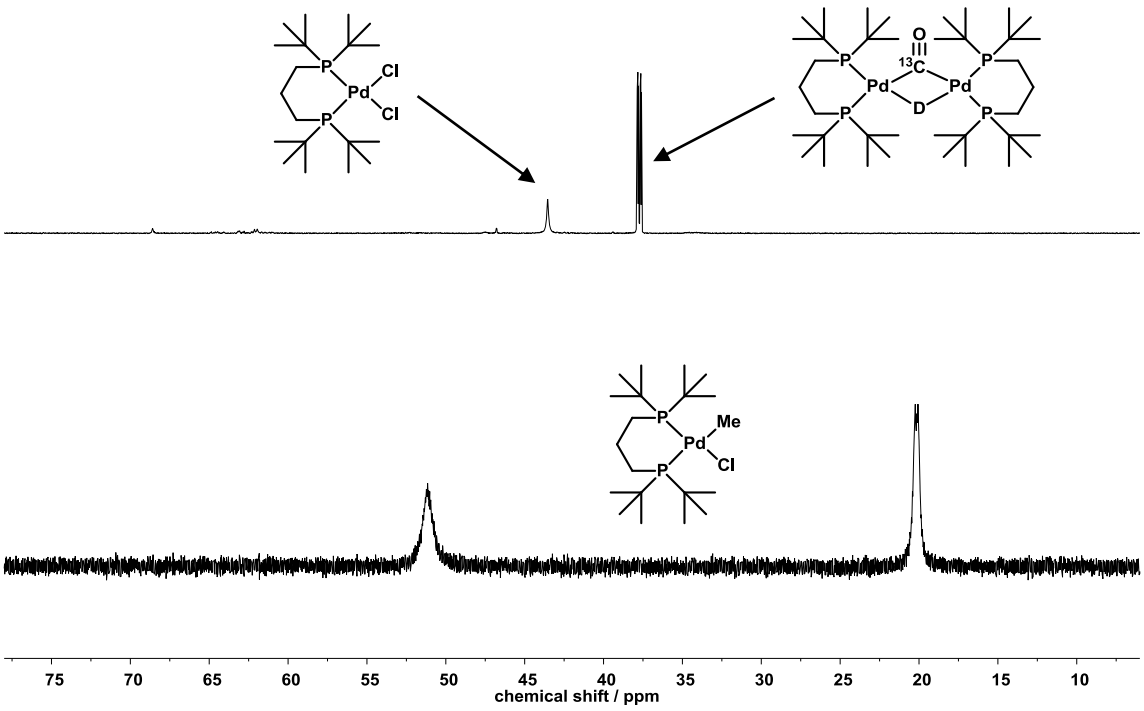


Figure S11: $^{31}$P{$^{1}$H} NMR spectra of [(dtbpp)Pd(Me)Cl] in methanol-$d_4$ at 25 °C before (bottom) and directly after (top) addition of 2 equiv. $^{13}$CO.

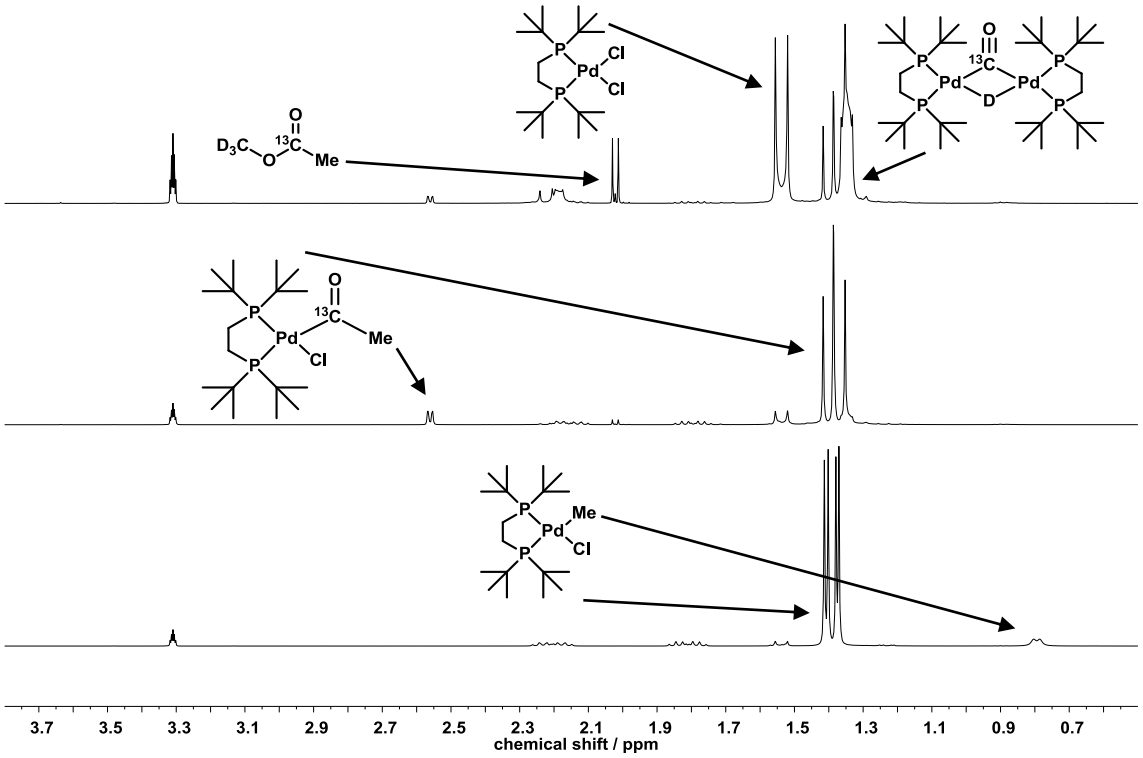


Figure S12: $^{1}$H NMR spectra of [(dtbpe)Pd(Me)Cl] in methanol-$d_4$ at 25 °C before (bottom), directly after (middle) and 30 hours after addition of 2 equiv. $^{13}$CO (Me-groups are assigned).

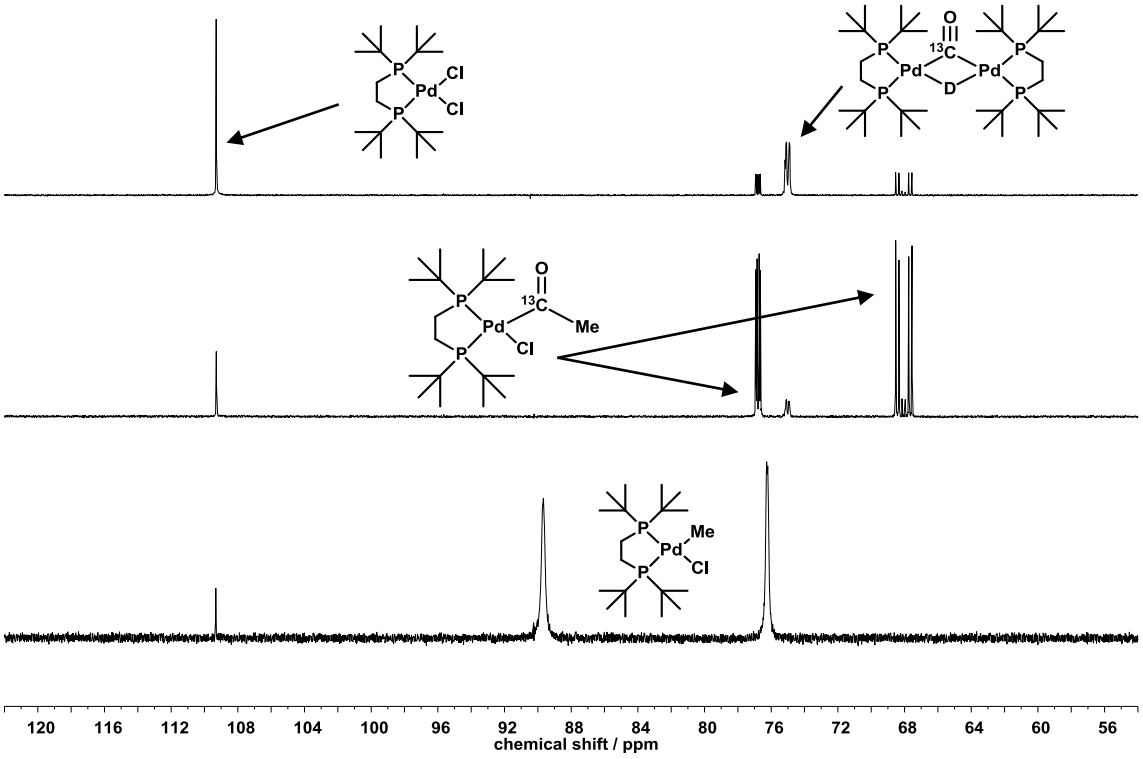


Figure S13: $^{31}$P{$^{1}$H} NMR spectra of [(dtbpe)Pd(Me)Cl] in methanol-$d_4$ at 25 °C before (bottom), directly after (middle) and 30 hours after addition of 2 equiv. $^{13}$CO.

**Alcoholysis of [(dtbpx)Pd(COMe)Cl]**

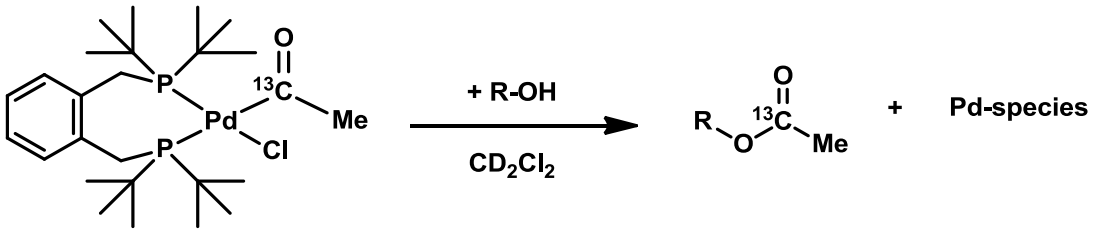


[(dtbpx)Pd(COMe)Cl] was generated in-situ in an NMR tube in methylene chloride as described above using 2 equiv. of $^{13}CO$. 10 Equiv. of the desired alcohol (methanol, ethanol, *n*-propanol or *iso*-propanol) were then added and the alcoholysis reaction was followed by $^{1}H$ NMR spectroscopy. Note that when methanol was used as the alcohol, the alcoholysis reaction was already completed before recording the NMR spectrum.

$$k_{obs}(ethanol) = (37.1 \pm 3.4) \cdot 10^{-4}\ s^{-1}$$
$$k_{obs}(n-propanol) = (28.4 \pm 1.3) \cdot 10^{-4}\ s^{-1}$$
$$k_{obs}(iso-propanol) = (5.6 \pm 0.1) \cdot 10^{-4}\ s^{-1}$$

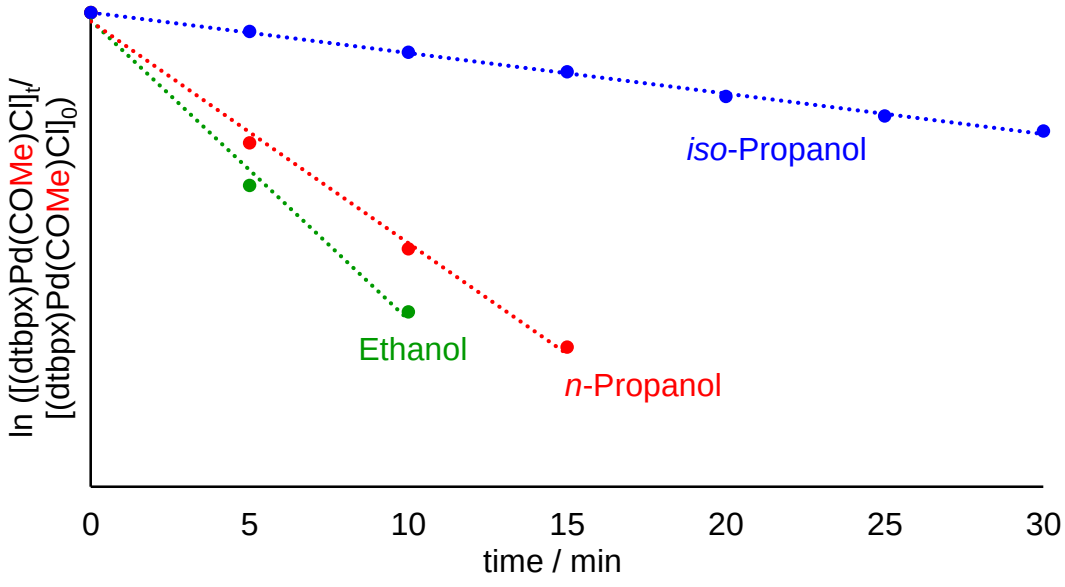


Figure S14: Alcoholysis reaction of [(dtbpx)Pd(COMe)Cl] with ethanol, *n*-propanol and *iso*-propanol at 25 °C followed by $^{1}H$ NMR spectroscopy.

**Reaction of [(dtbpx)Pd(D)(MeOD)]$^{+}$(OTf)$^{-}$ with double unsaturated compounds:**

In a typical experiment 20 – 30 mg [(dtbpx)Pd(OTf)$_2$] were dissolved in 0.6 mL methanol-$d_4$ in an NMR tube. Rapid formation of the deuteride species [(dtbpx)Pd(D)(MeOD)]$^{+}$(OTf)$^{-}$ was evidenced by $^{31}$P NMR spectroscopy. After addition of (sub)-stoichiometric amounts (0.7 – 1.0 equiv.) of the desired double unsaturated compound, the tube was shaken carefully and analyzed with NMR spectroscopy. To generate the respective linear / terminal Pd-allyl species, the NMR tube was heated for 1.5 hours to 55 °C. During this time the formation of Pd-black and deuterated diphosphine (dtbpx-D$_2$)$^{2+}$(OTf)$_2^{2-}$ was observed. The sample was thus filtered to remove Pd-black and analyzed with NMR spectroscopy.

**Reaction of [(dtbpx)Pd(D)(MeOD)]$^{+}$(OTf)$^{-}$ with methyl linoleate:**

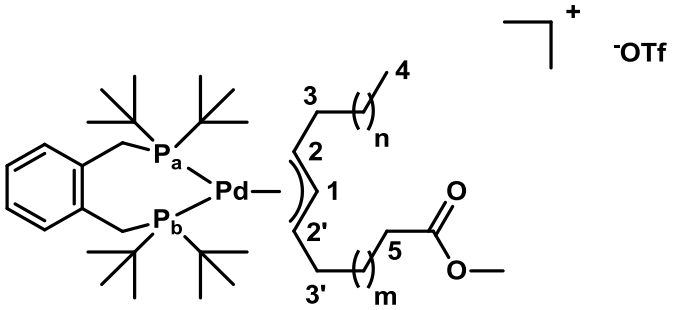


According to the above mentioned procedure, the disubstituted / internal Pd-allyl species was generated in-situ. Note that 2D-NMR spectra were recorded at 0 °C as slow isomerization towards the monosubstituted / terminal Pd-allyl species already occurred at 25 °C. **$^{1}$H NMR** (400 MHz, methanol-$d_4$, 298 K): δ 7.51 (m, aromatic CH), 7.22 (m, aromatic CH), 6.27 – 6.07 (s br., 1H, H-2), 5.15 (m, 1H, H-1), 4.69 (s br., 1H, H-2'), 3.96 – 3.70 (m, benzylic CH$_2$), 3.64 (s, 3H, -O-CH$_3$), 2.52 – 2.36 (s br., 1H, H-3), 2.31 (m, 2H, H-5), 2.06 – 1.92 (s br., 1H, H-3), 1.69 (m, 1H, H-3'), 1.65 – 1.01 (m, $^{t}$Bu-H, H-3' and residual CH$_2$ groups of methyl linoleate), 0.89 (m, 3H, H-4). **$^{31}$P{$^{1}$H} NMR** (162 MHz, methanol-$d_4$, 298 K): δ 51.7 – 47.7 (s br.), 46.6 (s br.).

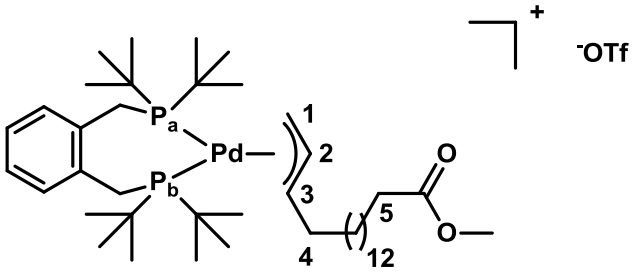


The monosubstituted / terminal Pd-allyl species was generated in-situ as described above. **$^{1}$H NMR** (400 MHz, methanol-$d_4$, 303 K): δ 7.51 (m, aromatic CH), 7.23 (m, aromatic CH), 6.51 (m, 1H, H-3), 5.25 (m, 1H, H-2), 4.63 (vt, $J$ = 6.7, 1H, H-1), 4.02 – 3.67 (m, benzylic $CH_2$), 3.40 (m, 1H, H-1), 3.35 (s, 3H, -O-$CH_3$), 2.31 (t, $^{3}J_{HH}$ = 7.2 Hz, 2H, H-5), 1.86 – 1.72 (s br., 1H, H-4), 1.70 – 1.03 (m, $^{t}$Bu-H, H-4 and residual $CH_2$ groups of methyl linoleate). **$^{31}$P{$^{1}$H} NMR** (162 MHz, methanol-$d_4$, 303 K): δ 49.5 (d, $^{2}J_{PP}$ = 40.6 Hz, $P_a$), 45.6 – 40.2 (s br., $P_b$). **$^{13}$C{$^{1}$H} NMR** (100 MHz, methanol-$d_4$, 303 K): δ 175.9 (s, carbonyl), 134.6 (s, aromatic C), 130.6 (s, aromatic CH), 128.3 (s, aromatic CH), 112.1 (m, C-2), 100.6 (m, C-3), 59.7 (d, $^{2}J_{CP}$ = 30.8 Hz, C-3), 49.9 (m, -O-$CH_3$), 39.2 (m, $^{t}$Bu-$C(CH_3)_3$), 31.7 – 28.4 (m, $^{t}$Bu-C($CH_3$)$_3$, benzylic $CH_2$ and residual $CH_2$ groups of methyl linoleate).

**<u>Reaction of [(dtbpx)Pd(D)(MeOD)]$^{+}$(OTf)$^{-}$ with 1,7-octadien:</u>**

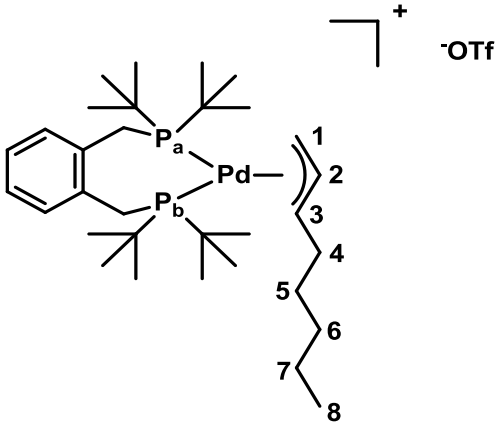


The monosubstituted / terminal Pd-allyl species was generated in-situ as described above. **$^{1}$H NMR** (400 MHz, methanol-$d_4$, 298 K): δ 7.52 (m, aromatic CH), 7.23 (m, aromatic CH), 6.50 (s, 1H, H-3), 5.25 (m, 1H, H-2), 4.63 (vt, $J$ = 6.6 Hz, 1H, H-1), 4.01 – 3.73 (m, benzylic $CH_2$), 3.39 (m, 1H, H-1), 1.77 (s, 1H, H-4), 1.66 – 1.13 (m, $^{t}$Bu-H, H-4 and H-5 to H-7), 0.89 (m, 3H, H-8). **$^{31}$P{$^{1}$H} NMR** (162 MHz, methanol-$d_4$, 298 K): δ 49.4 (d, $^{2}J_{PP}$ = 50.0 Hz, $P_a$), 45.1 – 40.3

(s br., $P_b$). **$^{13}C\{^1H\}$ NMR** (100 MHz, methanol-$d_4$, 298 K): δ 136.9 (s, aromatic C), 134.6 (s, aromatic CH), 128.3 (s, aromatic CH), 112.1 (s br., C-2), 100.5 (d, $J_{CP}$ = 21.3 Hz, C-3), 59.7 (d, $J_{CP}$ = 29.6, C-1), 39.9 – 38.6 (m, $^t$Bu-*C*($CH_3$)$_3$), 32.2 – 30.4 (m, $^t$Bu-C(*C*$H_3$)$_3$, C-4, C-5), 29.8 – 28.4 (m, benzylic $CH_2$), 27.8 (s, C-6) 23.0 (m, C-7), 14.2 (m, C-8).

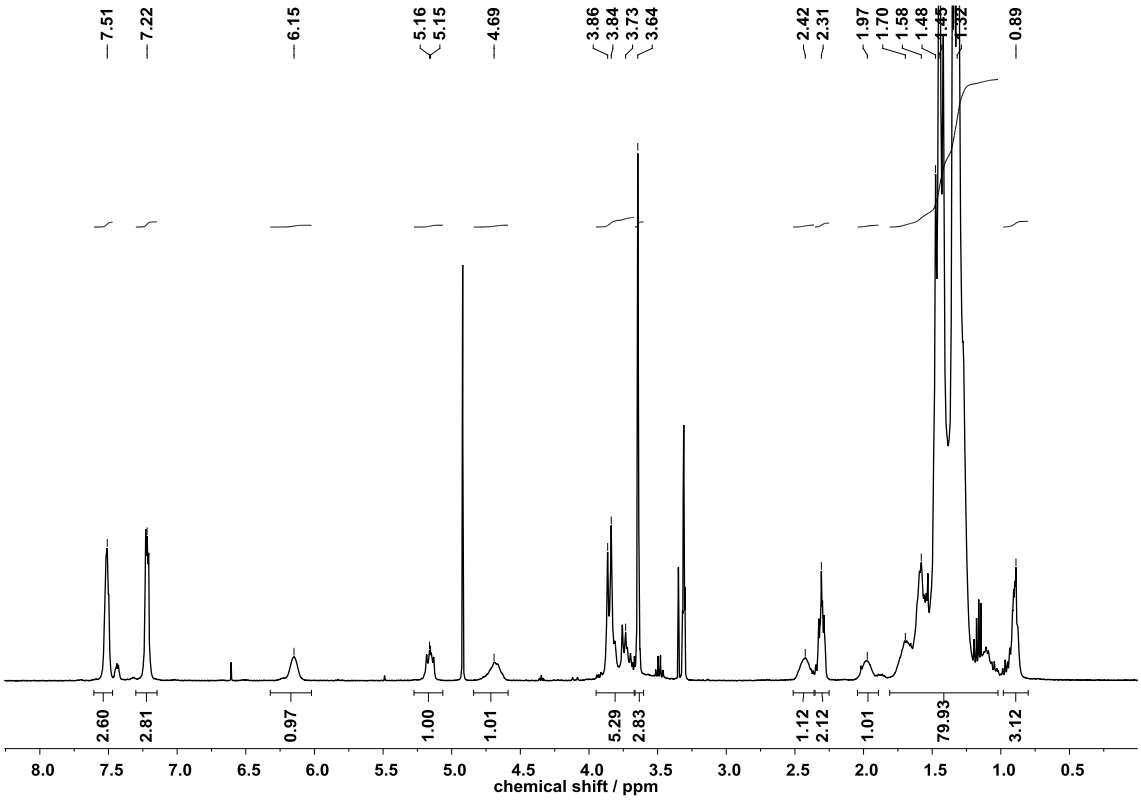


Figure S15: $^1$H NMR spectrum of the disubstituted / internal Pd-allyl species generated from [(dtbpx)Pd(D)(MeOD)]$^+$(OTf)$^-$ and methyl linoleate in methanol-$d_4$ at 25 °C.

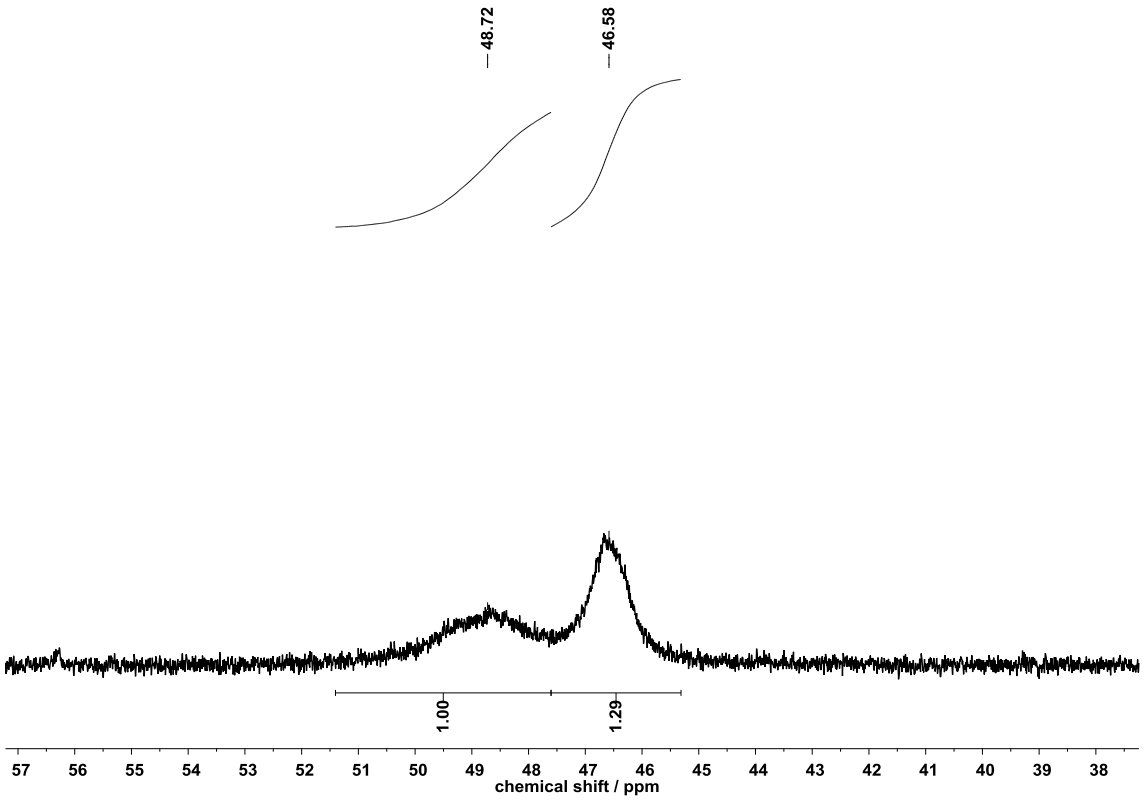


Figure S16: $^{31}P\{^{1}H\}$ NMR spectrum of the disubstituted / internal Pd-allyl species generated from $[(dtbpx)Pd(D)(MeOD)]^{+}(OTf)^{-}$ and methyl linoleate in methanol-$d_4$ at 25 °C.

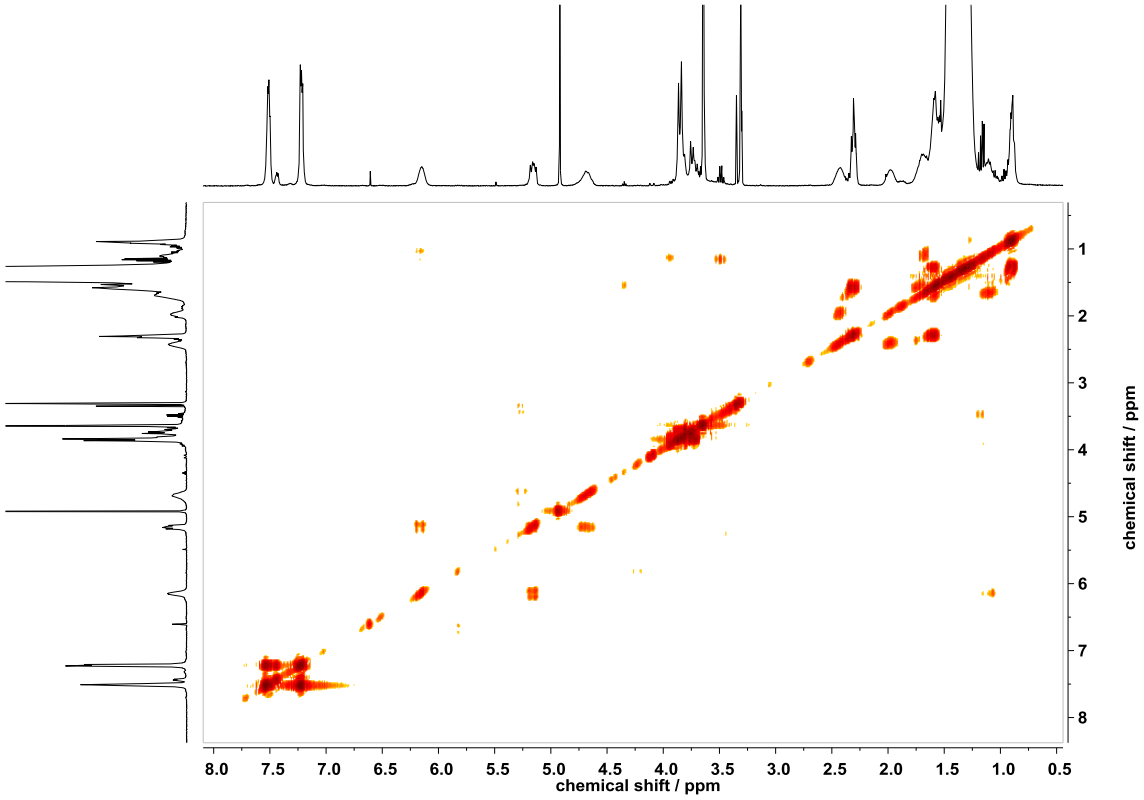


Figure S17: $^{1}H,^{1}H$-COSY NMR spectrum of the disubstituted / internal Pd-allyl species generated from $[(dtbpx)Pd(D)(MeOD)]^{+}(OTf)^{-}$ and methyl linoleate in methanol-$d_4$ at 25 °C.

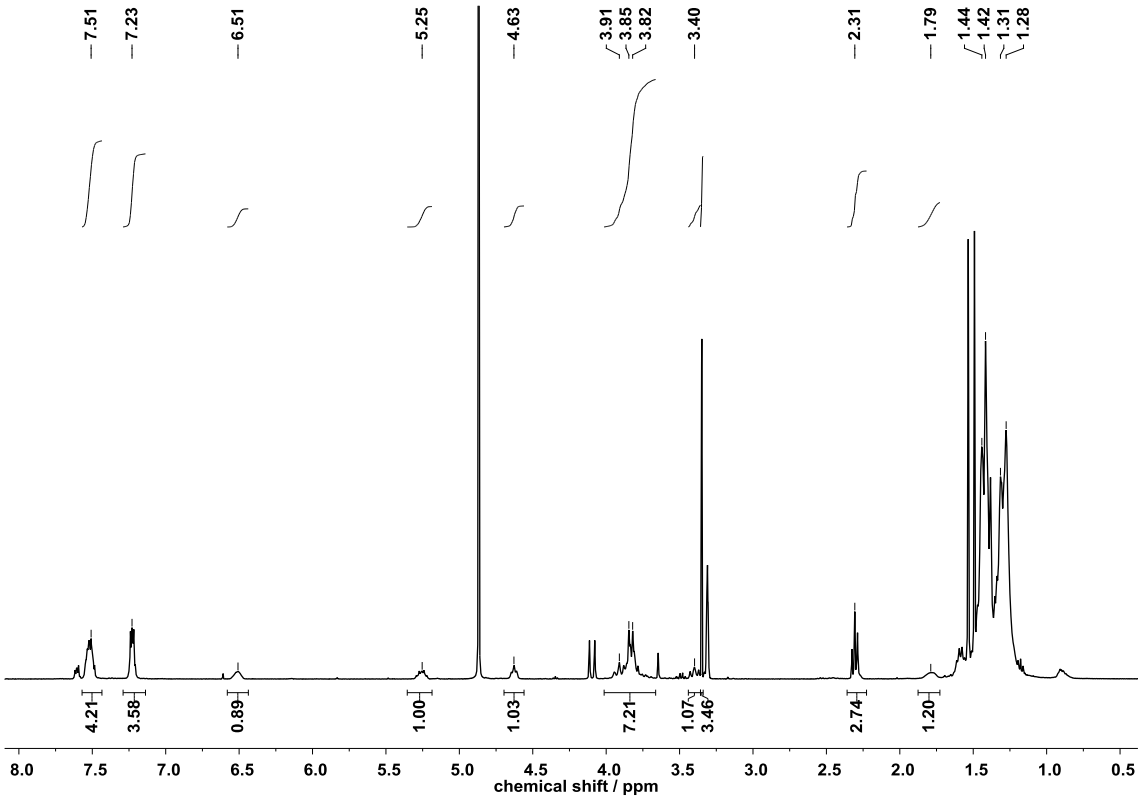


Figure S18: $^{1}$H NMR spectrum of the monosubstituted / terminal Pd-allyl species generated from [(dtbpx)Pd(D)(MeOD)]$^{+}$(OTf)$^{-}$ and methyl linoleate in methanol-$d_4$ at 30 °C.

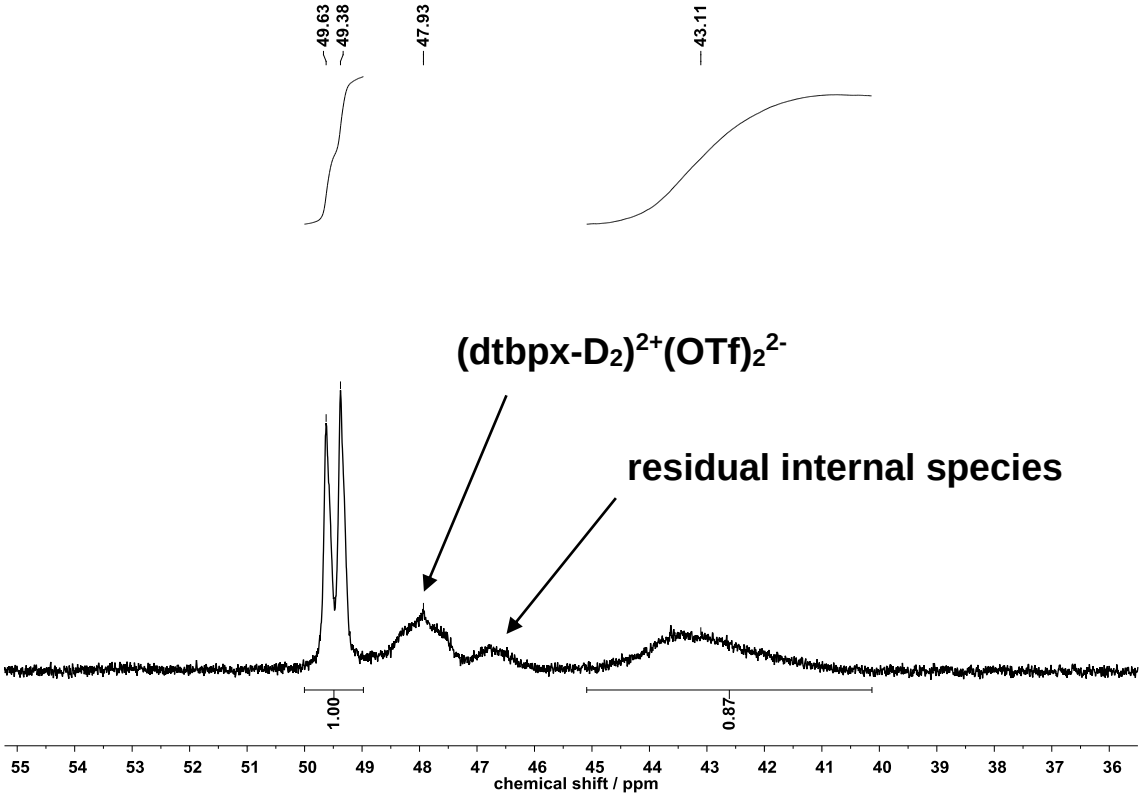


Figure S19: $^{31}$P{$^{1}$H} NMR spectrum of the monosubstituted / terminal Pd-allyl species generated from [(dtbpx)Pd(D)(MeOD)]$^{+}$(OTf)$^{-}$ and methyl linoleate in methanol-$d_4$ at 30 °C.

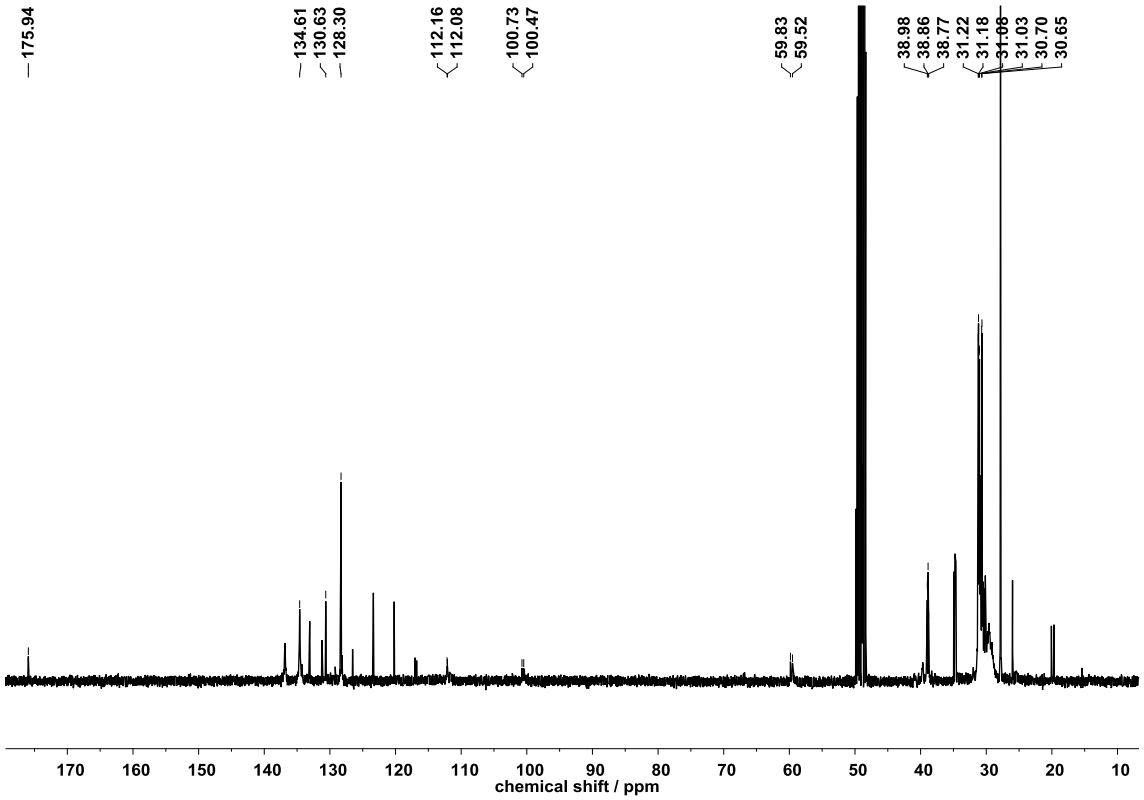


Figure S20: $^{13}C\{^{1}H\}$ NMR spectrum of the monosubstituted / terminal Pd-allyl species generated from [(dtbpx)Pd(D)(MeOD)]$^{+}$(OTf)$^{-}$ and methyl linoleate in methanol-$d_4$ at 30 °C.

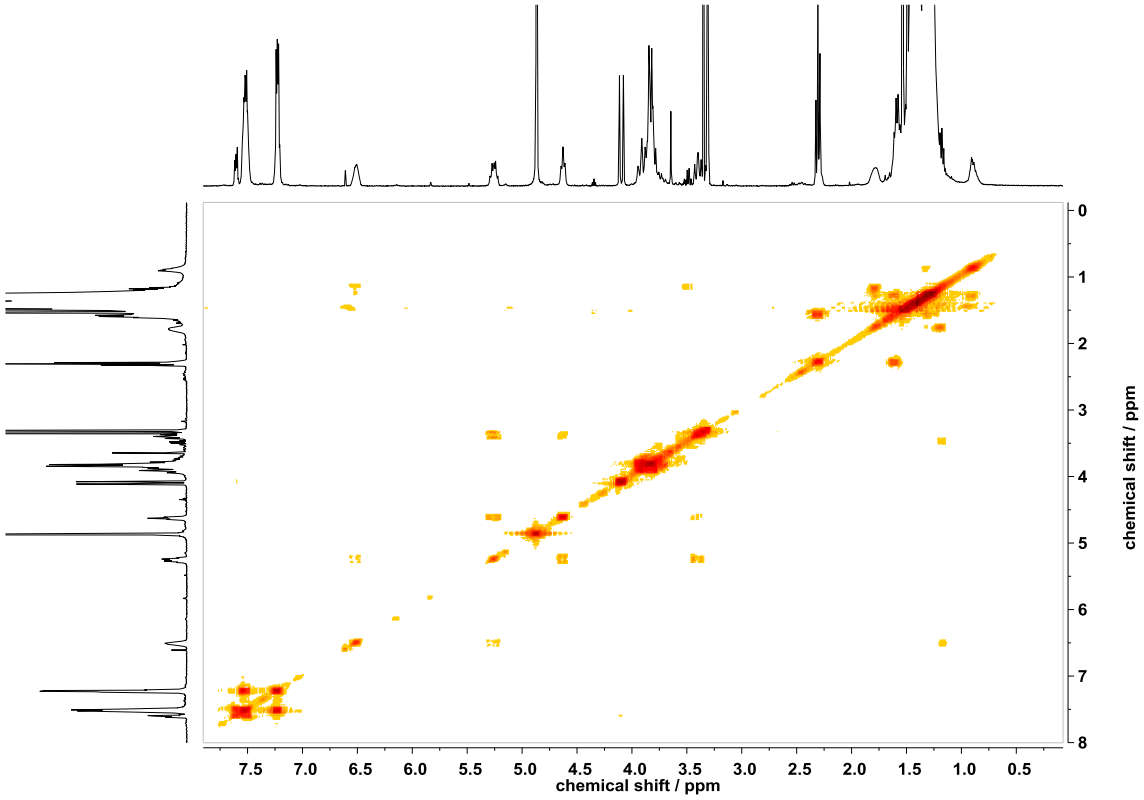


Figure S21: $^{1}H,^{1}H$-COSY NMR spectrum of the monosubstituted / terminal Pd-allyl species generated from [(dtbpx)Pd(D)(MeOD)]$^{+}$(OTf)$^{-}$ and methyl linoleate in methanol-$d_4$ at 30 °C.

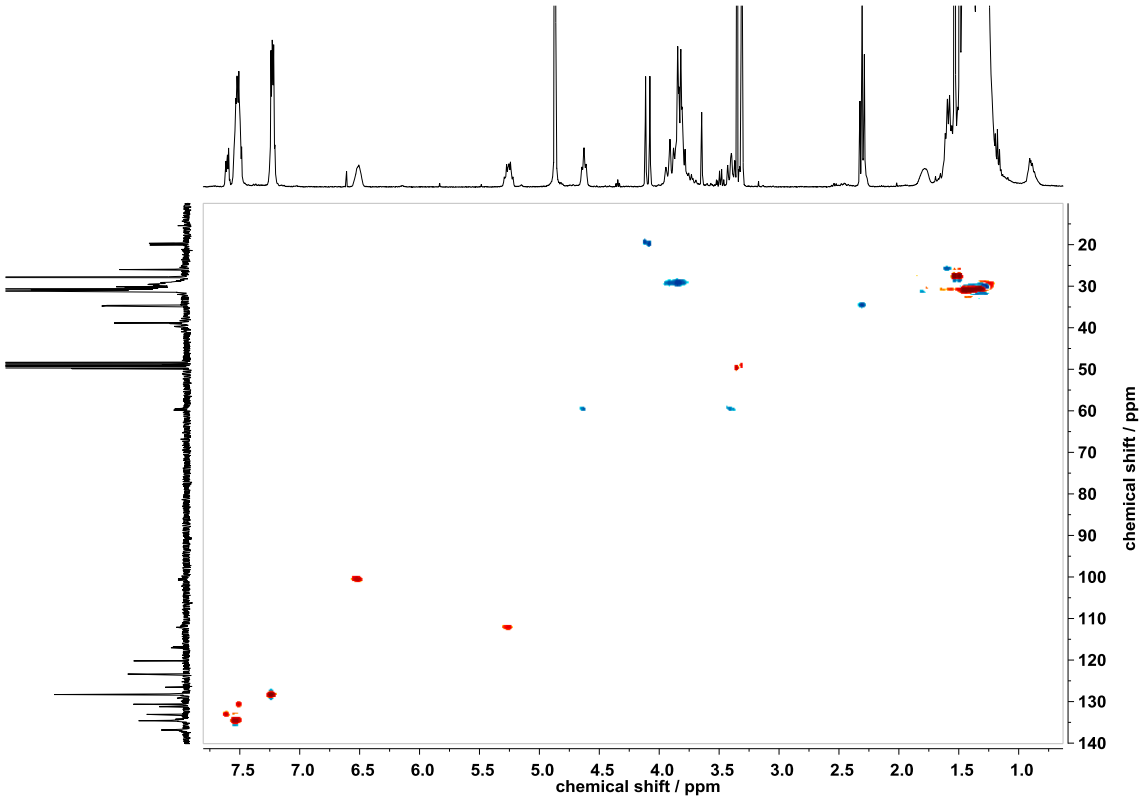


Figure S22: $^{1}H,^{13}C$-HSQC NMR spectrum of the monosubstituted / terminal Pd-allyl species generated from $[(dtbpx)Pd(D)(MeOD)]^{+}(OTf)^{-}$ and methyl linoleate in methanol-$d_4$ at 30 °C.

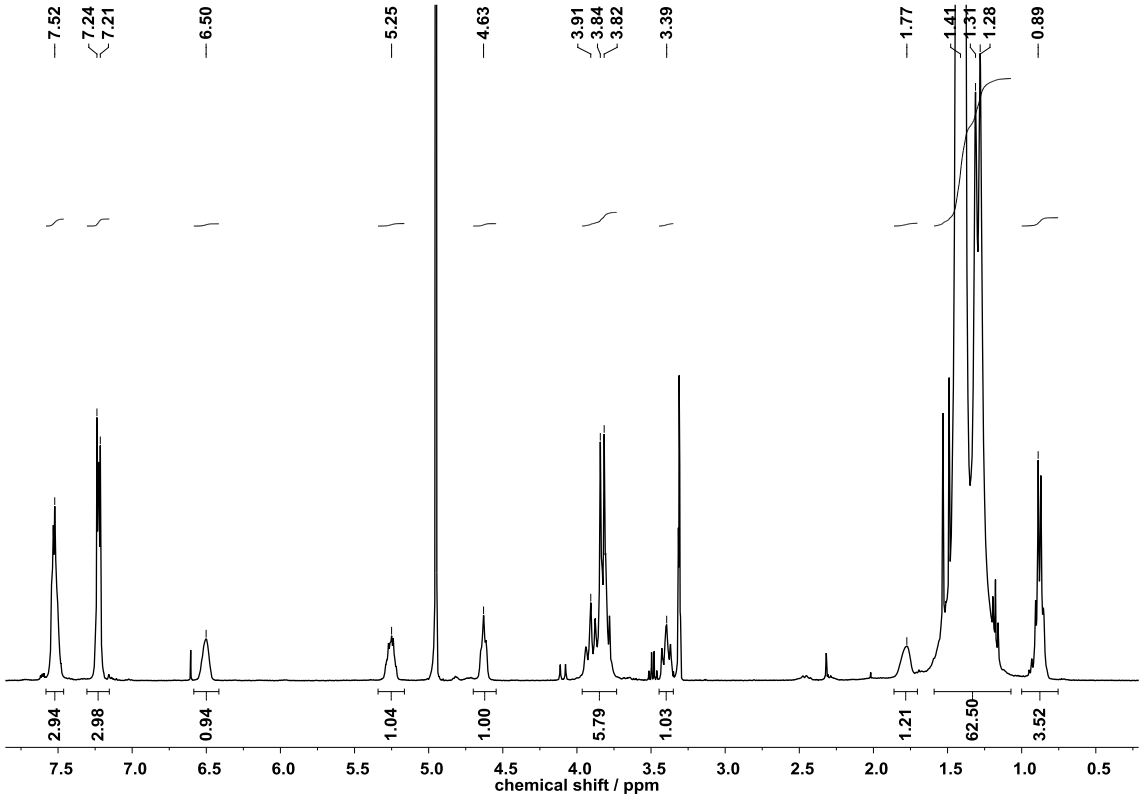


Figure S23: $^{1}H$ NMR spectrum of the monosubstituted / terminal Pd-allyl species generated from $[(dtbpx)Pd(D)(MeOD)]^{+}(OTf)^{-}$ and 1,7-octadiene in methanol-$d_4$ at 25 °C.

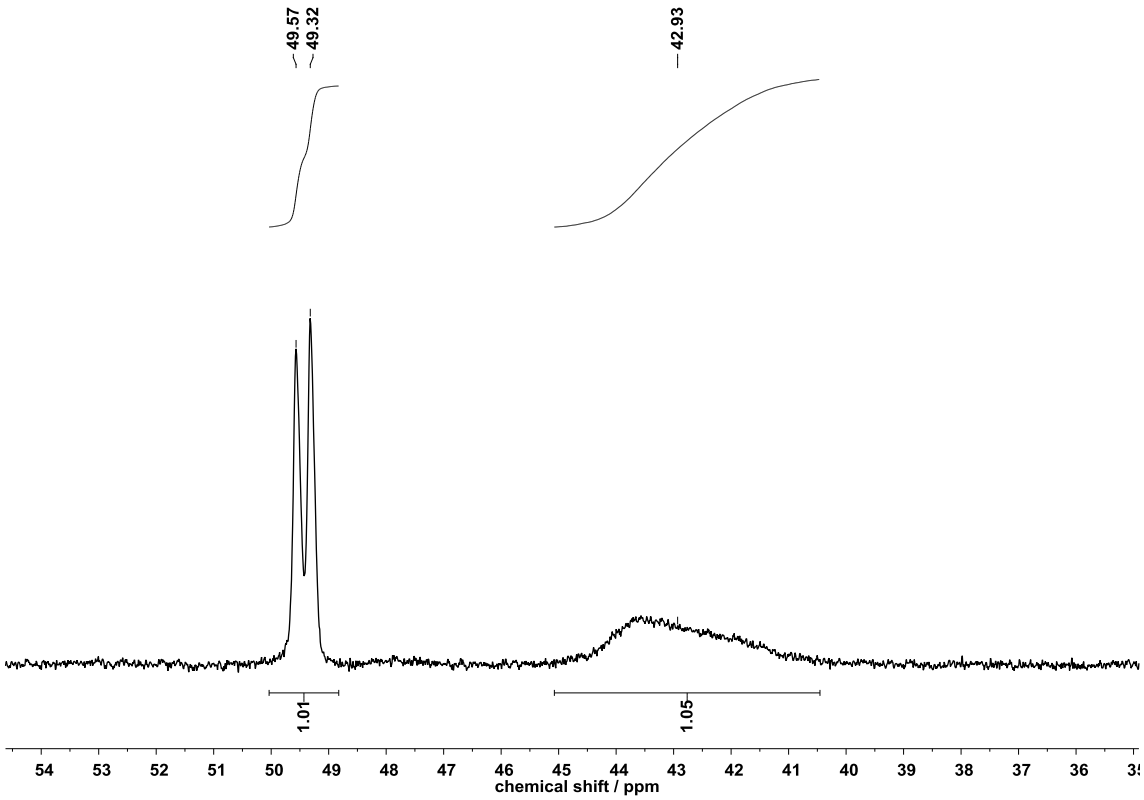


Figure S24: $^{31}P\{^{1}H\}$ NMR spectrum of the monosubstituted / terminal Pd-allyl species generated from $[(dtbpx)Pd(D)(MeOD)]^{+}(OTf)^{-}$ and 1,7-octadiene in methanol-$d_4$ at 25 °C.

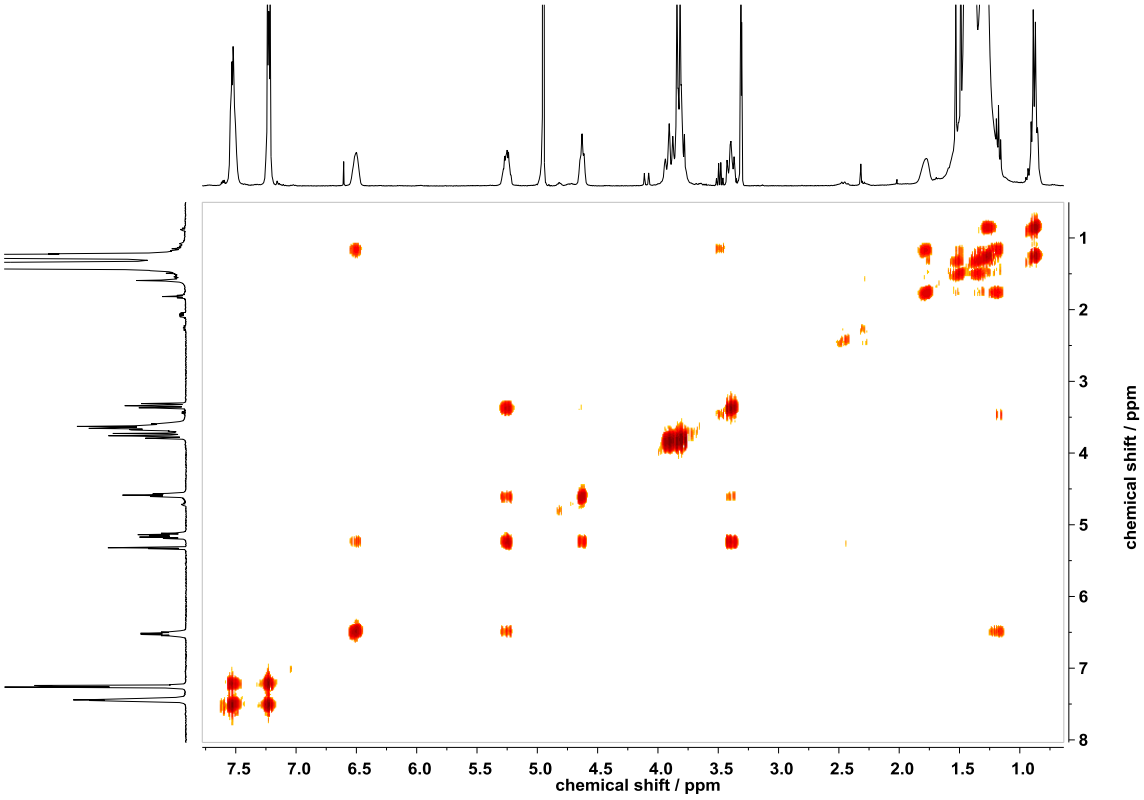


Figure S25: $^{1}H,^{1}H$-COSY NMR spectrum of the monosubstituted / terminal Pd-allyl species generated from $[(dtbpx)Pd(D)(MeOD)]^{+}(OTf)^{-}$ and 1,7-octadiene in methanol-$d_4$ at 25 °C.

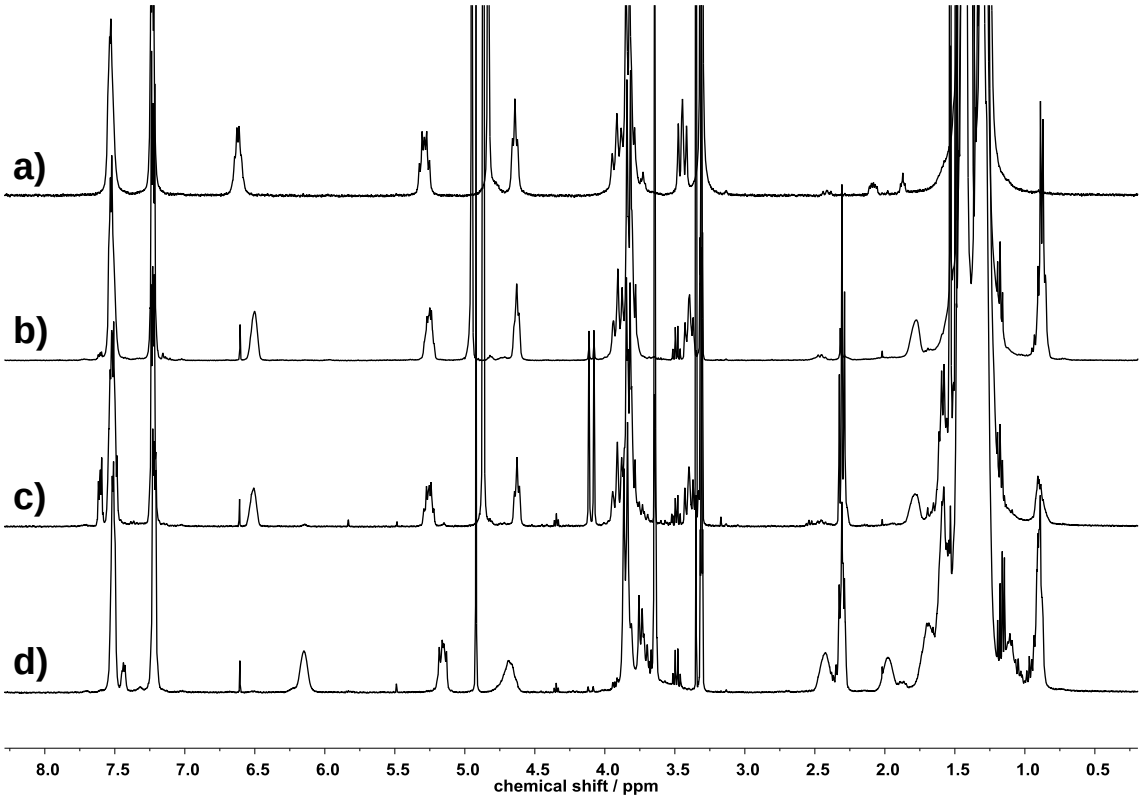


Figure S26: $^{1}$H NMR spectra of a) [(dtbpx)Pd($\eta^3$-$C_4H_7$)]$^+$(OTf)$^-$, b) the monosubstituted / terminal Pd-allyl species generated from [(dtbpx)Pd(D)(MeOD)]$^+$(OTf)$^-$ and 1,7-octadiene, c) the monosubstituted / terminal Pd-allyl species generated from [(dtbpx)Pd(D)(MeOD)]$^+$(OTf)$^-$ and methyl linoleate, and d) the disubstituted / internal Pd-allyl species generated from [(dtbpx)Pd(D)(MeOD)]$^+$(OTf)$^-$ and methyl linoleate in methanol-$d_4$ at 25 °C.

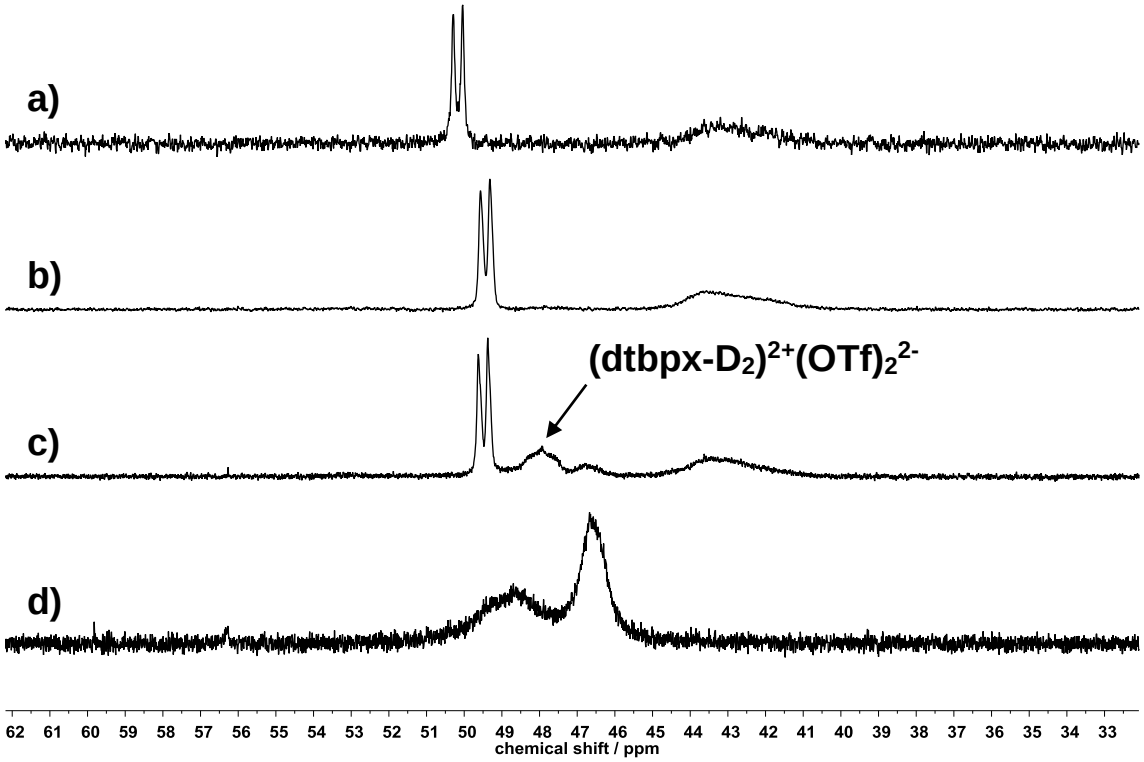


Figure S27: $^{31}P\{^{1}H\}$ NMR spectra of a) [(dtbpx)Pd($\eta^3$-$C_4H_7$)]$^+$(OTf)$^-$, b) the monosubstituted / terminal Pd-allyl species generated from [(dtbpx)Pd(D)(MeOD)]$^+$(OTf)$^-$ and 1,7-octadiene, c) the monosubstituted / terminal Pd-allyl species generated from [(dtbpx)Pd(D)(MeOD)]$^+$(OTf)$^-$ and methyl linoleate, and d) the disubstituted / internal Pd-allyl species generated from [(dtbpx)Pd(D)(MeOD)]$^+$(OTf)$^-$ and methyl linoleate in methanol-$d_4$ at 25 °C.

**Formation of dimethyl adipate from [(dtbpx)Pd($\eta^3$-$C_4H_7$)]$^+$(OTf)$^-$:**

According to the above general procedure of NMR experiments, the pressure NMR tube was charged with 20 mg [(dtbpx)Pd($\eta^3$-$C_4H_7$)]$^+$(OTf)$^-$, 0.5 mL methanol-$d_4$ and pressurized with 5 bar CO at room temperature. $^{13}C$ NMR was used to prove the presence of CO in solution. The sample was then heated to 90 °C for 3 days. $^{1}H$ NMR showed disappearance of the signals of the [(dtbpx)Pd($\eta^3$-$C_4H_7$)]$^+$(OTf)$^-$ and $^{2}H$ NMR showed the formation of deuterated dimethyl adipate.

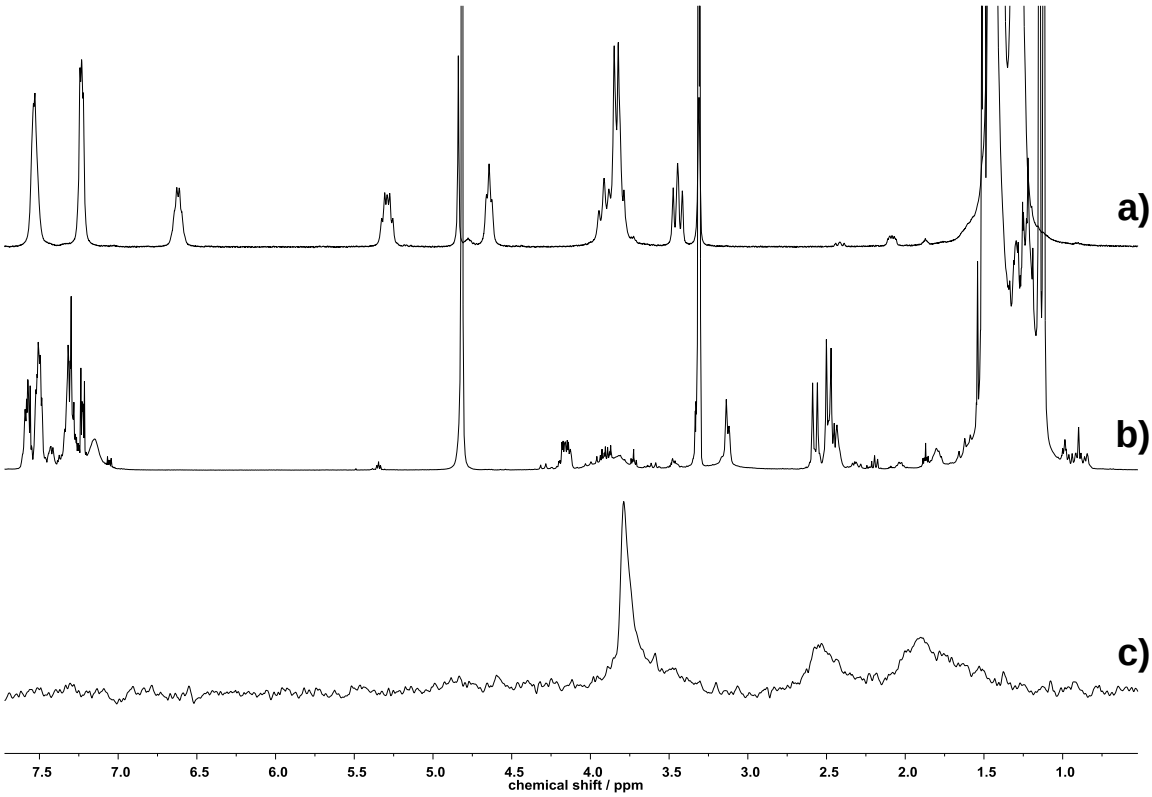


Figure S28: $^{1}H$ NMR spectra of $[(dtbpx)Pd(\eta^{3}\text{-}C_4H_7)]^{+}(OTf)^{-}$ in methanol-$d_4$ pressurized with 5 bar CO a) before and b) after heating to 90 °C for 3 days, and c) $^{2}H$ NMR spectrum after heating to 90 °C for 3 days.

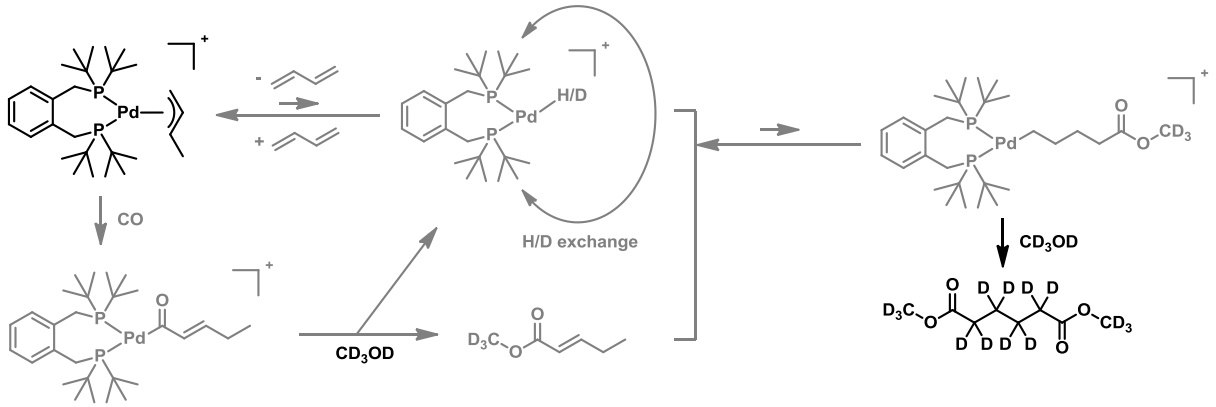


Figure S29: Possible reaction pathways leading to deuterated dimethyl adipate. Compounds in black were identified, compounds and pathways drawn in grey are hypothetical.

**Thermodynamic parameters of allylic isomerization:**

To determine thermodynamic parameters, the experiments were performed as described above using 20 mg (0.025 mmol) $[(dtbpx)Pd(OTf)_2]$ in 0.6 mL methanol-$d_4$ (c = 0.042 M) and 0.95 equiv. methyl linoleate which were added prior to the kinetic experiment. The NMR tube was

introduced into the pre-heated spectrometer and the progress of isomerization was followed by $^1$H NMR spectroscopy (signal at 6.15 ppm). As first order reaction was best suited for this transformation, $\ln([\int 6.15]_t/[\int 6.15]_0)$ was plotted *versus* time (Figure S31) and thermodynamic parameters were determined from isomerizations at temperatures between 25 – 55 °C.

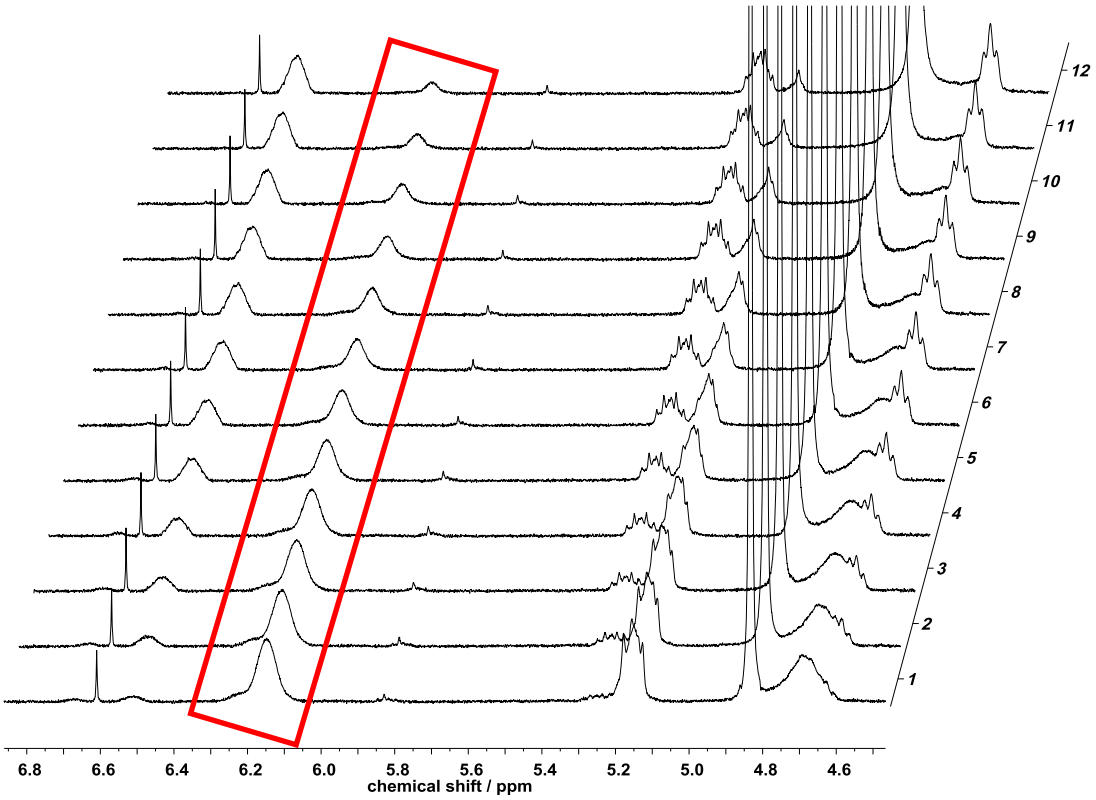


Figure S30: Stacked $^1$H NMR spectra of allylic isomerization in methanol-$d_4$ at 35 °C.

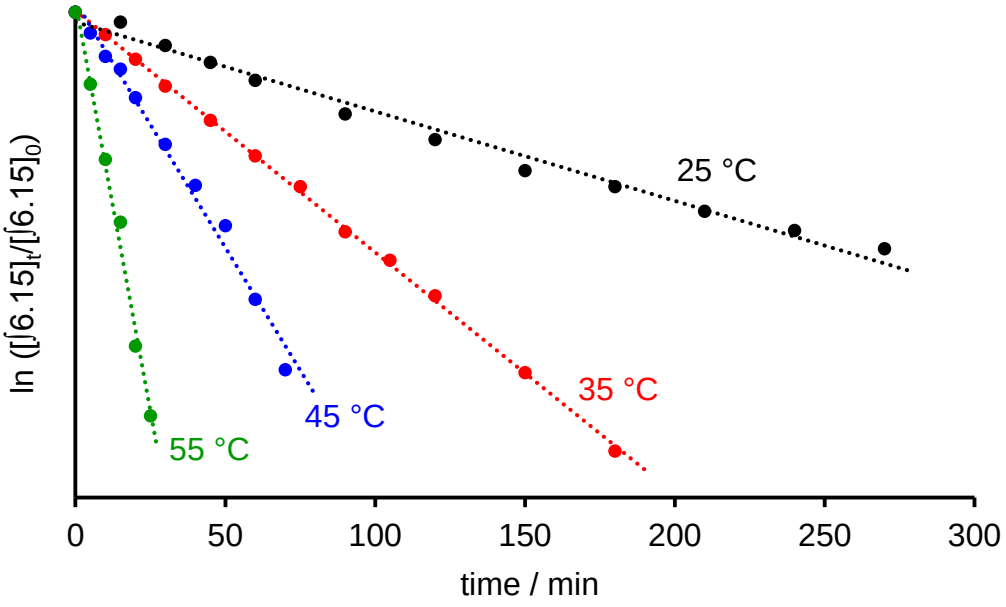


Figure S31: Allylic isomerization reaction followed by $^1$H NMR at denoted temperatures.

$k_{obs}(25\,°C) = (7.5 \pm 0.3) \cdot 10^{-5}\ s^{-1}$

$k_{obs}(35\,°C) = (20.2 \pm 0.2) \cdot 10^{-5}\ s^{-1}$

$k_{obs}(45\,°C) = (40.8 \pm 1.6) \cdot 10^{-5}\ s^{-1}$

$k_{obs}(55\,°C) = (129.1 \pm 6.2) \cdot 10^{-5}\ s^{-1}$

$$k_{obs} = \frac{k_b \cdot T}{h} \cdot \exp\left(-\frac{\Delta G^{\neq}}{RT}\right) \quad and \quad \Delta G^{\neq} = \Delta H^{\neq} - T\Delta S^{\neq}$$

$$\Rightarrow \ln\left(\frac{k_{obs} \cdot h}{k_b \cdot T}\right) \cdot R = -\Delta H^{\neq} \cdot \frac{1}{T} + \Delta S^{\neq}$$

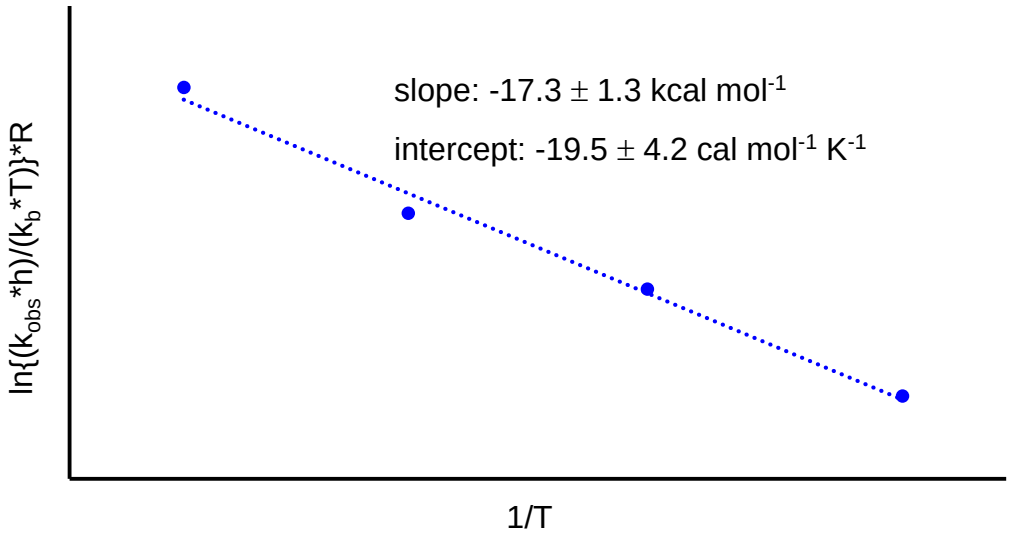


Figure S32: Eyring plot to determine $\Delta H^{\neq}$ (slope) and $\Delta S^{\neq}$ (intercept).

$\Delta H^{\neq}_{isom} = 17.3 \pm 1.3\ \text{kcal mol}^{-1}$

$\Delta S^{\neq}_{isom} = -19.5 \pm 4.2\ \text{cal mol}^{-1}\text{K}^{-1}$

$\Delta G^{\neq}_{isom}(25\,°C) = 23.1\ \text{kcal mol}^{-1}$

**Alkoxycarbonylations with different alcohols**

Alkoxycarbonylations were carried out according to the carbonylation procedure II. The respective oleates were synthesized by $H_2SO_4$ catalyzed esterification in neat alcohol as solvent and reagent from the fatty acids obtained from high-oleic sunflower oil, distilled and degassed prior to use and characterized by $^{1}H$ and $^{13}C$ NMR spectroscopy, and gas chromatography.

With all alcohols hydride formation from [(dtbpx)Pd(OTf)$_2$] within 5 minutes at room temperature by addition of 0.5 mL (methanol), 0.75 mL (ethanol), or 1 mL (*n*-propanol and *iso*-propanol) of the alcohol to a $CD_2Cl_2$ (0.5 mL) solution of [(dtbpx)Pd(OTf)$_2$] (20 mg) is evidenced by $^{1}H$ and $^{31}P$ NMR spectroscopy (Figure S33). Rapid isomerization of the respective oleates with these Pd-hydride species at room temperature is also evidenced by $^{1}H$ NMR spectroscopy.

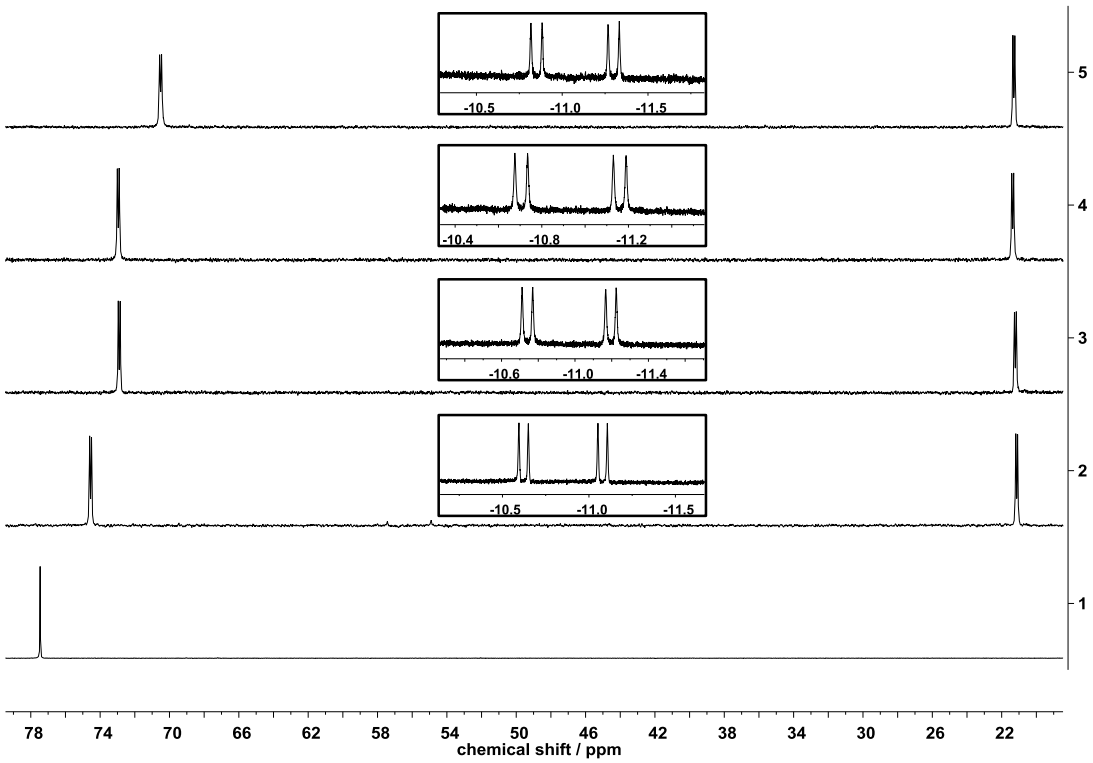


Figure S33: $^{31}P\{^{1}H\}$ NMR spectrum of [(dtbpx)Pd(OTf)$_2$] (1), [(dtbpx)PdH(MeOH)]$^+$ (2), [(dtbpx)PdH(EtOH)]$^+$ (3), [(dtbpx)PdH(*n*-PrOH)]$^+$ (4) and [(dtbpx)PdH(*i*-PrOH)]$^+$ (5) in $CD_2Cl_2$ / alcohol. Inset shows $^{1}H$ resonances of the hydride region.

**GC data of methoxycarbonylations with different substrates**

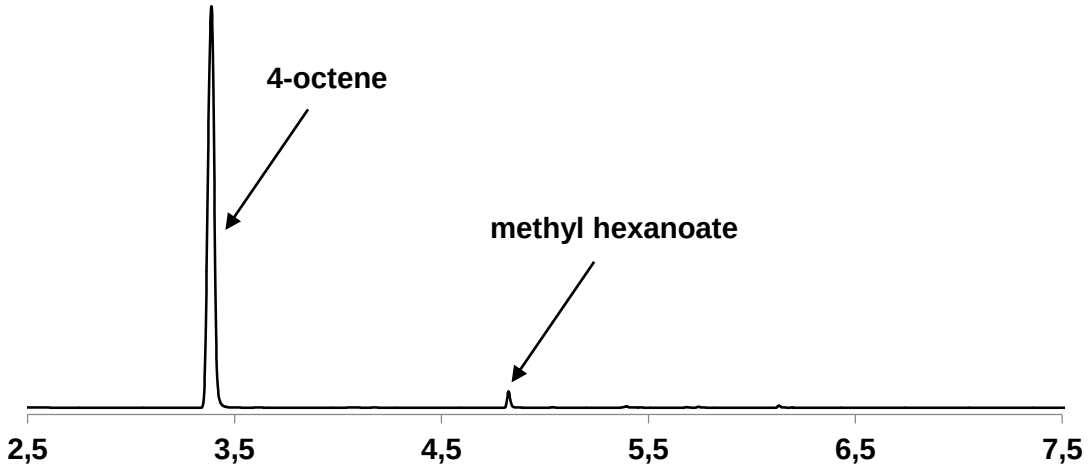


Figure S34: Gas chromatogram (time in minutes) of pure 4-octene + methyl hexanoate added as a standard.

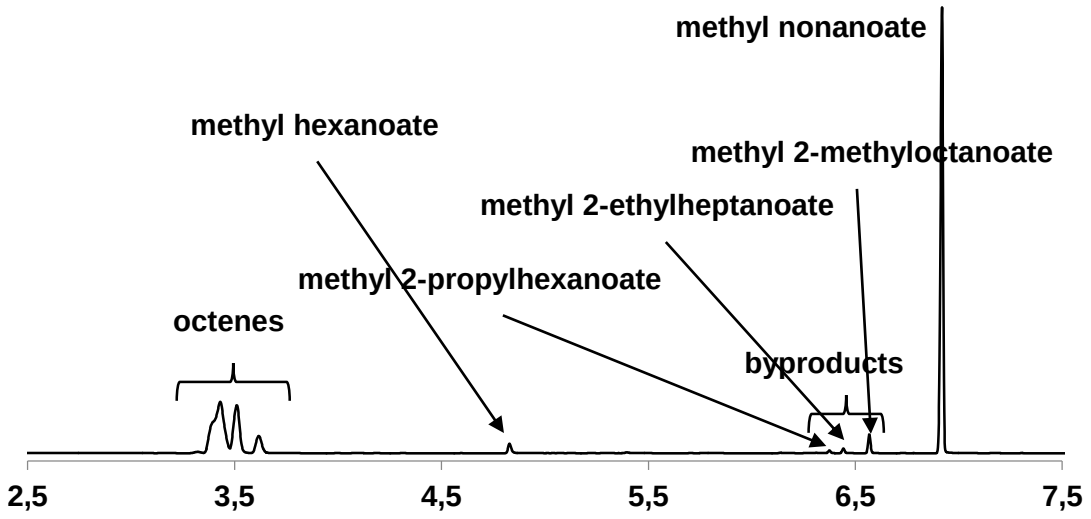


Figure S35: Gas chromatogram (time in minutes) of isomerizing methoxycarbonylation of 4-octene after a reaction time of 0.5 h. Methyl hexanoate was added as a standard.

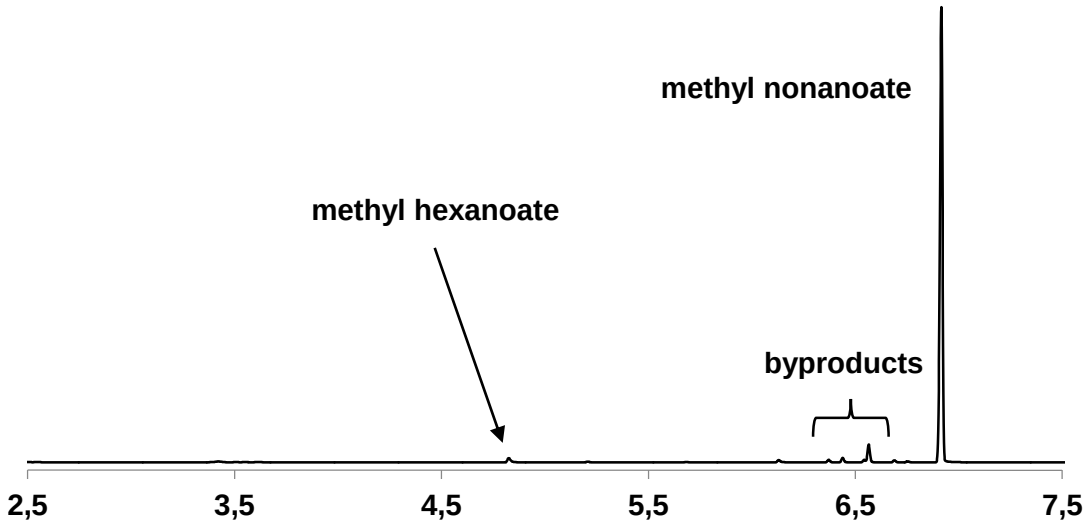


Figure S36: Gas chromatogram (time in minutes) of isomerizing methoxycarbonylation of 4-octene after a reaction time of 6 h. Methyl hexanoate was added as a standard.

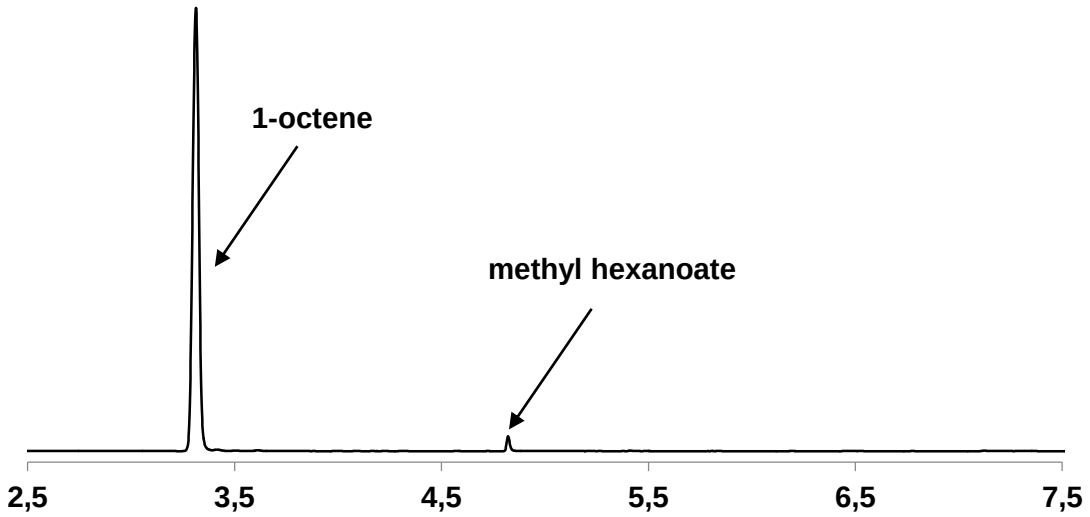


Figure S37: Gas chromatogram (time in minutes) of pure 1-octene + methyl hexanoate added as a standard.

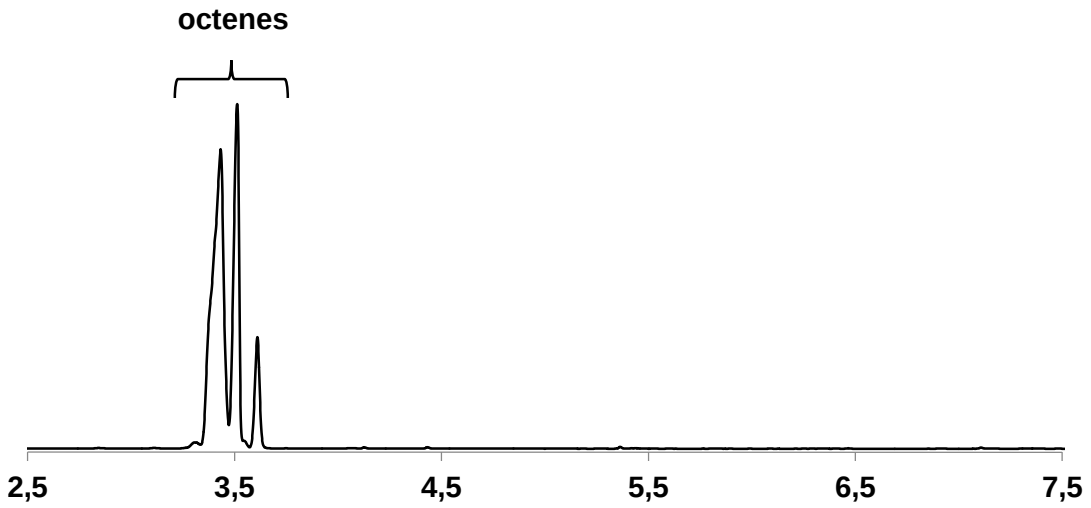


Figure S38: Gas chromatogram (time in minutes) of pure 1-octene with added [dtbpxPd(OTf)$_2$] (in methanol).

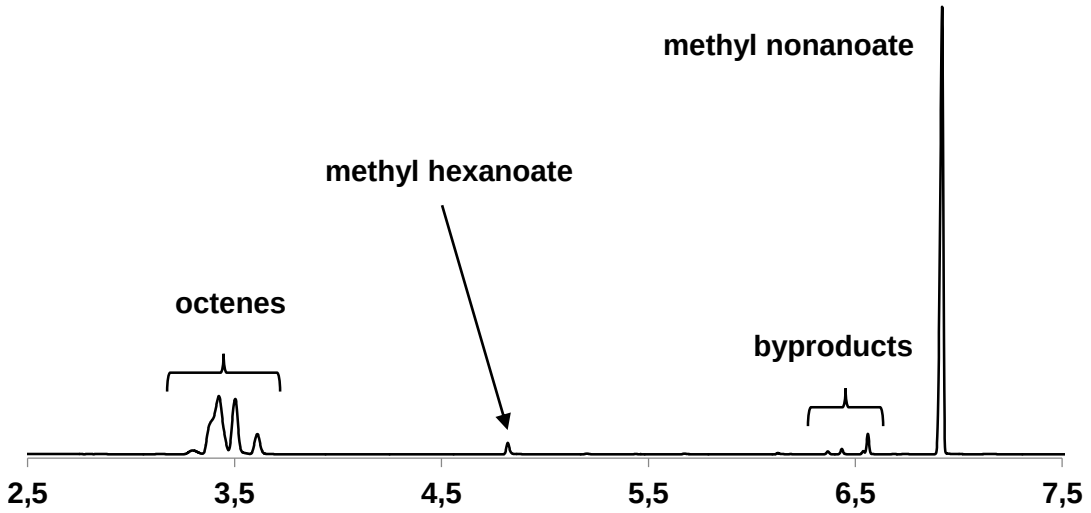


Figure S39: Gas chromatogram (time in minutes) of isomerizing methoxycarbonylation of 1-octene after a reaction time of 0.5 h. Methyl hexanoate was added as a standard.

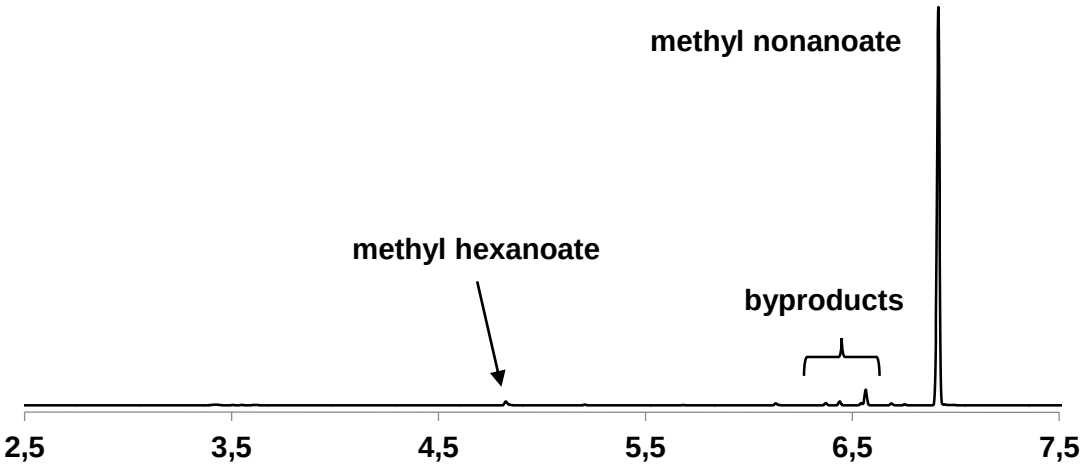


Figure S40: Gas chromatogram (time in minutes) of isomerizing methoxycarbonylation of 1-octene after a reaction time of 6 h. Methyl hexanoate was added as a standard.

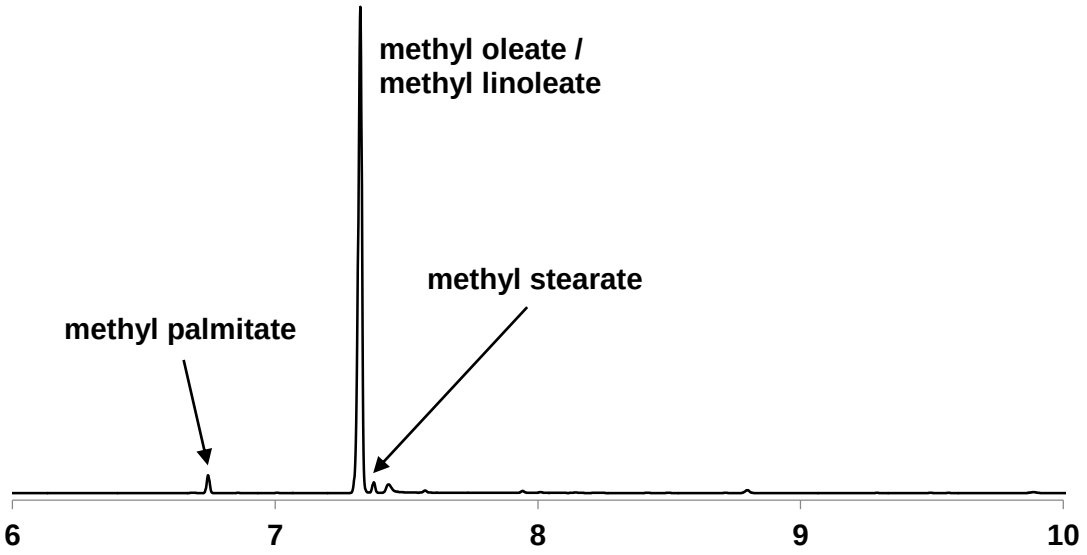


Figure S41: Gas chromatogram (time in minutes) of high oleic sunflower oil methyl ester (‘Dakolub MB 9001’).

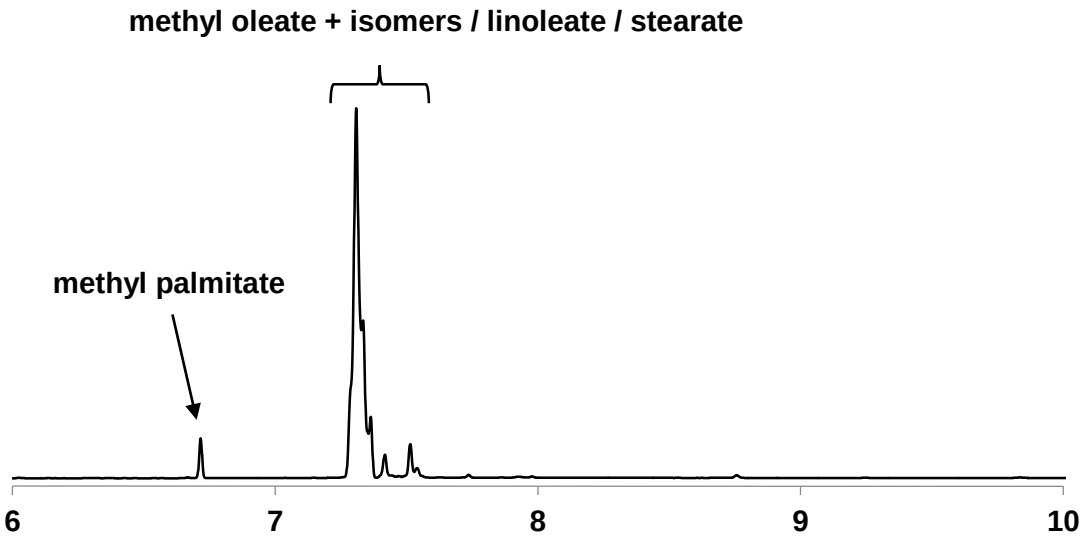


Figure S42: Gas chromatogram (time in minutes) of high oleic sunflower oil methyl ester ('Dakolub MB 9001') with added [dtbpxPd(OTf)$_2$] (in methanol).

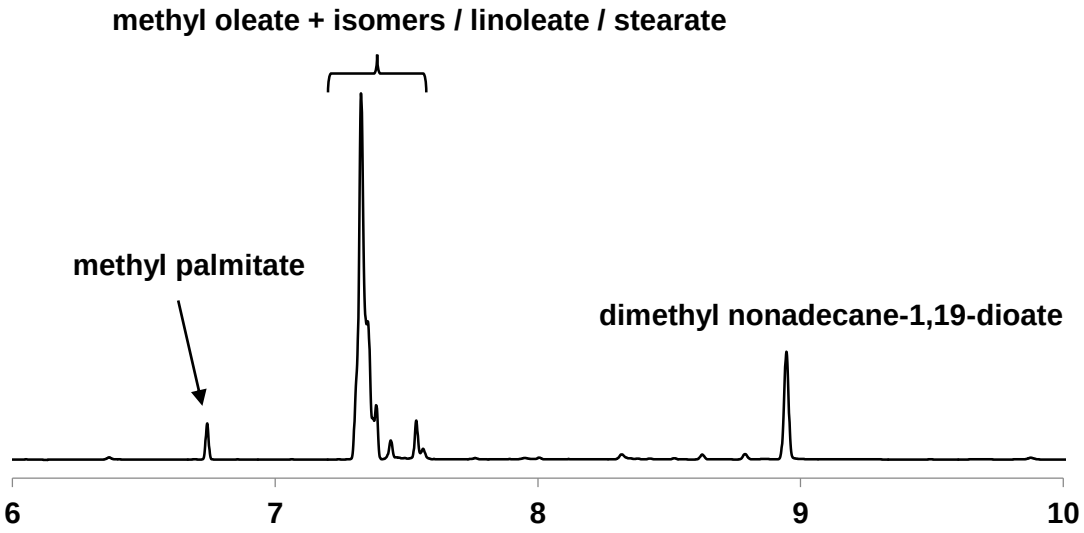


Figure S43: Gas chromatogram (time in minutes) of isomerizing methoxycarbonylation of high oleic sunflower oil methyl ester ('Dakolub MB 9001') after a reaction time of 1 h.

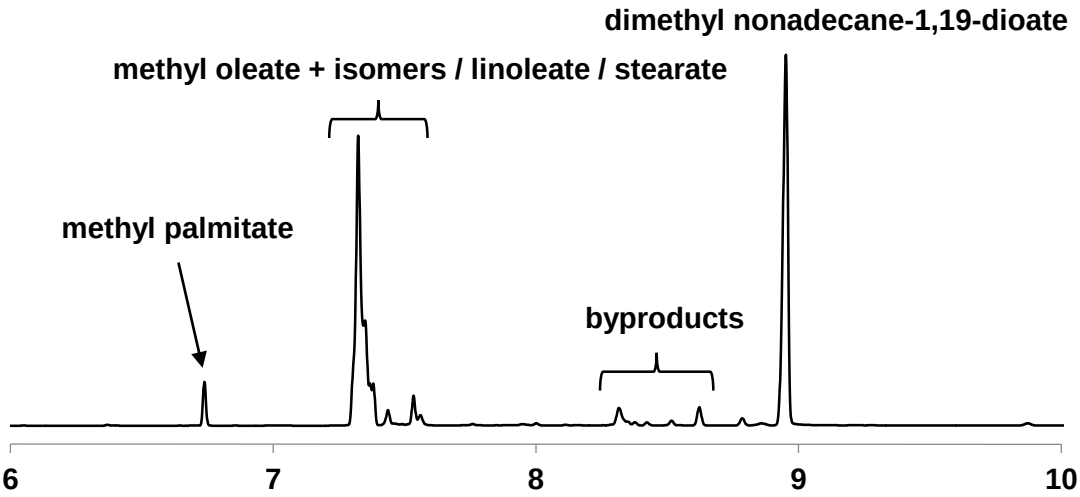


Figure S44: Gas chromatogram (time in minutes) of isomerizing methoxycarbonylation of high oleic sunflower oil methyl ester ('Dakolub MB 9001') after a reaction time of 5 h.

**Methoxycarbonylations with diphosphine Palladium(II) complexes**

Methoxycarbonylations were carried out according to the carbonylation procedure I. Catalyst precursor, reagents, reaction conditions, reaction time, conversion and selectivity are summarized in Table S1.

**Table S1: Methoxycarbonylations of methyl oleate and 1-octene with different Palladium(II) catalyst precursors.**

| complex | substrate | T | time | conversion[a)] | selectivity[b)] |
|---|---|---|---|---|---|
| [(dtbpm)Pd(OTf)$_2$][c)] | MO (techn.) | 90 °C | 90 h | < 0.5 % | - |
| [(dtbpe)Pd(OTf)$_2$][c)] | MO (techn.) | 90 °C | 90 h | < 0.5 % | - |
| [(dtbpp)Pd(OTf)$_2$][c)] | MO (techn.) | 90 °C | 18 h | 25.4 % | 82 % |
| [(dtbpp)Pd(OTf)$_2$][c)] | MO (techn.) | 90 °C | 90 h | 70.6 % | 82 % |
| [(dtbpb)Pd(OTf)$_2$][c)] | MO (techn.) | 90 °C | 90 h | < 0.5 % | - |
| [(dippp)Pd(OTf)$_2$][d)] | MO (techn.) | 90 °C | 90 h | < 0.5 % | - |
| [(depp)Pd(OTf)$_2$][d)] | MO (techn.) | 90 °C | 90 h | < 0.5 % | - |
| [(dtbpx)Pd(OTf)$_2$][c)] | MO (techn.) | 90 °C | 18 h | 94.8 % | 91 % |
| [(dtbpm)Pd(Me)Cl][d)] | MO (techn.) | 90 °C | 90 h | < 0.5 % | - |
| [(dtbpe)Pd(Me)Cl][d)] | MO (techn.) | 90 °C | 90 h | 2.3 % | 75 % |
| [(dtbpp)Pd(Me)Cl][d)] | MO (techn.) | 90 °C | 90 h | 80.7 % | 79 % |

| | | | | | |
|---|---|---|---|---|---|
| [(dtbpm)Pd(Me)Cl][e)] | 1-octene (> 99 %) | 90 °C | 90 h | 5.7 % | 73 % |
| [(dtbpe)Pd(Me)Cl][e)] | 1-octene (> 99 %) | 90 °C | 90 h | 33.8 % | 92 % |
| [(dtbpp)Pd(Me)Cl][e)] | 1-octene (> 99 %) | 90 °C | 90 h | 96.1 % | 90 % |

a) Determined from GC; for MO as a substrate: conversion = I(diesters) / I(MO in starting material); for octenes as a substrates: conversion = I(esters). b) Determined from GC; for MO as a substrate: selectivity = I(1,19-diester) / I(diesters); for octenes as a substrate: selectivity = I(methyl nonanoate) / I(esters); selectivity not determined for conversions < 0.5 %. c) Reaction conditions: n(Pd) = 0.048 mmol; V(MO) = 2 mL; V(MeOH) = 8 mL; p(CO) = 20 bar. d) Reaction conditions: n(Pd) = 0.024 mmol; V(MO) = 1 mL; V(MeOH) = 4 mL; p(CO) = 20 bar. e) Reaction conditions: n(Pd) = 0.051 mmol; V(1-octen) = 1 mL; V(MeOH) = 4 mL; p(CO) = 20 bar.

**X-ray crystal structure analysis of Palladium complexes**

[(dtbpm)Pd(Cl)$_2$], [(dtbpe)Pd(OTf)$_2$], [(dtbpb)Pd(OTf)$_2$], [(dippp)Pd(OTf)$_2$] and [(depp)Pd(OTf)$_2$] have square planar coordinated Palladium(II) centers. The coordination geometries contain the two phosphorous atoms of the chelating diphosphines with the other two coordination sites occupied by triflate oxygen atoms in [(dtbpb)Pd(OTf)$_2$] and [(depp)Pd(OTf)$_2$], by one triflate oxygen atom and one water molecule in [(dtbpe)Pd(OTf)$_2$] and [(dippp)Pd(OTf)$_2$] and by two chlorine anions in [(dtbpm)Pd(Cl)$_2$]. In [(dtbpb)Pd(OTf)$_2$] the triflate is coordinated in a bidentate fashion, whereas in [(depp)Pd(OTf)$_2$] both triflate anions are coordinated in a monodentate fashion. Water molecules coordinating in [(dtbpe)Pd(OTf)$_2$] and [(dippp)Pd(OTf)$_2$] may originate from traces of water in solvents or the trifluoromethanesulfonic acid reagent. Palladium-phosphorous bond length (vide infra) are in the typical range for these type of complexes. Bite angles (P-Pd-P, vide infra) range from 75.6° to 100.4° in [(dtbpm)Pd(Cl)$_2$] and [(dtbpb)Pd(OTf)$_2$], respectively. With increasing number of bridging methylene units between the two phosphorous moieties ([(dtbpm)Pd(Cl)$_2$], [(dtbpe)Pd(OTf)$_2$], [(dtbpp)Pd(OTf)$_2$] and [(dtbpb)Pd(OTf)$_2$]) the bite angle is increasing. In complexes with three bridging methylene units ([(dtbpp)Pd(OTf)$_2$] *vs* [(dippp)Pd(OTf)$_2$] *vs* [(depp)Pd(OTf)$_2$]) the bite angle is slightly decreasing with decreasing steric demand of the substituents on phosphorus. (*tert*-butyl in [(dtbpp)Pd(OTf)$_2$] > *iso*-propyl in [(dippp)Pd(OTf)$_2$] > ethyl in [(depp)Pd(OTf)$_2$]). However, this is not necessarily an effect of the substituents on phosphorous but rather due to the steric demand of the molecules occupying the other two coordination sites of the palladium center by only one bidentate triflate molecule in

[(dtbpp)Pd(OTf)$_2$], one triflate and one water molecule in [(dippp)Pd(OTf)$_2$] and two triflate molecules in [(depp)Pd(OTf)$_2$].

To quantify the steric demand around the palladium center we calculated the half-cone angle (vide supra), according to a previously described method,[18] from the available X-ray crystal structure data, whereas larger values indicate larger available space around the metal center. Half-cone angles of complexes [(dtbpp)Pd(OTf)$_2$], [(dtbpb)Pd(OTf)$_2$], and [(dtbpx)Pd(OTf)$_2$] are in the range of 86.1° to 87.5° and thus equal within this method. Increasing the number of bridging methylene units between the two phosphorpus moieties leads to decreasing available space around the metal center ([(dtbpm)Pd(Cl)$_2$] to [(dtbpp)Pd(OTf)$_2$]). However, the half-cone angle does not decrease significantly when four instead of three methylene units are used as a spacer. Decreasing steric demand of the substituents on phosphorous results in increasing available space around the metal center ([(dtbpp)Pd(OTf)$_2$], [(dippp)Pd(OTf)$_2$] and [(depp)Pd(OTf)$_2$]).

In the bridged hydrido-carbonyl complex [(dtbpe)Pd(μ-H)(μ-CO)Pd(dtbpe)]$^+$(OTf)$^-$ both Palladium(I) centers have square planar coordination geometry with the two phosphorous atoms of the chelating diphosphine and the other two coordination sites occupied by the bridging $\mu^2$-H and $\mu^2$-CO ligands. The Pd-Pd bond length is 2.7666(3) Å and is thus in the same range as previously reported for a similar complex by Milstein and co-workers.[21] The Pd-P bond length slightly increases by ca. 0.1 Å compared to the respective [(dtbpe)Pd(OTf)$_2$] complex and also the bite angle slightly inreases by 0.5°. Pd-H bond lengths of 1.72(2) and 1.69(2) Å, respectively, are increased by ca. 0.1 Å as compared to e.g. the previously published isolated hydride [(dtbpx)PdH(PPh$_3$)]$^+$(OTf)$^-$.[18]

In [(dtbpx)Pd($\eta^3$-C$_4$H$_7$)]$^+$(OTf)$^-$, the square planar coordination sphere around the Palladium(II) center is formed by the chelating diphosphine with the two other coordination sites occupied by the carbon atoms C1 and C3 of the butenyl ligand. The Pd-C2 distance is shorter than the Pd1-C1 and Pd1-C3 bond distances, respectively, as C2 is located above the square planar coordination sphere and the triangle C1-C2-C3 is tilted with its C2-tip towards the Pd-center. Bond distances C1-C2 and C2-C3 are nearly equal (1.376(6) versus 1.393(7) Å). With an average value of 1.385 Å these bond distances are in the typical range for aromatic systems, thus indicating delocalization of the double bound through the C1, C2 and C3 carbon atoms. In a previous study on the telomerization of 1,3-butadiene similar values were observed for C-C bond distances in a butenyl-diphosphine Palladium(II) complex.[22]

**Table S2: Half cone angles and selected bond angles and distances of Pd-complexes**

| compound | half cone angle / ° | bite angle / ° | Pd-P bond lengths / Å |
|---|---|---|---|
| [(dtbpm)Pd(Cl)$_2$] | 106.7 | 75.591(19) | 2.2633(5)<br>2.2578(5) |
| [(dtbpe)Pd(OTf)$_2$] | 96.3 | 87.677(18) | 2.2641(5)<br>2.2473(5) |
| [(dtbpp)Pd(OTf)$_2$][a)] | 87.5<br>87.5 | 96.92(7)<br>95.79(7) | 2.279(2)<br>2.267(2)<br>2.2589(19)<br>2.260(2) |
| [(dtbpb)Pd(OTf)$_2$] | 86.4 | 100.444(14) | 2.2607(4)<br>2.2778(4) |
| [(dippp)Pd(OTf)$_2$] | 98.8 | 94.553(18) | 2.2443(5)<br>2.2391(5) |
| [(depp)Pd(OTf)$_2$] | 111.9 | 93.62(2) | 2.2258(6)<br>2.2249(6) |
| [(dtbpx)Pd(OTf)$_2$][a)] | 86.1 | 99.30(2) | 2.2607(6)<br>2.2808(6) |
| [(dtbpe)Pd(μ-H)(μ-(CO)Pd(dtbpe)]$^+$(OTf)$^-$ | 99.0<br>99.5 | 88.07(3)<br>88.21(3) | 2.3697(7)<br>2.3861(7)<br>2.3647(7)<br>2.4137(7) |
| [(dtbpx)Pd($\eta^3$-C$_4$H$_7$)]$^+$(OTf)$^-$ | 89.3 | 103.05(3) | 2.3584(9)<br>2.3623(9) |

a) Previously reported data from our group was used for [(dtbpp)Pd(OTf)$_2$] (CCDC 893845) and [(dtbpx)Pd(OTf)$_2$] (CCDC 817578).

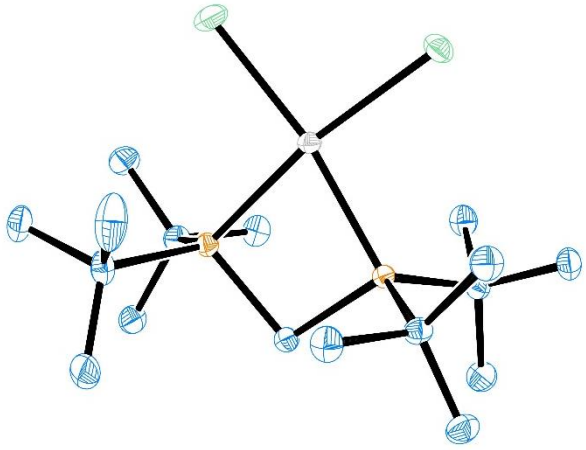

Figure S45: X-ray crystal structure of [(dtbpm)Pd(Cl)$_2$] (CCDC 1010350). Hydrogen atoms were omitted for clarity. Displacement ellipsoids are shown at the 50 % probability level.

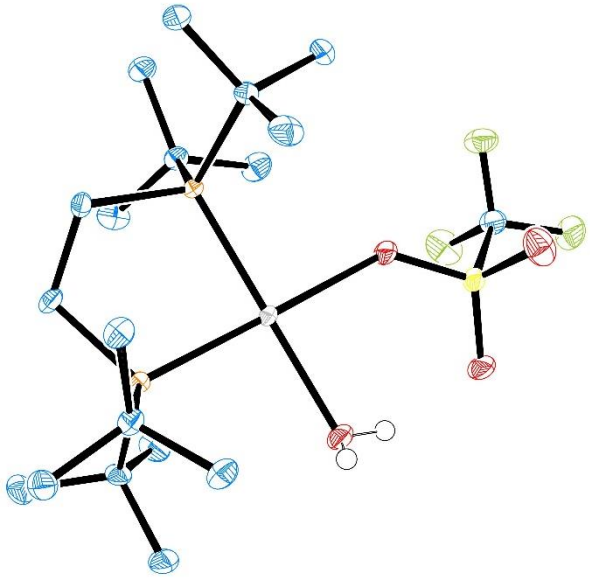

Figure S46: X-ray crystal structure of [(dtbpe)Pd(OTf)$_2$] (CCDC 1010349). Hydrogen atoms (except from coordinated water) and a non-coordinating triflate counterion were omitted for clarity. Displacement ellipsoids are shown at the 50 % probability level.

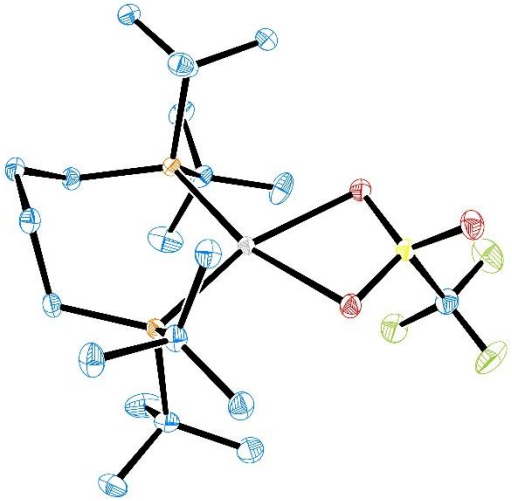

Figure S47: X-ray crystal structure of [(dtbpb)Pd(OTf)$_2$] (CCDC 1010347). Hydrogen atoms and a non-coordinating triflate counterion were omitted for clarity. Displacement ellipsoids are shown at the 50 % probability level.

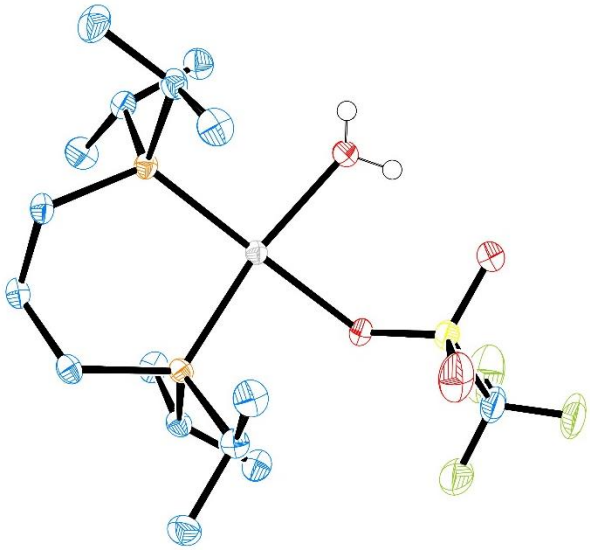

Figure S48: X-ray crystal structure of [(dippp)Pd(OTf)$_2$] (CCDC 1010346). Hydrogen atoms (except from coordinated water) and a non-coordinating triflate counterion were omitted for clarity. Displacement ellipsoids are shown at the 50 % probability level.

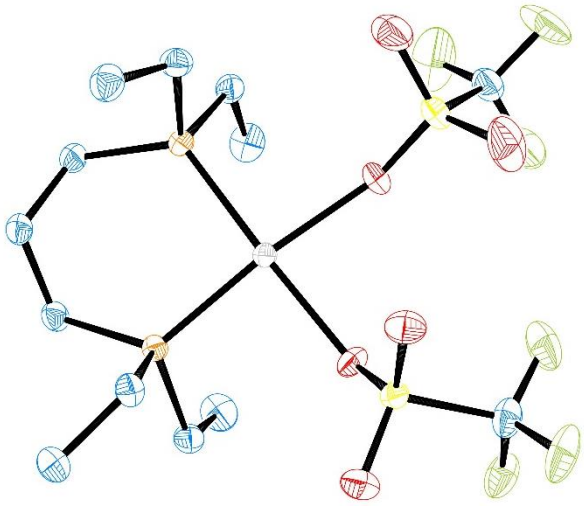

Figure S49: X-ray crystal structure of [(depp)Pd(OTf)$_2$] (CCDC 1010345). Hydrogen atoms were omitted for clarity. Displacement ellipsoids are shown at the 50 % probability level.

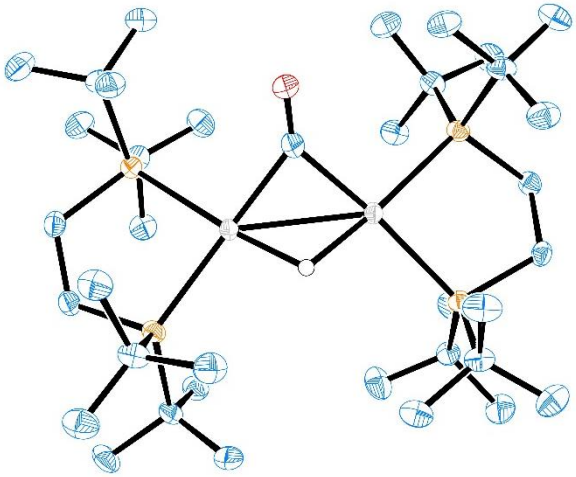

Figure S50: X-ray crystal structure of [(dtbpe)Pd(μ-H)(μ-(CO)Pd(dtbpe)]$^+$(OTf)$^-$ (CCDC 1010348). Hydrogen atoms (except $\mu^2$-H) and a non-coordinating triflate counterion were omitted for clarity. Displacement ellipsoids are shown at the 50 % probability level.

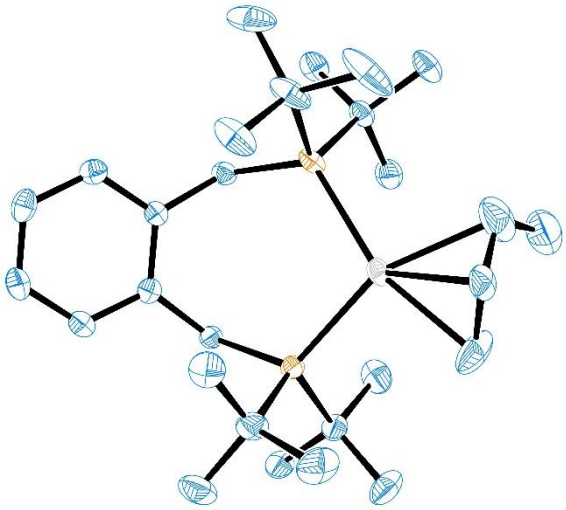

Figure S51: X-ray crystal structure of [(dtbpx)Pd($\eta^3$-$C_4H_7$)]$^+$(OTf)$^-$ (CCDC 1010351). Hydrogen atoms and a non-coordinating triflate counterion were omitted for clarity. Displacement ellipsoids are shown at the 50 % probability level.

**Byproducts in isomerizing alkoxycarbonylation of methyl linoleate**

The carbonylation was carried out according to the carbonylation procedure II using 29.5 mmol (8.7 g, 9.8 mL) methyl linoleate (> 99 %), 0.235 mmol (188 mg) of the [(dtbpx)Pd(OTf)$_2$] catalyst precursor, 20 bar CO, at 90 °C in methanol at a total volume of 180 mL. After an overall reaction time of 190 h, the reaction was stopped, the crude reaction mixture was diluted with methylene chloride and filtered to remove Pd-black. To identify the byproducts and to calculate the selectivity of the reaction, the crude reaction mixture was hydrogenated using Pd/charcoal in a methanol/ethyl acetate mixture (1/1 by volume) at atmospheric hydrogen pressure. Complete hydrogenation was proved by the absence of any olefinic signal in $^{1}$H and $^{13}$C NMR spectroscopy. Conversion was calculated via GC from the remaining signal of methyl stearate after hydrogenation of the crude reaction mixture (conversion = 100 % - integral (methyl stearate)). Selectivity was calculated via GC from the signal of the linear 1,19-diester and the conversion after hydrogenation of the crude reaction mixture (selectivity = integral (linear 1,19-diester) / conversion).

To identify byproducts, the hydrogenated reaction mixture was crystallized from methanol twice to remove substantial amounts of methyl stearate and the linear 1,19-diester (note that both methyl stearate and the linear 1,19-diester were not completely removed by these crystallizations). The supernatant of the recrystallization was then separated by column chromatography (eluent: ethyl acetate/pentane = 1/10 by volume) into 4 different fractions (a-d) which were then used to identify the byproducts by NMR spectroscopy and ESI-MS. In addition to the known, branched byproducts also formed in the isomerizing alkoxycarbonylation of methyl oleate,[18] 4 more byproducts were identified: a triester, formed by double alkoxycarbonylation of the substrate, a methoxy substituted diester, formed by mono alkoxycarbonylation and hydromethoxylation of the remaining double bond of the substrate, a C18 keto monoester product, and a terminal dimethylacetal monoester. The first three were identified by NMR spectroscopy ($^{1}$H, $^{13}$C, $^{1}$H,$^{1}$H-COSY, $^{1}$H,$^{13}$C-HSQC, $^{1}$H,$^{13}$C-HMBC) and ESI-MS and GC. The latter was identified by NMR spectroscopy only.

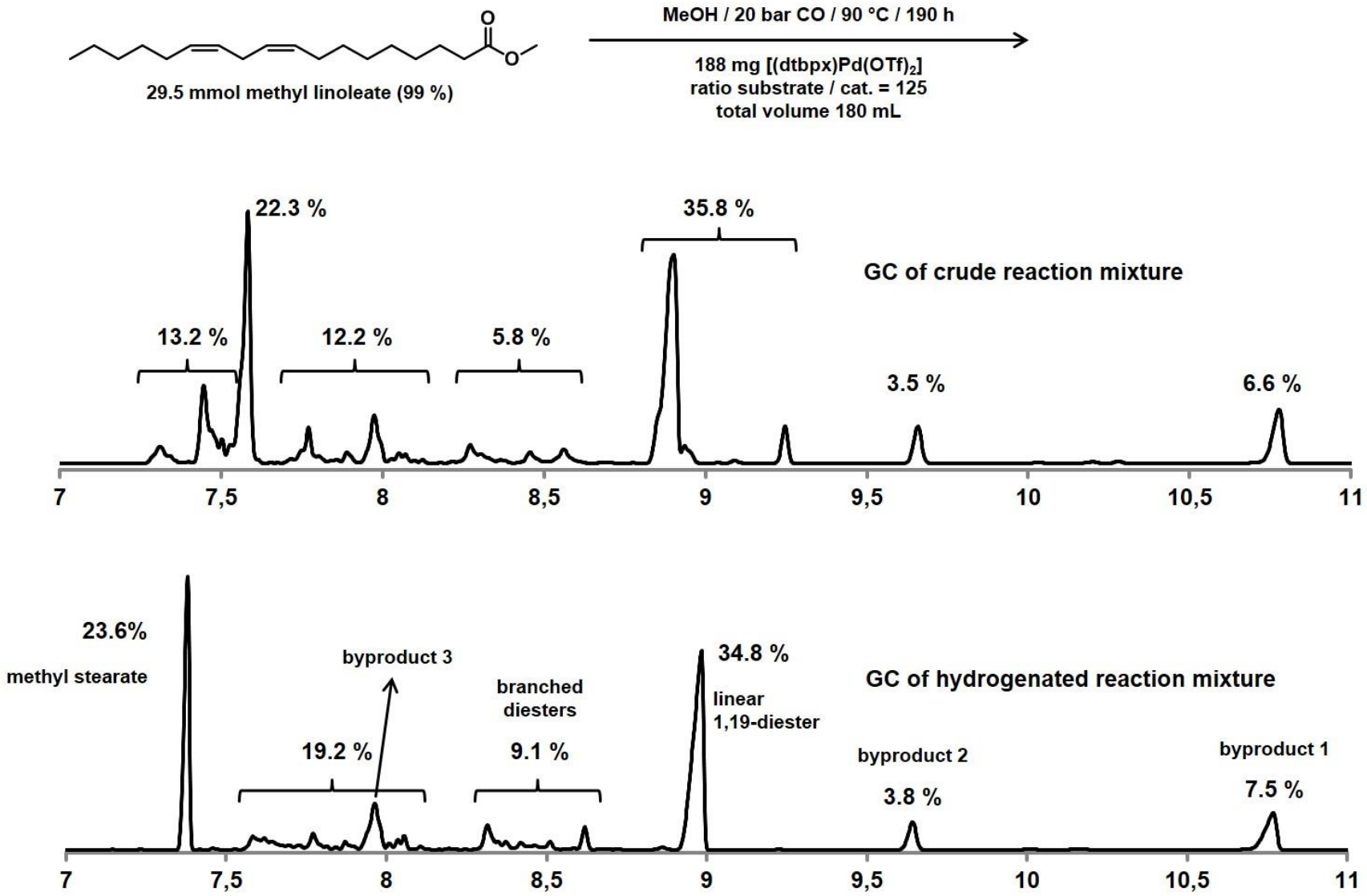


Figure S52: GC of crude reaction mixture before (top) and after (bottom) hydrogenation.

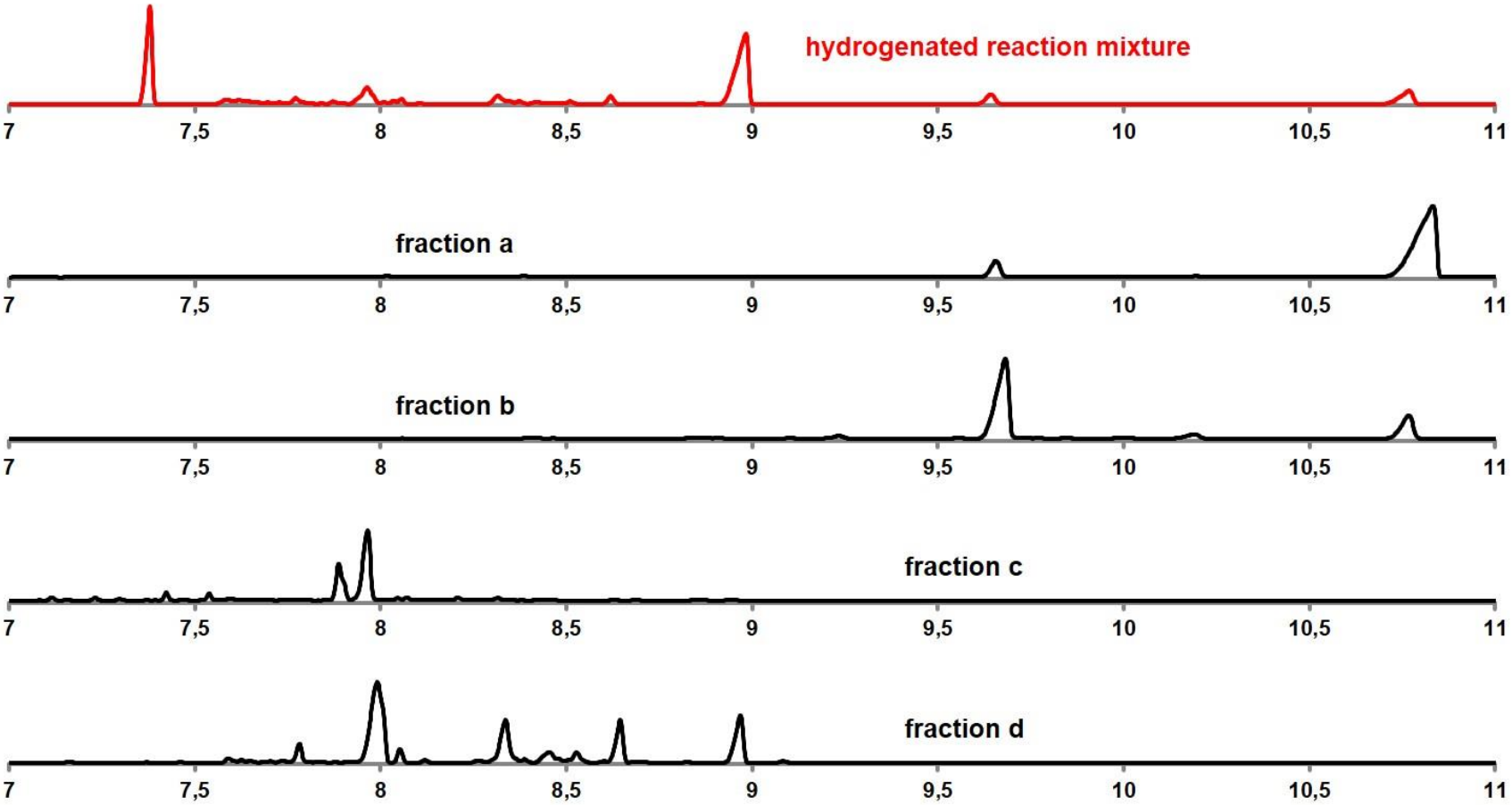


Figure S53: GC traces of hydrogenated reaction mixture (top, red) and the four fractions obtained by column chromatography.

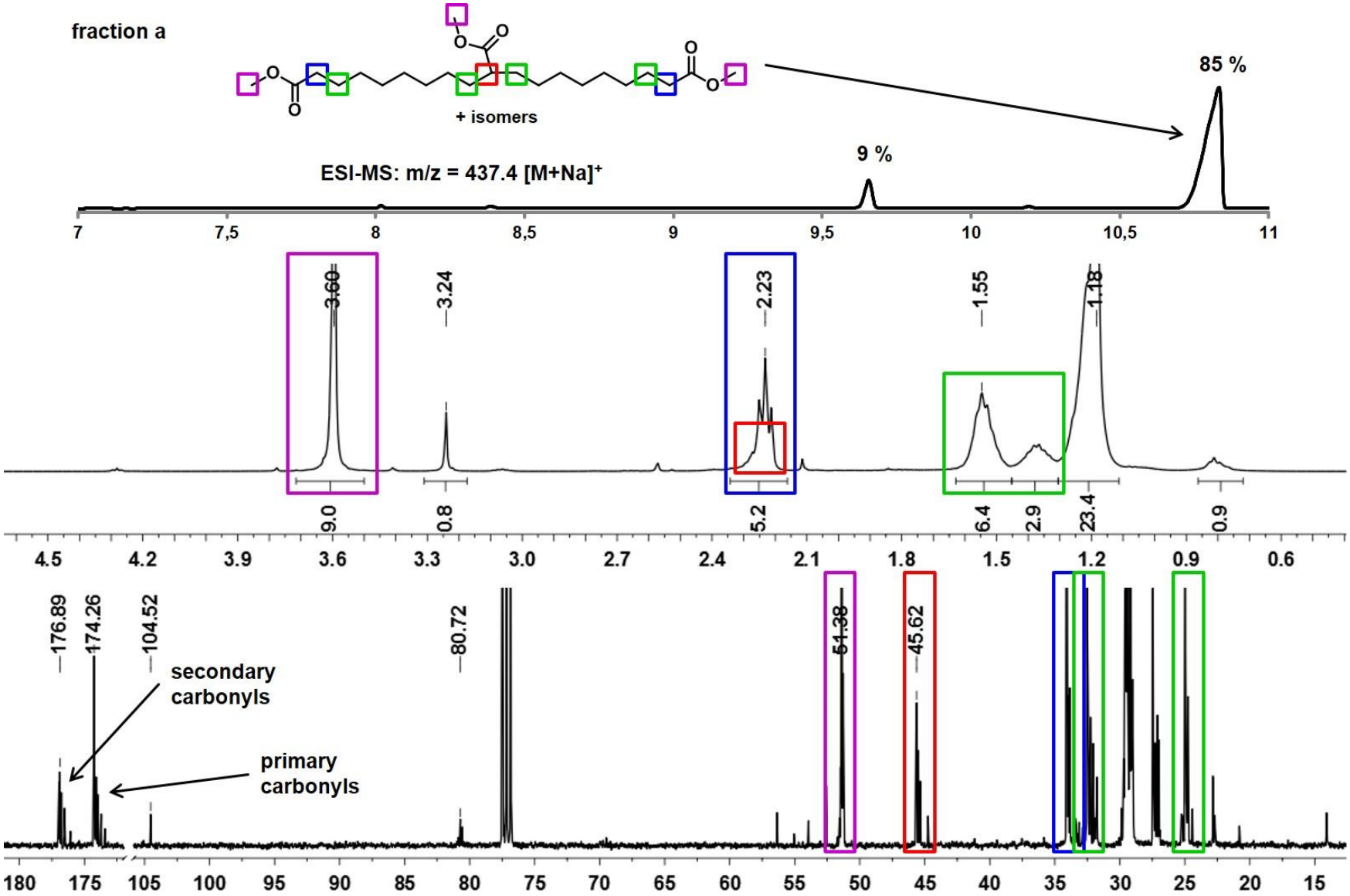


Figure S54: GC trace and $^{1}H$ (top) and $^{13}C$ (bottom) NMR spectra of fraction a (byproduct 1 is identified).

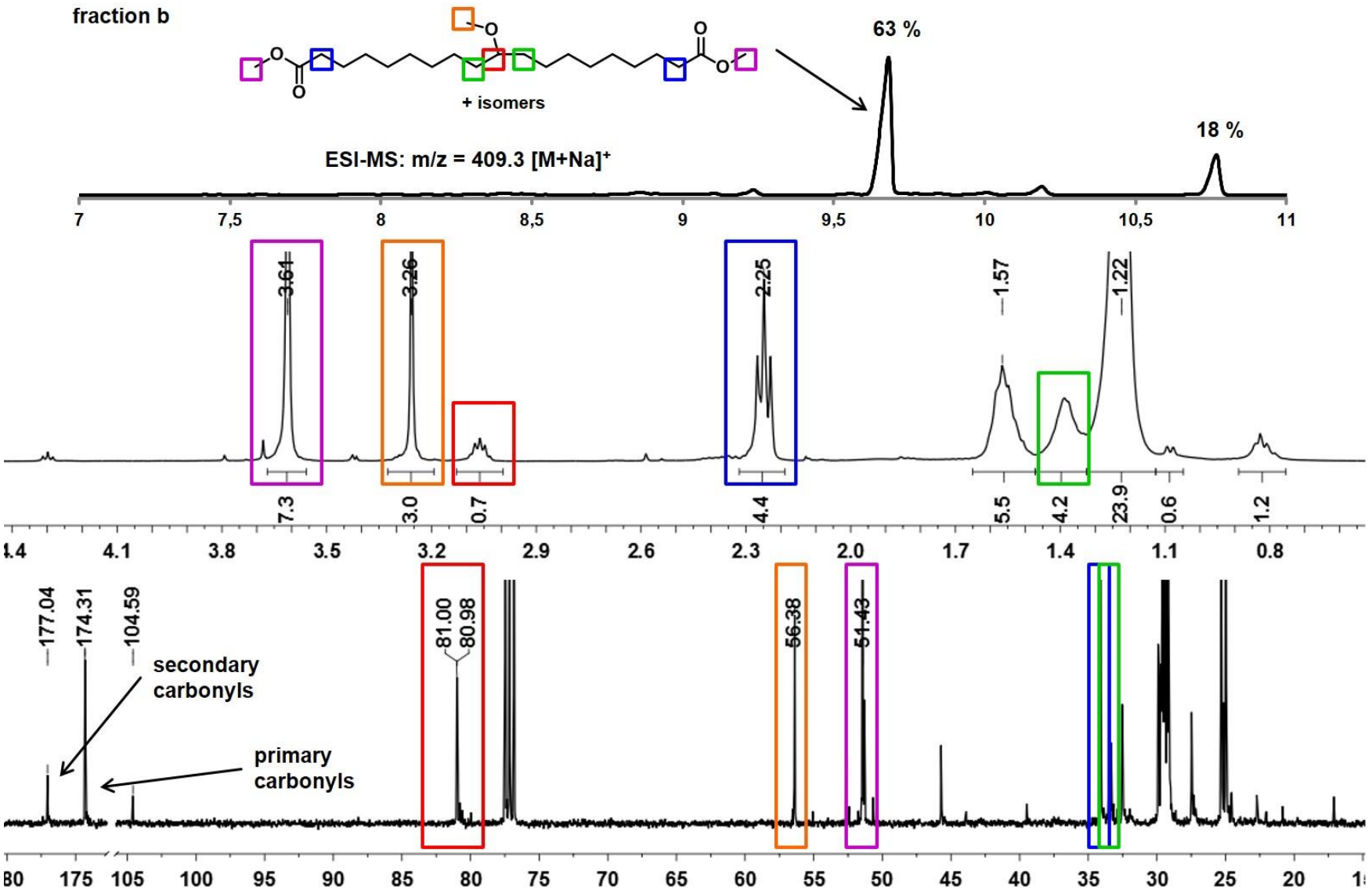


Figure S55: GC trace and $^{1}H$ (top) and $^{13}C$ (bottom) NMR spectra of fraction b (byproduct 2 is identified).

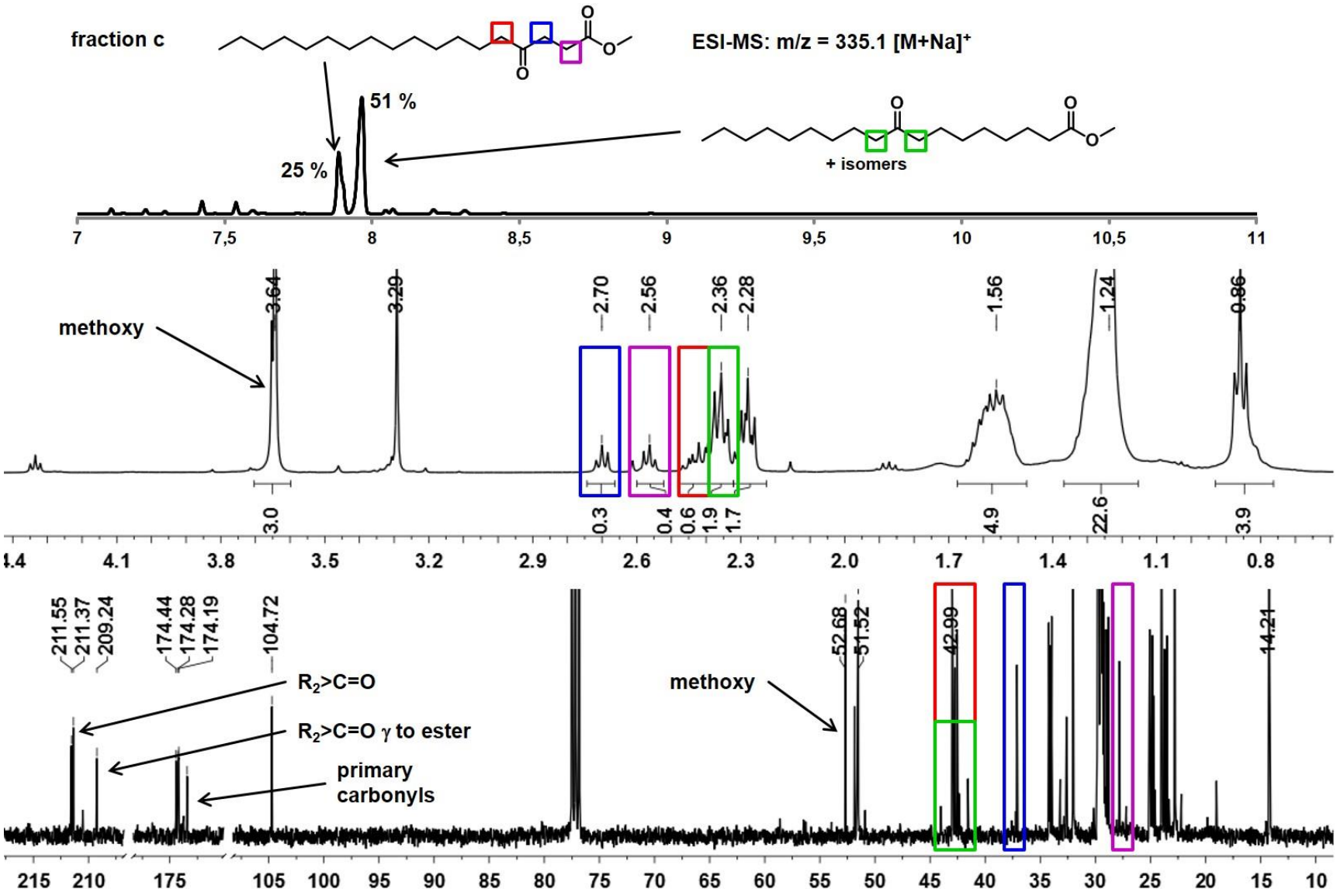


Figure S56: GC trace and $^{1}H$ (top) and $^{13}C$ (bottom) NMR spectra of fraction c (byproduct 3 is identified).

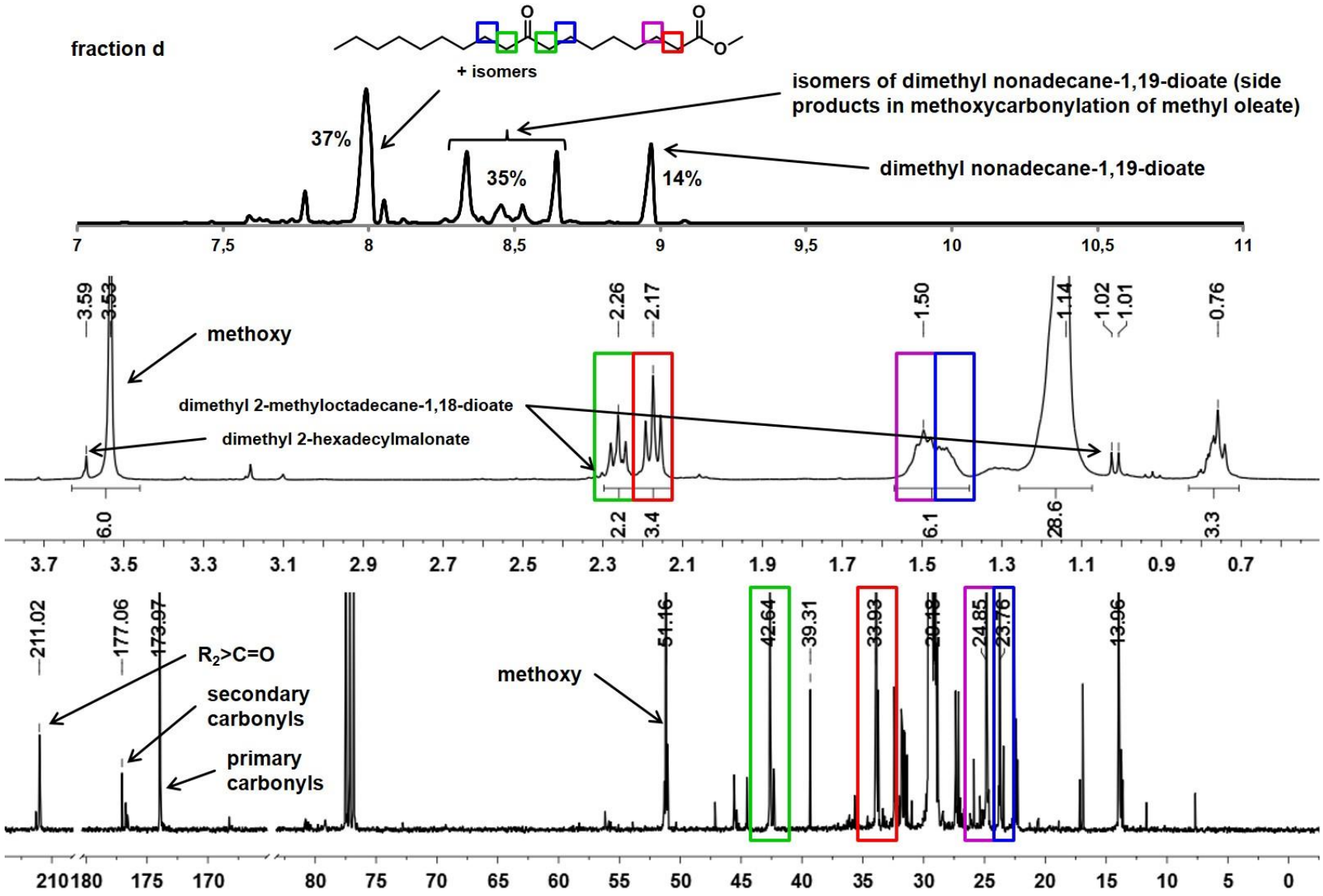


Figure S57: GC trace and $^{1}H$ (top) and $^{13}C$ (bottom) NMR spectra of fraction d (byproduct 3 is identified).

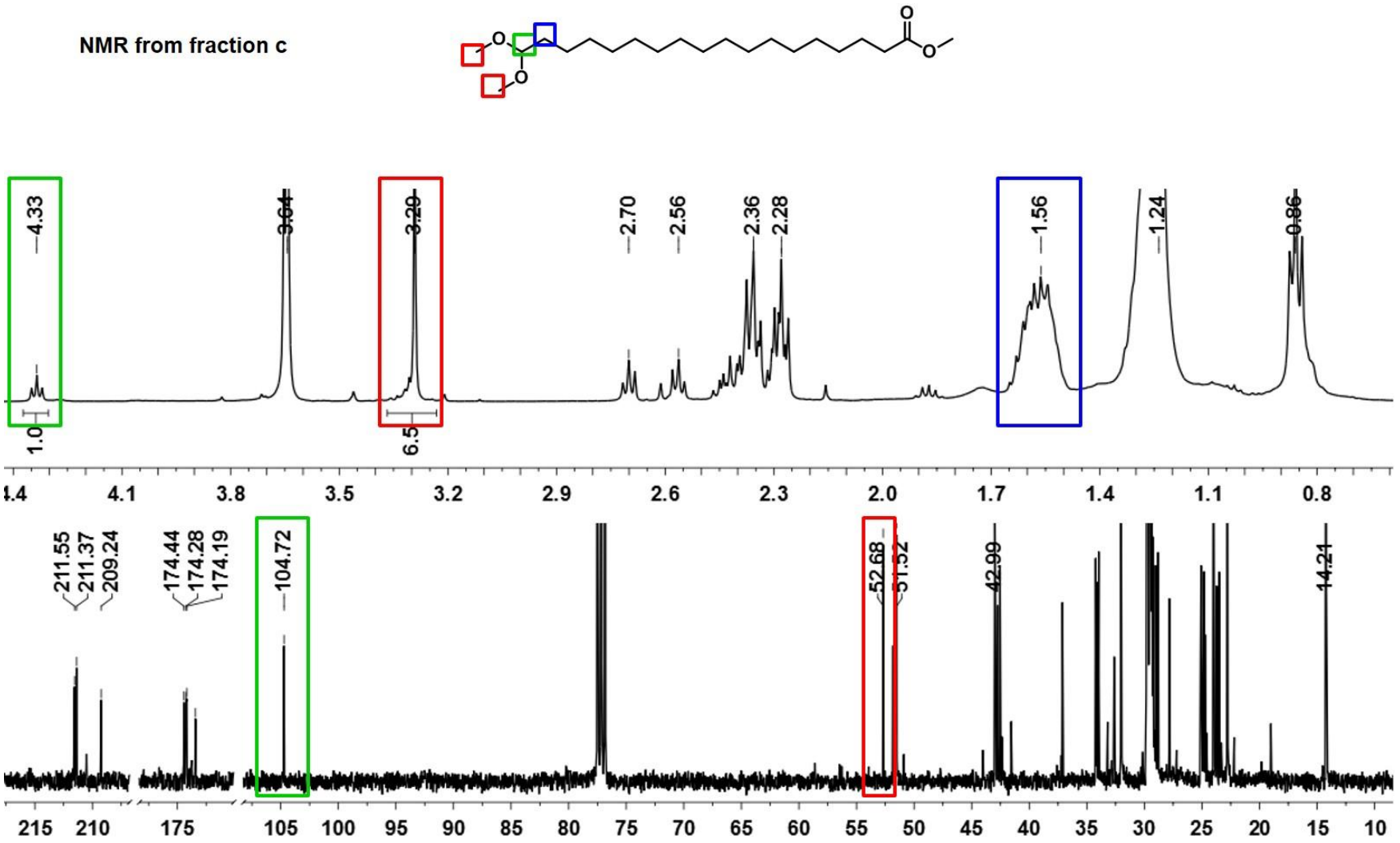


Figure S58: $^{1}H$ (top) and $^{13}C$ (bottom) NMR spectra of fraction c with the assigned signals of the dimethylacetal monoester.

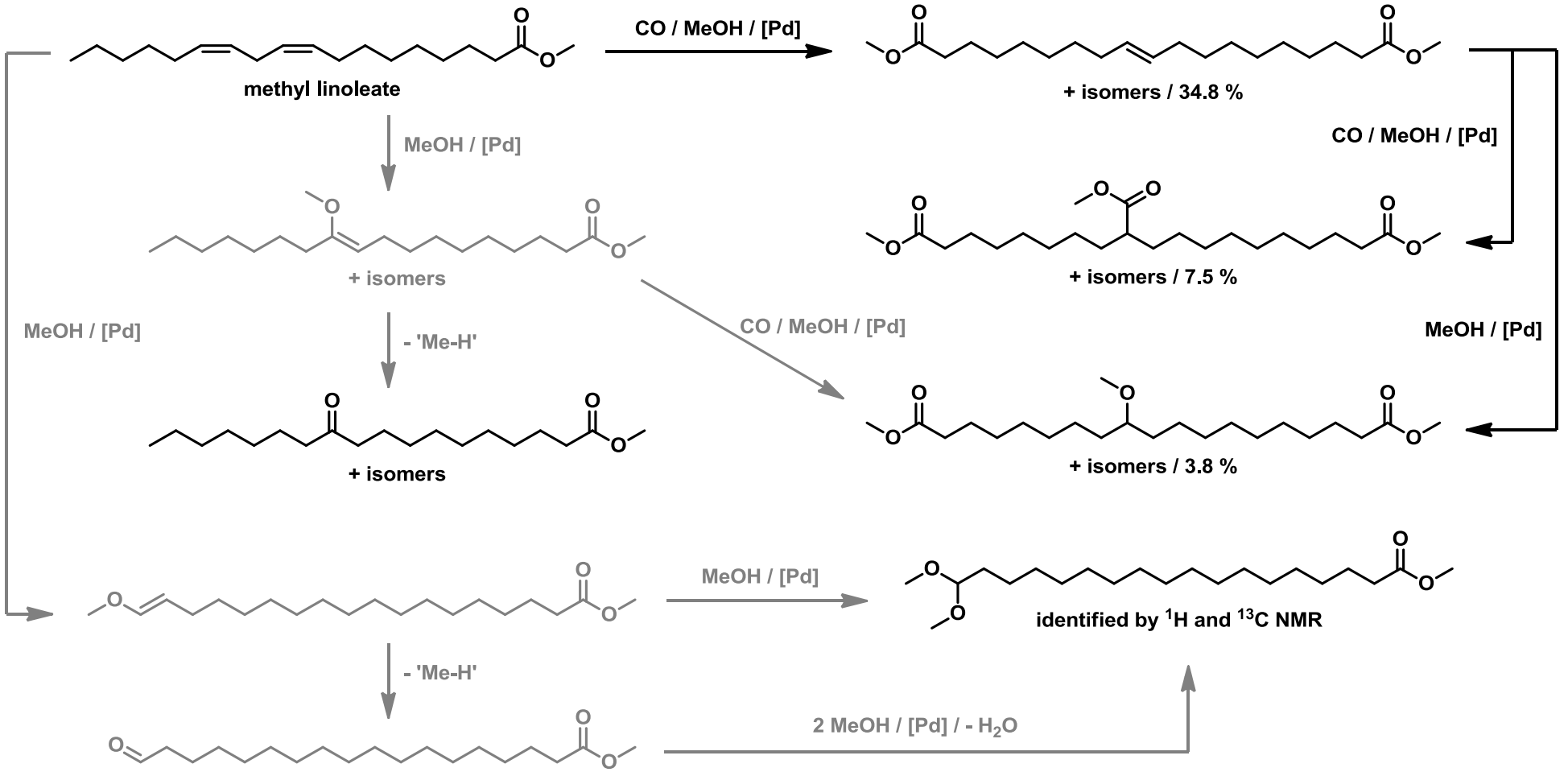


Figure S59: Possible reaction pathways leading to the identified byproducts. Compounds in black were identified, compounds and pathways drawn in grey are hypothetical.

**Computational details**

DFT calculations were performed with the Gaussian09 package[23] using the B3LYP[24] functional and the LANL2DZ ECP[25] with the associated valence basis set on the Pd-atom, and the 6-31G(d)[26] basis set on all the other atoms. All geometries were localized in the gas phase at the B3LYP level. Minima were localized by full optimization of the starting structures, while transition states were approached through a linear transit procedure starting from the coordination intermediate and then located by a full transition state search. All structures were confirmed as minimum or transition state through frequency calculations. In addition, single point energy calculations with the triple-ζ plus polarization TZVP basis set were performed on selected Pd-alkyl species (**5-β-4**, **5-β-6** and **7-β-6**) to validate the chemical scenario derived with the 6-31G(d) basis set. Isomerization reactions, were studied via classical metal hydride insertion/β-H-elimination mechanism using methyl 4-hepteneoate as a model substrate, with the sterically demanding 1,2-$(CH_2P^tBu_2)_2C_6H_4$ (dtbpx) diphosphine and the less demanding 1,2-$(CH_2PMe_2)_2C_6H_4$ (dmpx) diphosphine Palladium(II) hydride fragments $[(P\hat{}P)Pd(H)]^+$. Calculations on the CO insertion reactions and the following methanolysis reactions were performed starting from the linear Pd-alkyl species $[(P\hat{}P)Pd(CH_2)_6COOCH_3]^+$ (**7-β-6**), the branched Pd-alkyl species $[(P\hat{}P)PdCH(CH_3)\{(CH_2)_4COOCH_3\}]^+$ (**6-β-5** or **6-β-7**, respectively, depending on which of them is energetically favored), $[(P\hat{}P)PdCH(CH_2CH_3)\{(CH_2)_3COOCH_3\}]^+$ (**5-β-4**), $[(P\hat{}P)PdCH\{(CH_2)_3CH_3\}(CH_2COOCH_3)]^+$ (**5-m.c.**), and $[(P\hat{}P)PdCH\{(CH_2)_4CH_3\}COOCH_3]^+$ (**4-m.c.**), with the 1,2-$(CH_2P^tBu_2)_2C_6H_4$ (dtbpx)[17] and 1,2-$(CH_2PMe_2)_2C_6H_4$ (dmpx) coordinated Palladium center. For the CO insertion reaction into the Pd-alkyl species, the CO coordination intermediate (**CO-Coord**), the CO insertion transition state (**CO-Ins-TS**), and the corresponding CO insertion product (Pd-Acyl) was calculated.[17] For almost all Pd-Acyl species, the three membered $\eta^2$-Pd-acyl intermediate is lowest in energy, except for the CO insertion product formed from **4-m.c** for dtbpx[17] and dmpx which results in a five-membered chelate Pd-acyl, and from **5-m.c.** for dmpx which results in a six-membered chelate Pd-acyl. The methanolysis reaction pathway with a three MeOH molecules cluster (methanol coordination **3MeOH-Coord** and methanolysis transition state **3MeOH-TS**) and with a single MeOH molecule (methanol coordination **MeOH-Coord** and methanolysis transition state **MeOH-TS**) were compared for all species with both systems dtbpx and dmpx. As in our previous publication,[17] the methanolysis reaction pathway with a three MeOH molecules cluster is favored for the linear dtbpx coordinated Pd-acyl species while in case of the more hindered branched dtbpx coordinated Pd-acyl species the reaction pathway with a single MeOH molecule is lower in energy. The lowest reaction pathways for complexes

dtbpx[17] and dmpx with Gibbs free energy in kcal/mol, are reported in Figures S63 and S64. The calculations for **7-β-6** and **5-m.c.** with dtbpx are those already reported in ref. 17, with exception of the **3MeOH-TS** for **7-β-6**. The new TS herein reported is more stable than the corresponding TS in ref. 17 by 0.6 kcal/mol.

**Isomerization along the hydrocarbon chain:**

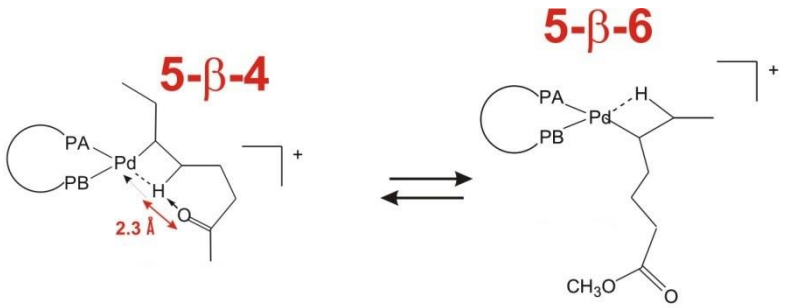


Figure S60: Favorable interaction of the substrates ester group with the β-hydrogen atom interacting with the metal center in **5-β-4** (left) thus being energetically favored over **5-β-6** (right), for the dmpx coordinated metal center.

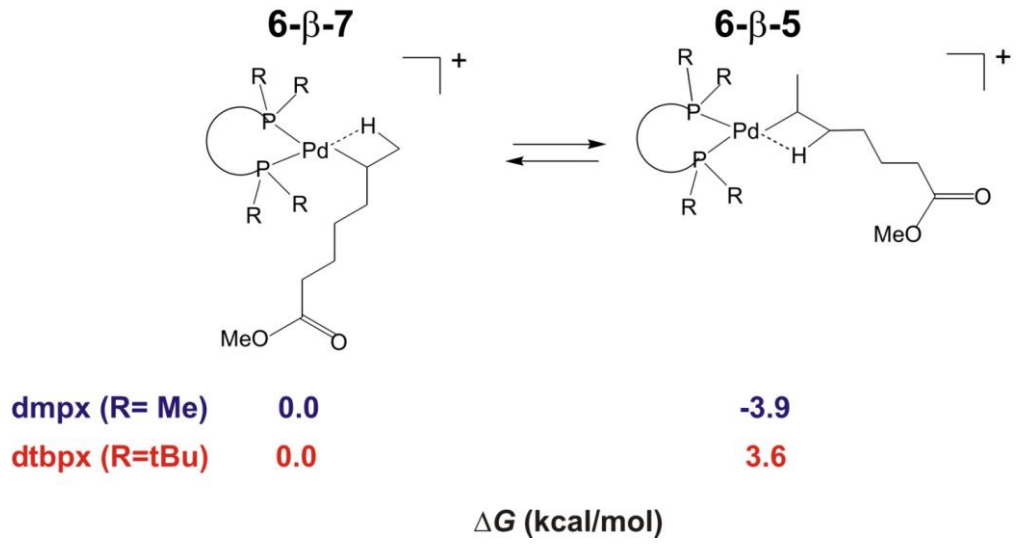


Figure S61: Energy differences (ΔG, kcal/mol) of **6-β-7** *versus* **6-β-5** with the dtbpx and dmpx coordinated metal center. From electronic point of view **6-β-5** is favored because the beta agostic interaction involves an H atom bound to a secondary carbon atom, whereas in **6-β-7** it is bound to a primary carbon atom. From steric point of view **6-β-7** is favored because its less steric demanded. As a consequence **6-β-7** is favored for the encumbered dtbpx coordinated metal center and **6-β-5** is favored for the less encumbered dmpx coordinated metal center.

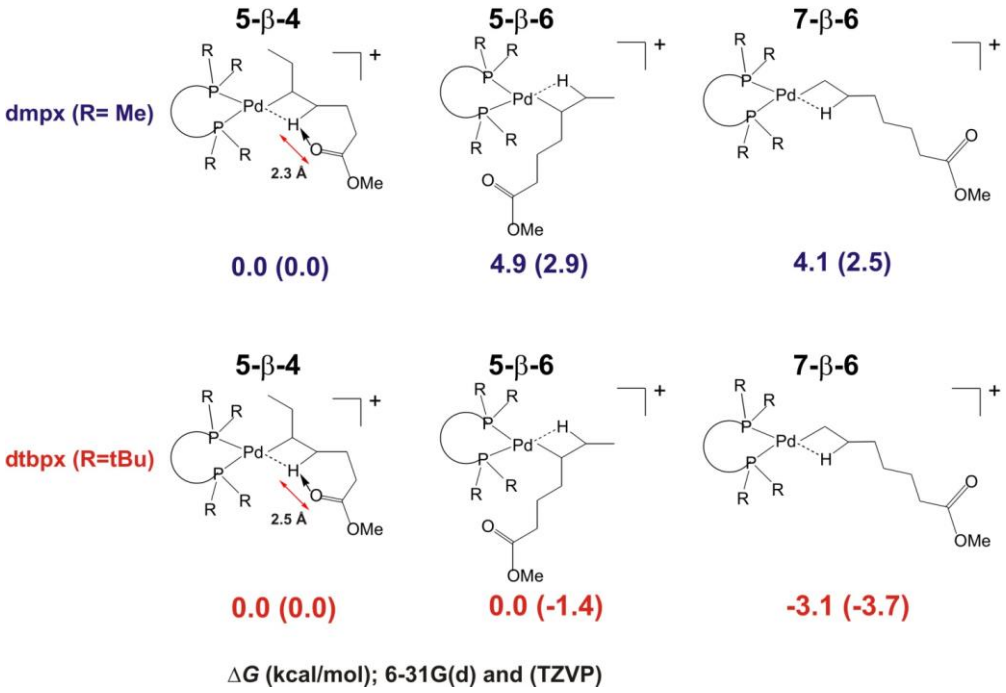


Figure S62: Free energies (ΔG, kcal/mol) obtained with the 6-31G(d) and the TZVP (values in brackets) basis sets for the **5-β-4**, **5-β-6** and **7-β-6** alkyl species with the dmpx (blue, top) and the dtbpx (red, bottom) coordinated Pd(II)-center. The free energy values given are relative to the energy of **5-β-4** as a reference point, set to zero. For both ligands, the energetic series of these Pd-alkyl species are replicated by the single point energy calculation with the TZVP basis set, although energy differences are different.

**Methanolysis of Pd-acyl species:**

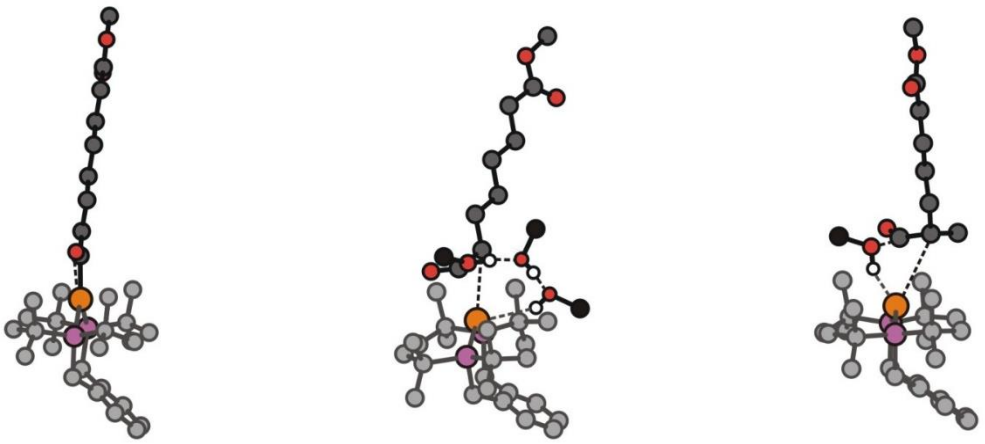

Figure S63: The dtbpx coordinated linear Pd-acyl species $[(dtbpx)PdC(=O)(CH_2)_6COOMe]^+$ (left), the three methanol coordinated transition state of methanolysis of this linear Pd-acyl species (middle), and the single methanol coordinated transition state of methanolysis of the methyl branched acyl species $[(dtbpx)PdC(=O)CH(CH_3)\{(CH_2)_4COOMe\}]^+$.

**Energy profiles of DFT studies:**

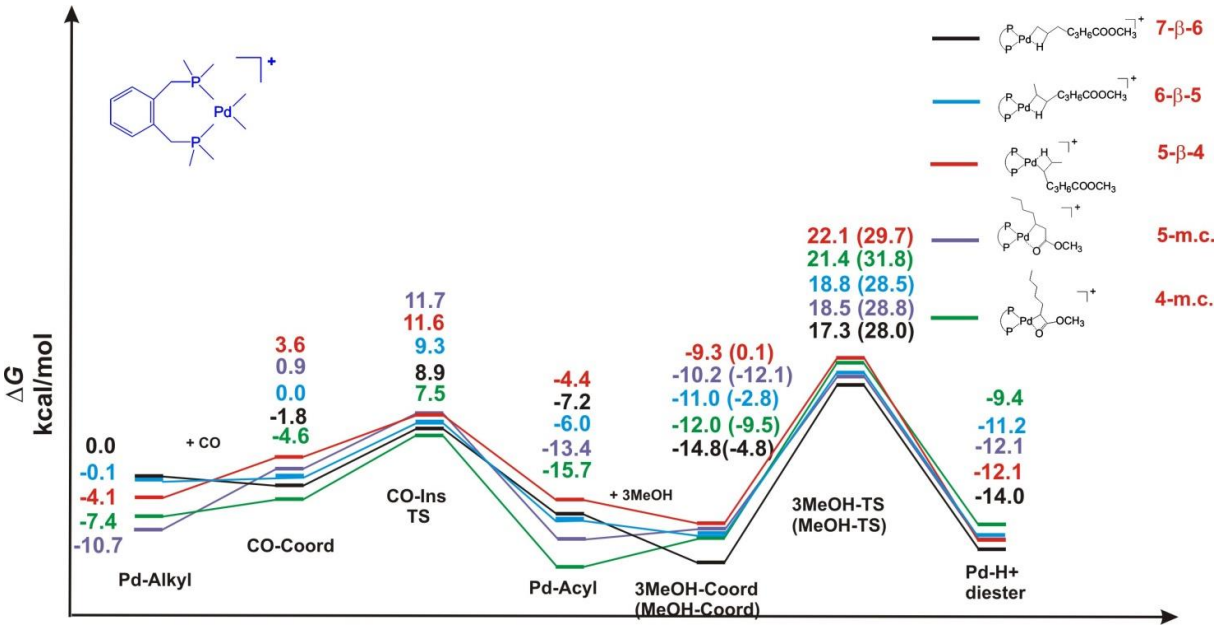


Figure S64: DFT calculations of the energy profile of CO insertion and methanolysis reaction of the dmpx coordinated Pd-alkyl species.

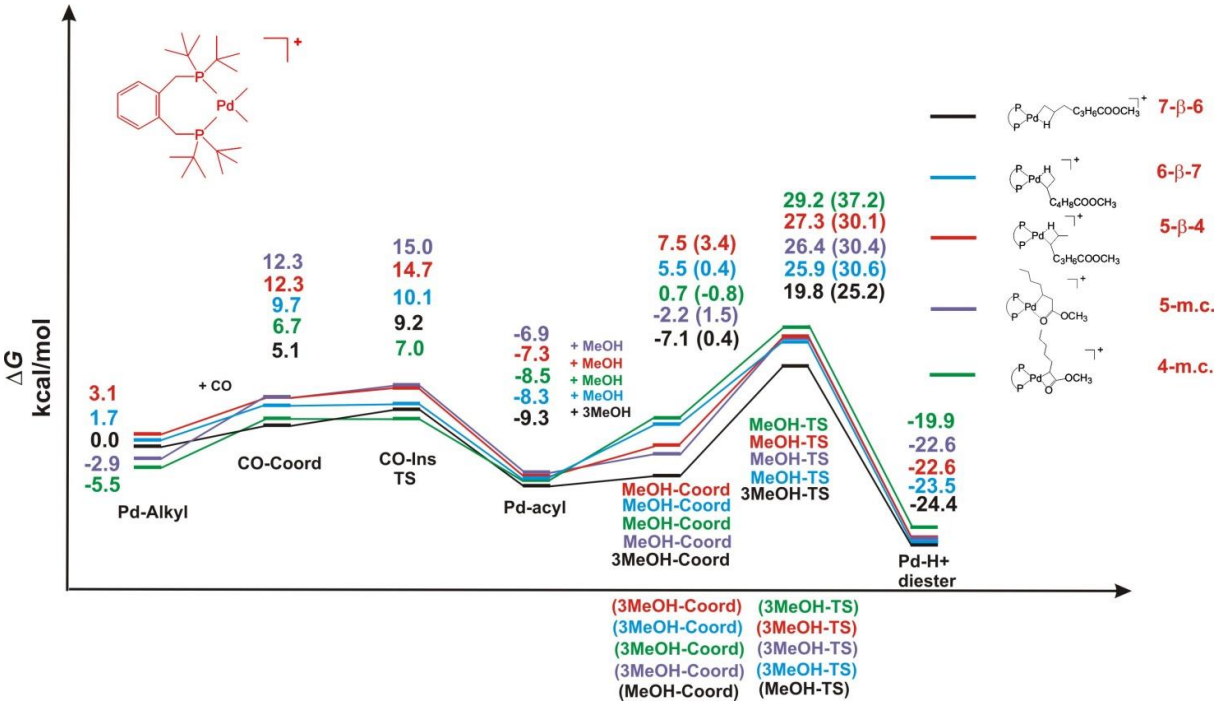


Figure S65: DFT calculations of the energy profile of CO insertion and methanolysis reaction of the dtbpx coordinated Pd-alkyl species.

**Table S3: Internal energy (E) and free energy (G) in gas phase (in Hartrees) of isomerization along the hydrocarbon chain of the model substrate methyl heptenoate with the dtbpx coordinated Pd-hydride species.**

| | dtbpx_7_beta_6 | dtbpx_7_beta_6_BHE_TS | dtbpx_Me_6_heptenoate_Coor | dtbpx_6_beta_7_BHE_TS | dtbpx_6_beta_7 |
|---|---|---|---|---|---|
| **E** | -2214.682936 | -2214.667742 | -2214.668608 | -2214.66368 | -2214.67984 |
| **G** | -2213.905380 | -2213.892894 | -2213.892815 | -2213.888 | -2213.902718 |
| | **dtbpx_6_beta_5** | **dtbpx_6_beta_5_BHE_TS** | **dtbpx_Me_5_heptenoate_Coor** | **dtbpx_5_beta_6_BHE_TS** | **dtbpx_5_beta_6** |
| **E** | -2214.6762 | -2214.6666 | -2214.6697 | -2214.66634 | -2214.6799 |
| **G** | -2213.8970 | -2213.8893 | -2213.8944 | -2213.89054 | -2213.9005 |
| | **dtbpx_5_beta_4** | **dtbpx_5_beta_4_BHE_TS** | **dtbpx_Me_4_heptenoate_Coor** | **dtbpx_4_beta_5_BHE_TS** | **dtbpx_4_beta_5** |
| **E** | -2214.682829 | -2214.6688 | -2214.67303 | -2214.66517 | -2214.68049 |
| **G** | -2213.90046 | -2213.8926 | -2213.89572 | -2213.88903 | -2213.90035 |
| | **dtbpx_4_beta_3** | **dtbpx_4_beta_3_BHE_TS** | **dtbpx_Me_3_heptenoate_Coor** | **dtbpx_3_beta_4_BHE_TS** | **dtbpx_3_beta_4** |
| **E** | -2214.68301 | -2214.66685 | -2214.6701 | -2214.6646 | -2214.6806 |
| **G** | -2213.90097 | -2213.89012 | -2213.8948 | -2213.8878 | -2213.8994 |
| | **dtbpx_3_beta_2** | **dtbpx_3_beta_2_BHE_TS** | **dtbpx_Me_2_heptenoate_Coor** | **dtbpx_2_beta_3_BHE_TS** | **dtbpx_2_beta_3** |
| **E** | -2214.68221 | -2214.66703 | -2214.67261 | -2214.6712 | -2214.68915 |
| **G** | -2213.90158 | -2213.88891 | -2213.89482 | -2213.89292 | -2213.90757 |
| | **dtbpx_5MC** | **dtbpx_4MC** | **dtbpx_Pd_H** | | |
| **E** | -2214.695609 | -2214.697274 | -1750.933994 | | |
| **G** | -2213.910067 | -2213.914227 | -1750.351441 | | |

**Table S4: Internal energy (E) and free energy (G) in gas phase (in Hartrees) of isomerization along the hydrocarbon chain of the model substrate methyl heptenoate with the dmpx coordinated Pd-hydride species.**

| | dmpx_7_beta_6 | dmpx_7_beta_6_BHE_TS | dmpx_Me_6_heptenoate_Coor | dmpx_6_beta_7_BHE_TS | dmpx_6_beta_7 |
|---|---|---|---|---|---|
| **E** | -1742.981874 | -1742.967954 | -1742.969629 | -1742.96498 | -1742.97681 |
| **G** | -1742.533826 | -1742.522722 | -1742.52304 | -1742.51938 | -1742.52779 |
| | **dmpx_6_beta_5** | **dmpx_6_beta_5_BHE_TS** | **dmpx_Me_5_heptenoate_Coor** | **dmpx_5_beta_6_BHE_TS** | **dmpx_5_beta_6** |
| **E** | -1742.983764 | -1742.9711 | -1742.9734 | -1742.96804 | -1742.98211 |
| **G** | -1742.534043 | -1742.5243 | -1742.5274 | -1742.52296 | -1742.53257 |
| | **dmpx_5_beta_4** | **dmpx_5_beta_4_BHE_TS** | **dmpx_Me_4_heptenoate_Coor** | **dmpx_4_beta_5_BHE_TS** | **dmpx_4_beta_5** |
| **E** | -1742.989327 | -1742.9709 | -1742.97576 | -1742.96942 | -1742.98389 |
| **G** | -1742.540353 | -1742.5249 | -1742.52827 | -1742.52344 | -1742.534 |
| | **dmpx_4_beta_3** | **dmpx_4_beta_3_BHE_TS** | **dmpx_Me_3_heptenoate_Coor** | **dmpx_3_beta_4_BHE_TS** | **dmpx_3_beta_4** |
| **E** | -1742.9877 | -1742.9716 | -1742.9738 | -1742.9685 | -1742.9833 |
| **G** | -1742.53724 | -1742.52474 | -1742.5266 | -1742.5227 | -1742.5342 |
| | **dmpx_3_beta_2** | **dmpx_3_beta_2_BHE_TS** | **dmpx_Me_2_heptenoate_Coor** | **dmpx_2_beta_3_BHE_TS** | **dmpx_2_beta_3** |
| **E** | -1742.98226 | -1742.96735 | -1742.97439 | -1742.97427 | -1742.9903 |
| **G** | -1742.53368 | -1742.52125 | -1742.52671 | -1742.52597 | -1742.53886 |
| | **dmpx_5MC** | **dmpx_4MC** | **dmpx_Pd_H** | | |
| **E** | -1743.004666 | -1742.998449 | -1279.21782 | | |
| **G** | -1742.550936 | -1742.545708 | -1278.963175 | | |

**Table S5: Internal energy (E) and free energy (G) in gas phase (in Hartrees) of CO coordination, CO insertion, methanol coordination and methanolysis for the dtbpx coordinated linear 7-β-6 and methyl branched 6-β-7 Pd-alkyl species.**

| | dtbpx_7_beta_6 | dtbpx_7_beta_6_CO_Coor | dtbpx_7_beta_6_CO_TS | dtbpx_7_beta_6_CO_RS |
|---|---|---|---|---|
| **E** | -2214.682936 | -2328.006167 | -2327.999167 | -2328.028573 |
| **G** | -2213.905380 | -2327.220859 | -2327.214211 | -2327.243781 |
| | **dtbpx_7_beta_6_MeOH_Coor** | **dtbpx_7_beta_6_3(MeOH)_Coor** | **dtbpx_7_beta_6_MeOH_TS** | **dtbpx_7_beta_6_3(MeOH)_TS** |
| **E** | -2443.750003 | -2675.223300 | -2443.70548 | -2675.17780 |
| **G** | -2442.913992 | -2674.289843 | -2442.87449 | -2674.24709 |
| | **dtbpx_7_beta_6_product** | | | |
| **E** | -692.830658 | | | |
| **G** | -692.602106 | | | |
| | **dtbpx_6_beta_7** | **dtbpx_6_beta_7_CO_Coor** | **dtbpx_6_beta_7_CO_TS** | **dtbpx_6_beta_7_CO_RS** |
| **E** | -2214.67984 | -2328.000119 | -2327.997193 | -2328.029198 |
| **G** | -2213.902718 | -2327.213483 | -2327.212800 | -2327.242094 |
| | **dtbpx_6_beta_7_MeOH_Coor** | **dtbpx_6_beta_7_3(MeOH)_Coor** | **dtbpx_6_beta_7_MeOH_TS** | **dtbpx_6_beta_7_3(MeOH)_TS** |
| **E** | -2443.742965 | -2675.214042 | -2443.70362 | -2675.16408 |
| **G** | -2442.905884 | -2674.277891 | -2442.87335 | -2674.22986 |
| | **dtbpx_6_beta_7_product** | | | |
| **E** | -692.828793 | | | |
| **G** | -692.600568 | | | |

**Table S6: Internal energy (E) and free energy (G) in gas phase (in Hartrees) of CO coordination, CO insertion, methanol coordination and methanolysis for the dtbpx coordinated 4- and 5-membered chelate 4-m.c. and 5-m.c. Pd-alkyl species.**

| | dtbpx_4MC | dtbpx_4MC_CO_Coor | dtbpx_4MC_CO_TS | dtbpx_4MC_CO_RS |
|---|---|---|---|---|
| **E** | -2214.697274 | -2328.00732 | -2328.003214 | -2328.034437 |
| **G** | -2213.914227 | -2327.218272 | -2327.217806 | -2327.242480 |
| | **dtbpx_4MC_MeOH_Coor** | **dtbpx_4MC_3(MeOH)_Coor** | **dtbpx_4MC_MeOH_TS** | **dtbpx_4MC_3(MeOH)_TS** |
| **E** | -2443.757326 | -2675.21398 | -2443.70009 | -2675.15564 |
| **G** | -2442.913407 | -2674.279898 | -2442.86808 | -2674.21935 |
| | **dtbpx_4MC_product** | | | |
| **E** | -692.827783 | | | |
| **G** | -692.59489 | | | |
| | **dtbpx_5MC** | **dtbpx_5MC_CO_Coor** | **dtbpx_5MC_CO_TS** | **dtbpx_5MC_CO_RS** |
| **E** | -2214.695609 | -2327.995566 | -2327.992544 | -2328.028829 |
| **G** | -2213.910067 | -2327.209279 | -2327.205102 | -2327.237296 |
| | **dtbpx_5MC_MeOH_Coor** | **dtbpx_5MC_3(MeOH)_Coor** | **dtbpx_5MC_MeOH_TS** | **dtbpx_5MC_3(MeOH)_TS** |
| **E** | -2443.758639 | -2675.2143 | -2443.70436 | -2675.16810 |
| **G** | -2442.918150 | -2674.276125 | -2442.87257 | -2674.23013 |
| | **dtbpx_5MC_product** | | | |
| **E** | -692.828997 | | | |
| **G** | -692.599206 | | | |

**Table S7: Internal energy (E) and free energy (G) in gas phase (in Hartrees) of CO coordination, CO insertion, methanol coordination and methanolysis for the dtbpx coordinated branched 5-β-4 Pd-alkyl species.**

| | dtbpx_5_beta_4 | dtbpx_5_beta_4_CO_Coor | dtbpx_5_beta_4_CO_TS | dtbpx_5_beta_4_CO_RS |
|---|---|---|---|---|
| **E** | -2214.682829 | -2327.99522 | -2327.991081 | -2328.027202 |
| **G** | -2213.90046 | -2327.209333 | -2327.205439 | -2327.240645 |
| | **dtbpx_5_beta_4_MeOH_Coor** | **dtbpx_5_beta_4_3(MeOH)_Coor** | **dtbpx_5_beta_4_MeOH_TS** | **dtbpx_5_beta_4_3(MeOH)_TS** |
| **E** | -2443.739388 | -2675.209698 | -2443.70268 | -2675.16988 |
| **G** | -2442.902716 | -2674.273192 | -2442.87106 | -2674.23053 |
| | **dtbpx_5_beta_4_product** | | | |
| **E** | -692.827775 | | | |
| **G** | -692.599185 | | | |

**Table S8: Internal energy (E) and free energy (G) in gas phase (in Hartrees) of CO coordination, CO insertion, methanol coordination and methanolysis for the dmpx coordinated linear 7-β-6 and methyl branched 6-β-7 Pd-alkyl species.**

| | dmpx_7_beta_6 | dmpx_7_beta_6_CO_Coor | dmpx_7_beta_6_CO_TS | dmpx_7_beta_6_CO_RS |
|---|---|---|---|---|
| **E** | -1742.981874 | -1856.314422 | -1856.296482 | -1856.323943 |
| **G** | -1742.533826 | -1855.860245 | -1855.843151 | -1855.868823 |
| | **dmpx_7_beta_6_MeOH_Coor** | **dmpx_7_beta_6_3(MeOH)_Coor** | **dmpx_7_beta_6_MeOH_TS** | **dmpx_7_beta_6_3(MeOH)_TS** |
| **E** | -1972.054455 | -2203.532609 | -1972.00042 | -2203.48143 |
| **G** | -1971.550755 | -2202.930652 | -1971.49849 | -2202.87942 |
| | **dmpx_7_beta_6_product** | | | |
| **E** | -692.830658 | | | |
| **G** | -692.602106 | | | |
| | **dmpx_6_beta_5** | **dmpx_6_beta_5_CO_Coor** | **dmpx_6_beta_5_CO_TS** | **dmpx_6_beta_5_CO_RS** |
| **E** | -1742.983764 | -1856.312710 | -1856.296039 | -1856.323203 |
| **G** | -1742.534043 | -1855.857482 | -1855.842532 | -1855.866957 |
| | **dmpx_6_beta_5_MeOH_Coor** | **dmpx_6_beta_5_3(MeOH)_Coor** | **dmpx_6_beta_5_MeOH_TS** | **dmpx_6_beta_5_3(MeOH)_TS** |
| **E** | -1972.051637 | -2203.527932 | -1972.00157 | -2203.47876 |
| **G** | -1971.547508 | -2202.924610 | -1971.49769 | -2202.87701 |
| | **dmpx_6_beta_5_product** | | | |
| **E** | -692.828793 | | | |
| **G** | -692.600568 | | | |

**Table S9: Internal energy (E) and free energy (G) in gas phase (in Hartrees) of CO coordination, CO insertion, methanol coordination and methanolysis for the dmpx coordinated 4- and 5-membered chelate 4-m.c. and 5-m.c. Pd-alkyl species.**

| | dmpx_4MC | dmpx_4MC_CO_Coor | dmpx_4MC_CO_TS | dmpx_4MC_CO_RS |
|---|---|---|---|---|
| **E** | -1742.998449 | -1856.322524 | -1856.301915 | -1856.342464 |
| **G** | -1742.545708 | -1855.864702 | -1855.845424 | -1855.882433 |
| | **dmpx_4MC_MeOH_Coor** | **dmpx_4MC_3(MeOH)_Coor** | **dmpx_4MC_MeOH_TS** | **dmpx_4MC_3(MeOH)_TS** |
| **E** | -1972.067995 | -2203.530659 | -1971.99588 | -2203.47612 |
| **G** | -1971.558263 | -2202.926135 | -1971.49238 | -2202.87294 |
| | **dmpx_4MC_product** | | | |
| **E** | -692.827783 | | | |
| **G** | -692.59489 | | | |
| | **dmpx_5MC** | **dmpx_5MC_CO_Coor** | **dmpx_5MC_CO_TS** | **dmpx_5MC_CO_RS** |
| **E** | -1743.004666 | -1856.311918 | -1856.295164 | -1856.323573 |
| **G** | -1742.550936 | -1855.855964 | -1855.839578 | -1855.864080 |
| | **dmpx_5MC_MeOH_Coor** | **dmpx_5MC_3(MeOH)_Coor** | **dmpx_5MC_MeOH_TS** | **dmpx_5MC_3(MeOH)_TS** |
| **E** | -1972.072534 | -2203.529139 | -1972.00066 | -2203.48264 |
| **G** | -1971.562408 | -2202.923189 | -1971.49713 | -2202.87757 |
| | **dmpx_5MC_product** | | | |
| **E** | -692.828997 | | | |
| **G** | -692.599206 | | | |

**Table S10: Internal energy (E) and free energy (G) in gas phase (in Hartrees) of CO coordination, CO insertion, methanol coordination and methanolysis for the dmpx coordinated branched 5-β-4 Pd-alkyl species.**

| | dmpx_5_beta_4 | dmpx_5_beta_4_CO_Coor | dmpx_5_beta_4_CO_TS | dmpx_5_beta_4_CO_RS |
|---|---|---|---|---|
| **E** | -1742.989327 | -1856.306568 | -1856.292928 | -1856.322098 |
| **G** | -1742.540353 | -1855.851719 | -1855.838851 | -1855.864438 |
| | **dmpx_5_beta_4_MeOH_Coor** | **dmpx_5_beta_4_3(MeOH)_Coor** | **dmpx_5_beta_4_MeOH_TS** | **dmpx_5_beta_4_3(MeOH)_TS** |
| **E** | -1972.048956 | -2203.52417 | -1972.00009 | -2203.47415 |
| **G** | -1971.542886 | -2202.921826 | -1971.49566 | -2202.87185 |
| | **dmpx_5_beta_4_product** | | | |
| **E** | -692.827775 | | | |
| **G** | -692.599185 | | | |

**Table S11: Internal energy (E) and free energy (G) in gas phase (in Hartrees) of ethylene coordination, ethylene insertion, CO coordination, CO insertion, methanol coordination and methanolysis for the dtbpx coordinated Pd-hydride species.**

| | dtbpx_Ethylene_Coor | dtbpx_Ethylene_Ins_TS | dtbpx_Ethyl | dtbpx_Ethyl_CO_Coor |
|---|---|---|---|---|
| **E** | -1829.541773 | -1829.541673 | -1829.560146 | -1942.884247 |
| **G** | -1828.906839 | -1828.906975 | -1828.924352 | -1942.239728 |
| | **dtbpx_Ethyl_CO_TS** | **dtbpx_Ethyl_CO_RS** | **dtbpx_Ethyl _MeOH_Coor** | **dtbpx_Ethyl _MeOH_TS** |
| **E** | -1942.876661 | -1942.906312 | -2058.628028 | -2058.582139 |
| **G** | -1942.233249 | -1942.263304 | -2057.934018 | -2057.894119 |
| | **dtbpx_Ethyl _3(MeOH)_Coor** | **dtbpx_Ethyl _3(MeOH)_TS** | **dtbpx_Ethyl _product** | |
| **E** | -2290.101381 | -2290.055373 | -307.7015633 | |
| **G** | -2289.310809 | -2289.267818 | -307.612393 | |

**Table S12: Internal energy (E) and free energy (G) in gas phase (in Hartrees) of *iso*-propanol coordination and alcoholysis for the dtbpx coordinated linear 7-β-6 Pd-alkyl species and of miscellaneous compounds.**

| | dtbpx_7_beta_6_iPrOH_Coor | dtbpx_7_beta_6_iPrOH_TS | dtbpx_7_beta_6_3(iPrOH)_Coor | dtbpx_7_beta_6_3(iPrOH)_TS |
|---|---|---|---|---|
| **E** | -2522.384608 | -2522.340006 | -2911.127842 | -2911.075099 |
| **G** | -2521.49706 | -2521.455109 | -2910.034045 | -2909.984222 |
| | **dtbpx_7_beta_6_iPrOH_product** | **Me_2_heptenoate** | **Me_3_heptenoate** | **Me_4_heptenoate** |
| **E** | -771.4679512 | -463.7309692 | -463.7254957 | -463.7261545 |
| **G** | -771.18753 | -463.560346 | -463.556672 | -463.556374 |
| | **Me_5_heptenoate** | **Me_6_heptenoate** | **MeOH** | **3(MeOH)** |
| **E** | -463.726692 | -463.7212023 | -115.7144073 | -347.1736537 |
| **G** | -463.557844 | -463.551741 | -115.685661 | -347.049626 |
| | **Ethylene** | **CO** | **iPrOH** | **3(iPrOH)** |
| **E** | -78.587458 | -113.3094543 | -194.3533176 | -583.0977305 |
| **G** | -78.557105 | -113.323561 | -194.272151 | -582.817555 |

## References


[1] Rettig, M. F.; Maitlis, P. M.; Cotton, F. A.; Webb, T. R. *Inorg. Synth.* **2007**, *28*, pp 110-113.

[2] *Organikum*, 21st Edition, Wiley-VCH, Weinheim, **2001**, pp 518-522.

[3] Chatt, J.; Vallarino, L. M.; Venanzi, L. M. *J. Chem. Soc.* **1957**, 3413-3416.

[4] Rulke, R. E.; Ernsting, J. M.; Spek, A. L.; Elsevier, C. J.; van Leeuwen, P. W. N. M.; Vrieze, K. *Inorg. Chem.* **1993**, *32*, 5769-5778.

[5] (a) Hoffmann, H.; Schellenbeck, P. *Chem. Ber.* **1966**, *99*, 1134-1142. (b) Rithner, C. D.; Bushweller, C. H. *J. Am. Chem. Soc.* **1985**, *107*, 7823-7836.

[6] Eisenträger, F.; Göthlich, A.; Gruber, I.; Heiss, H.; Kiener, C. A.; Krüger, C.; Notheis, J. U.; Rominger, F.; Scherhag, G.; Schultz, M.; Straub, B. F.; Volland, M. A. O.; Hofmann, P. *New J. Chem*. **2003**, *27*, 540-550.

[7] Pörschke, K.-R.; Pluta, C.; Proft, B.; Lutz, F.; Krüger, C. *Z. Naturforsch.* **1993**, 608-626.

[8] Carr, N.; Dunne, B. J.; Mole, L.; Orpen, A. G.; Spencer, J. L. *J. Chem. Soc., Dalton Trans.* **1991**, 863-871.

[9] Huber, J.; Mecking, S. *Macromolecules* **2010**, *43*, 8718-8723.

[10] Tani, K.; Tanigawa, E.; Tatsuno, Y.; Otsuka, S. *J. Organomet. Chem.* **1985**, *279*, 87-101.

[11] depp was synthesized according to ref. 10, by using diethylphosphine instead of di-*iso*-propylphosphine.

[12] Stempfle, F.; Quinzler, D.; Heckler, I.; Mecking, S. *Macromolecules* **2011**, *44*, 4159-4166.

[13] *X-RED* version 1.31 (2005) Stoe Data Reduction Program, Darmstadt, Germany.

[14] Sheldrick, G. M. *SHELXS-97* Program for Crystal Structure Analysis, University of Göttingen, Germany, **1997**.

[15] Sheldrick, G. M. *SHELXL-97* Program for Crystal Structure Refinement, University of Göttingen, Germany, **1997**.

[16] Faruggia, L. J. ORTEP-3 V2.02 for Windows, University of Glasgow, Scotland, **2008**.

[17] Roesle, P.; Dürr, C. J.; Möller, H. M.; Cavallo, L.; Caporaso, L.; Mecking, S. *J. Am. Chem. Soc.* **2012**, *134*, 17696-17703.

[18] Christl, J. T.; Roesle, P.; Stempfle, F.; Wucher, P.; Göttker-Schnetmann, I.; Müller, G.; Mecking, S. *Chem. Eur. J.* **2013**, *19*, 17131-17140.

[19] Clegg, W.; Eastham, G. R.; Elsegood, M. R. J.; Heaton, B. T.; Iggo, J. A.; Tooze, R. P.; Whyman, R.; Zacchini, S. *Organometallics* **2002**, *21*, 1832-1840.

[20] Beller, M.; Krotz, A.; Baumann W. *Adv. Synth. Catal.* **2002**, *344*, 517-524.

[21] Portnoy, M.; Frolow, F.; Milstein, D. *Organometallics* **1991**, *10*, 3960-3962.

[22] Hausoul, P. J. C.; Lutz, M.; Jastrzebski, J. T. B. H.; Bruijnincx, P. C. A.; Weckhuysen, B. M.; Klein Gebbink R. J. M. *Organometallics* **2013**, *32*, 5047-5057.

[23] Frisch, M. J.; Trucks, G. W.; Schlegel, H. B.; Scuseria, G. E.; Robb, M. A.; Cheeseman, J. R.; Scalmani, G.; Barone, V.; Mennucci, B.; Petersson, G. A.; Nakatsuji, H.; Caricato, M.; Li, X.; Hratchian, H. P.; Izmaylov, A. F.; Bloino, J.; Zheng, G.; Sonnenberg, J. L.; Hada, M.; Ehara, M.; Toyota, K.; Fukuda, R.; Hasegawa, J.; Ishida, M.; Nakajima, T.; Honda, Y.; Kitao, O.; Nakai, H.; Vreven, T.; Montgomery, Jr., J. A.; Peralta, J. E.; Ogliaro, F.; Bearpark, M.; Heyd, J. J.; Brothers, E.; Kudin, K. N.; Staroverov, V. N.; Kobayashi, R.; Normand, J.; Raghavachari, K.; Rendell, A.; Burant, J. C.; Iyengar, S. S.; Tomasi, J.; Cossi, M.; Rega, N.; Millam, J. M.; Klene, M.; Knox, J. E.; Cross, J. B.; Bakken, V.; Adamo, C.; Jaramillo, J.; Gomperts, R.; Stratmann, R. E.; Yazyev, O.; Austin, A. J.; Cammi, R.; Pomelli, C.; Ochterski, J. W.; Martin, R. L.; Morokuma, K.; Zakrzewski, V. G.; Voth, G. A.; Salvador, P.; Dannenberg, J. J.; Dapprich, S.; Daniels, A. D.; Farkas, Ö.; Foresman, J. B.; Ortiz, J. V.; Cioslowski, J.; Fox, D. J. Gaussian, Inc., Wallingford CT, **2009**.

[24] Becke, A. D. *J. Chem. Phys.* **1993**, *98*, 5648-5652.

[25] (a) Dunning Jr., T. H.; Hay, P. J. in *Modern Theoretical Chemistry*, Schaefer III, H. F., Ed.; Plenum, New York, **1976**, pp. 1-28. (b) Hay, P. J.; Wadt, W. R. *J. Chem. Phys*, **1985**, *82*, 270-283.

[26] (a) Ditchfield, R.; Hehre, W. J.; Pople, J. A. *J. Chem. Phys.* **1971**, *54*, 724-728. (b) Hehre, W. J.; Ditchfield, R.; Pople, J. A. *J. Chem. Phys.* **1972**, *56*, 2257-2261. (c) Hariharan, P. C.; Pople, J. A. *Mol. Phys.* **1974**, *27*, 209-214. (d) Gordon, M. S. *Chem. Phys. Lett.* **1980**, *76*, 163-168. (e) Hariharan, P. C.; Pople, J. A. *Theor. Chim. Acta* **1973**, *28*, 213-222.